



**TECHNISCHE
UNIVERSITÄT
WIEN**
Vienna University of Technology

DIPLOMARBEIT

Inkjet Printed CVD-Graphene Devices

Ausgeführt am Forschungszentrum
CRANN des Trinity College Dublin
der University of Dublin

unter der Anleitung von
Prof. Georg S. Duesberg

eingereicht am Institut für
Chemische Technologien und Analytik
der Technischen Universität Wien

zur Beurteilung durch
Ao.Prof. Dr. Roland Haubner

von

Sarah Hurch, BSc

Hauptstraße 61a Top 10
3021 Pressbaum
Austria

Inkjet Printed CVD-Graphene Devices

Abstract

Due to its unique properties graphene has become of great interest these past years and many diverse and innovative routes to its synthesis have been realised. However, to implement its potential it is crucial to fabricate devices and to develop a commercially relevant production route.

This work demonstrates the fabrication of chemical vapour deposition (CVD) grown graphene-based devices using inkjet printing for both device pattern definition and electrical contact deposition. First a pre-patterning step of the catalyst substrate for graphene growth was developed to yield well defined high quality graphene structures. Secondly, after transfer to an arbitrary insulating substrate, these structures were contacted with inkjet printed leads. As a result high performance graphene field effect transistors (GFETs) entirely defined by a commercial inkjet printer with channel lengths of 50 μm were fabricated. This study examines the patterned graphene growth using optical and electronic microscopy, Raman spectroscopy and XPS. The resultant devices were characterised by electrical transport measurements.

Carrier mobilities exceeding $2100 \text{ cm}^2 \text{ V}^{-1} \text{ s}^{-1}$ at room temperature were realised. This novel device fabrication route, combining CVD growth of high quality graphene and inkjet printing, opens a pathway to the production of high performance, cheap, flexible and transparent electronics.

Kurzfassung

Aufgrund seiner einzigartigen Eigenschaften hat Graphen in den letzten Jahren großes Interesse in der Forschung geweckt und viele innovative Herstellungsmethoden wurden entwickelt. Um das Potential von Graphen auszunützen, ist es jedoch essentiell, Anwendungen und deren kommerziell relevante Produktionsrouten zu entwickeln.

Diese Arbeit beschreibt die Fabrikation von Feld-Effekt-Transistoren aus Chemical-Vapour-Deposition (CVD) Graphen. Inkjetdruck wurde dabei eingesetzt, sowohl um das Graphen zu strukturieren, als auch um dieses elektrisch zu kontaktieren. Zuerst wurde ein Maskierungsschritt des katalytischen Substrats für das Graphenwachstum entwickelt, um klar definierte Graphenstrukturen zu erzeugen. Dann, nach der Überführung dieser Strukturen auf ein isolierendes Material, wurden sie mit inkjetgedruckten Kontakten versehen. Daraus resultierten ausschließlich durch Inkjetdruck geformte Graphen-Feld-Effect-Transistoren (GFETs) mit Channelweiten von 50 μm , die hohe Mobilitätswerte aufwiesen. Die Herstellung von definierten Graphenmustern wurde mittels optischer und Elektronenmikroskopie, Raman Spektroskopie und XPS analysiert. Die erzeugten Transistoren wurden mit Hilfe von elektrischen Transportmessungen charakterisiert.

Ladungsträgermobilitäten bei Raumtemperatur von über $2100 \text{ cm}^2 \text{ V}^{-1} \text{ s}^{-1}$ wurden erzielt. Diese neue Fabrikationsroute, die die hohe Qualität von CVD Graphen mit der Anpassungsfähigkeit des Inkjetdrucks kombiniert, öffnet einen möglichen Weg zu billiger, flexibler, transparenter Elektronik.

Acknowledgements

So many people helped in so many ways to finish this study. First of all Prof. Georg Duesberg, who put his trust in me and gave me the opportunity to work on this interesting subject. Prof. Roland Haubner gave me the freedom to carry out this project in Dublin.

My fellow members of the ASIN research group, namely Dr. Nina Berner, Dr. Toby Hallam, Dr. Kay Lee, Dr. Niall McEvoy, Dr. Rohit Mishra, Dr. Ashok Kumar Nanjundan, Dr. Hye-Young Kim, Chris Murray, Riley Gatensby, Hugo Nolan, Ehsan Rezvani, Sinéad Winters, Christian Wirtz and Chanyoung Yim, were a great pleasure to work with and supported me at work and in private. Dr. Toby Hallam supervised me and was a constant source of knowledge and aid. Hugo Nolan and Dr. Niall McEvoy answered endless questions and helped with EDX measurements and the subtleties of the English language. Dr. Nina Berner conducted XPS measurements, Riley Gatensby electropolished the copper foil substrates used in this study and Sinéad Winters took the presented AFM scans. Richard Coull introduced me to the mysteries of inkjet printing. Many members of CRANN and AML helped as well.

Prof. Wolfgang Linert, Prof. Eoin Scanlan and Traude Krausler were responsible for the coordination and organisation of my ERASMUS stay in Trinity College Dublin.

My mother, my father and my siblings always supported me and last but not least Andreas, who was always there for me, even when he was not with me.

I thank you all!!!

Table of Contents

ABSTRACT	2
KURZFASSUNG	3
ACKNOWLEDGEMENTS	4
I. INTRODUCTION.....	8
1. MOTIVATION.....	9
2. THEORY.....	12
2.1. <i>Graphene and its potential uses.....</i>	<i>12</i>
2.1.1. Properties of graphene.....	13
2.1.2. Applications of graphene	14
2.2. <i>Synthesis of graphene</i>	<i>16</i>
2.2.1. Top-down graphene synthesis.....	16
2.2.1.1. Mechanical exfoliation.....	16
2.2.1.2. Liquid phase exfoliation	17
2.2.1.3. Unzipping carbon nanotubes	17
2.2.2. Bottom-up graphene synthesis.....	17
2.2.2.1. Growth on silicon carbide.....	17
2.2.2.2. Chemical synthesis	18
2.2.2.3. Chemical vapour deposition on metals.....	18
2.3. <i>Graphene design</i>	<i>21</i>
2.3.1. Post growth patterning	21
2.3.1.1. Lithography.....	21
2.3.1.2. Metal etch masks	21
2.3.1.3. Focused ion beam	21
2.3.1.4. Solution processing.....	21
2.3.2. Pre growth patterning.....	21
2.3.2.1. Growth substrate template	22
2.3.2.2. Masking the growth substrate.....	22
2.4. <i>Analysis of graphene</i>	<i>23</i>
2.4.1. Optical microscopy.....	23
2.4.2. Raman spectroscopy	23
2.4.3. AFM.....	27
2.4.4. SEM.....	27
2.4.5. TEM.....	27
2.4.6. Electrical Measurements.....	28
2.5. <i>Inkjet printing</i>	<i>29</i>
2.5.1. Inkjet printer.....	29
2.5.2. Inks for inkjet printing.....	30
2.5.3. Sintering of Ag nanoparticle ink.....	31

II. EXPERIMENTAL	32
3. MATERIALS AND METHODS	33
3.1. Production of CVD grown graphene	33
3.1.1. Growth substrate preparation.....	33
3.1.1.1. Polishing of Cu-foil.....	33
3.1.1.2. Cleaning the copper foil	33
3.1.2. CVD graphene growth.....	34
3.1.3. Graphene growth control - “hotplate test”	35
3.1.4. Graphene transfer from copper foil to wafer	35
3.1.4.1. Adding a PMMA transfer handling layer to graphene	35
3.1.4.2. Removal of copper-foil.....	35
3.1.4.3. Transferring graphene to a wafer.....	36
3.1.4.4. PMMA removal.....	37
3.2. Inkjet printed graphene device fabrication.....	38
3.2.1. Prepatterned graphene growth.....	38
3.2.2. Inkjet printing of silver electrodes.....	39
3.2.3. Sintering of Ag nanoparticle ink.....	40
3.3. Analysis.....	41
3.3.1. Analysis of CVD grown graphene.....	41
3.3.1.1. Raman spectroscopy.....	41
3.3.1.2. Optical microscopy	41
3.3.1.3. SEM.....	41
3.3.2. Influence of marker ink/chromium on the graphene growth.....	41
3.3.2.1. Analysis of Staedtler Lumocolor® permanent marker 385 + 388 ink black	41
3.3.2.2. Sputtering chromium on substrate.....	41
3.3.3. Analysis of SunTronic® silver ink	42
3.3.3.1. SEM.....	42
3.3.3.2. Sheet resistance.....	42
3.3.3.3. Resistance	43
3.3.4. Characterisation of fabricated GFETs.....	43
3.3.4.1. 4-point-probe geometry.....	43
3.3.4.2. 4-point-probe geometry without a gate sweep.....	44
3.3.4.3. 2-point-probe geometry.....	44
4. RESULTS	45
4.1. Production of graphene	45
4.1.1. Graphene growth on unpolished copper foils.....	45
4.1.2. Graphene growth on electropolished copper foils.....	48
4.2. Patterned graphene growth	52
4.2.1. Ink masking the growth substrate prior to graphene growth.....	52
4.2.2. Quality of prepatterned graphene	53
4.2.3. Analysis of Staedtler Lumocolor® permanent marker black ink	54
4.2.4. Influence of chromium on graphene growth.....	57
4.2.4.1. Border of ink-prepatterned features	57
4.2.4.2. Sputter deposited chromium.....	58

4.3.	<i>Production and characterisation of GFETs</i>	64
4.3.1.	Printing electrical contacts onto graphene	64
4.3.1.1.	Inkjet printing silver nanoparticle ink	64
4.3.1.2.	Sintering of silver nanoparticle ink	64
4.3.1.3.	Electrical characterisation of silver contacts	65
4.3.1.4.	Sintering of silver nanoparticle ink printed on graphene	66
4.3.2.	Device characterisation	67
4.3.2.1.	Sheet resistance and charge carrier mobility	69
4.3.2.2.	Current on-off ratio	73
5.	DISCUSSION OF RESULTS	74
5.1.	<i>Graphene growth on unpolished vs. growth on polished copper foils</i>	74
5.2.	<i>Staedtler Lumocolor® permanent marker ink</i>	76
5.3.	<i>Chromium influenced graphene growth</i>	76
5.4.	<i>Printing silver ink</i>	78
5.5.	<i>Electrical performance of the fabricated graphene devices</i>	79
6.	CONCLUSION AND FUTURE WORK	82
	APPENDIX	84
	LIST OF ACRONYMS	89
	LIST OF REFERENCES	90

I. Introduction

1. Motivation

In the last decade graphene has attracted much attention and fuelled by graphene's promising properties much effort has been put into the development of synthesis routes [1]. Nevertheless to harness its potential it is essential not only to produce graphene but to find ways of fabricating devices based on it.

Printed electronics is an evolving field, with improvements and developments in both techniques and materials used being reported frequently [2] [3]. Inkjet printing is a simple method that can be used in versatile applications. It is an economic process that requires minimum amounts of material and energy and is up-scalable for mass production. It gives access to the fabrication of devices on a multitude of substrates, such as plastics, wafers or glass. Inkjet printing is a quickly adjustable and immensely versatile direct writing process. Due to the fact that it is a contactless fabrication the introduction of impurities can be eliminated. For example, different products such as sensors, solar cells, display backplanes, electronic packaging and RF antennas have been successfully fabricated by inkjet printing [4]. Printed conductive inks can contain a big variety of materials such as metal nanoparticles, organometallics or polymers. The disadvantage of devices fabricated with these inks is that the reported mobilities of $\mu < 0.5 \text{ cm}^2\text{V}^{-1}\text{s}^{-1}$ are quite low [5]. Much effort is constantly put into the development of new inks to overcome this hindrance. As an example inkjet printed thin film transistors (TFTs) made of carbon nanotube (CNT) inks with carrier mobilities μ up to $50 \text{ cm}^2\text{V}^{-1}\text{s}^{-1}$ have been reported [6].

Its outstanding properties [1], especially its high possible carrier mobility (reported up to $200,000 \text{ cm}^2\text{V}^{-1}\text{s}^{-1}$ [7]), make graphene a very interesting material for various electrical applications and thus a possible component of conductive inks for printed electronics. One approach is the liquid phase exfoliation of graphite in N-methylpyrrolidone (NMP) to produce printable graphene dispersions [8]. For this process carrier mobilities in thin film transistors (TFTs) of up to $95 \text{ cm}^2\text{V}^{-1}\text{s}^{-1}$ have been reported [5]. Another approach uses Graphene Oxide (GO) dispersions as inks that are subsequently reduced to form conducting features [9]. Unfortunately the resulting Reduced Graphene Oxide (RGO) does not perform to the same standard as other graphene materials (such as CVD-grown) in electronic applications and usually mobilities not exceeding $90 \text{ cm}^2\text{V}^{-1}\text{s}^{-1}$ have been reported [5].

On the other hand, graphene grown by CVD provides a promising route towards large scale production of high quality, monolayer graphene films. CVD-grown graphene is of

great interest in the electronics industry as large areas of graphene can be grown on copper foils and transferred to arbitrary substrates [10]. Reported mobilities in the tens of thousands $\text{cm}^2\text{V}^{-1}\text{s}^{-1}$ range [11] affirm the high quality of CVD graphene; making it a prime candidate for incorporation into wafer scale production of graphene devices [12]. The mono-layered nature of such a graphene film combined with the well documented mechanical properties could prove invaluable in flexible electronics. Its high optical transparency suggests that it could also be employed in transparent electronics [13].

Many different methods of producing patterns of CVD graphene have been reported in the literature. A widespread approach is to grow a continuous graphene sheet and later decompose specific areas. This is commonly achieved by a lithographically patterned masking layer and etching of the exposed graphene areas through oxygen reactive ions (RIE), lasers or accelerated ion beams. These methods, though, tend to decrease the quality of the graphene layer [14], and are restricted to flat surfaces. Additionally, the substrate must be able to withstand the sometimes harsh chemical environment associated with the technique. Most importantly, lithography requires the graphene to be coated with polymer, which has been shown to deteriorate the quality of graphene [15].

Another way of patterning graphene is to restrict its growth to defined areas. This can either be achieved by pre-shaping a pattern of catalytic growth substrate (usually copper) on an inert basis substrate [16] or by physically blocking the growth in certain catalyst areas. Pre-shaped growth substrates tend to restructure under the temperatures involved in CVD graphene growth conditions so the resolution and the sharpness of the resulting graphene features is severely limited. Preventing the graphene growth in certain areas on the growth substrate has been successfully performed using alumina (Al_2O_3) masks. The Al_2O_3 efficiently prevents the growth of graphene by preventing the nucleation and growth of graphene crystallites in certain areas of the growth substrate [17]. A problem associated with this technique is that Al_2O_3 recrystallises at growth temperatures and forms hard structures that cannot be easily removed. Further, ALD (Atomic Layer Deposition) is a time consuming, relatively expensive process, and it requires a preceding patterning step.

This work shows, for the first time, the use of commercially available permanent marker inks to define graphene growth patterns on the copper CVD catalyst. Microscopic and spectroscopic techniques were used to characterise the graphene patterns in conjunction with electrical device measurements. Electrical devices were fabricated by printing electrical contacts using a silver nanoparticle-based ink and forming GFETs. Many

advantages are afforded by producing devices entirely via printing techniques including simplicity, flexibility and economy of the process. As such, it is ideally suited for the fabrication of prototypes as well as large scale production. Due to the low temperatures involved and the fact that no aggressive chemicals are required, this production route makes flexible, transparent electronics possible using inexpensive materials and fabrication techniques.

2. Theory

Graphite is an allotrope of carbon. It has a layered structure consisting of carbon atoms that are arranged in a regular hexagonal lattice. Graphene can be seen as one such isolated honeycomb sheet – a 2D crystal with remarkable properties [18].

2.1. Graphene and its potential uses

Graphene existed for many years as a theoretical model but was believed unstable in its free state [19] until it was proved otherwise in 2004 [20]. A. Geim and K. Novoselov received the Nobel Prize of Physics in 2010 for the discovery of graphene and their follow-up experiments [21].

In monolayer graphene the carbon atoms are sp^2 hybridised and hence form a flat sheet of high mechanical stability. Stacking single graphene layers results in graphite. Nonetheless ‘multilayer graphene’ is an accepted term in relevant literature. Mono- and bilayer graphene have distinctive simple electronic structures. With an increasing number of layers this structure becomes more and more complicated, merging into the electronic spectrum of 3D graphite at about 10 layers. It therefore can be distinguished between single-, double- and few-layered graphene and graphite [19].

Each atom in graphene contributes one s-orbital and two p-orbitals to form bonds with its neighbour atoms. The remaining p-orbital is oriented perpendicular to the carbon sheet. These p-orbitals form a delocalised π -system. The π (valence) and π^* (conduction) bands touch at 6 points in the first Brillouin zone, the so called Dirac points (see also Figure 1). This interesting band structure is responsible for the extraordinary electronic behaviour of

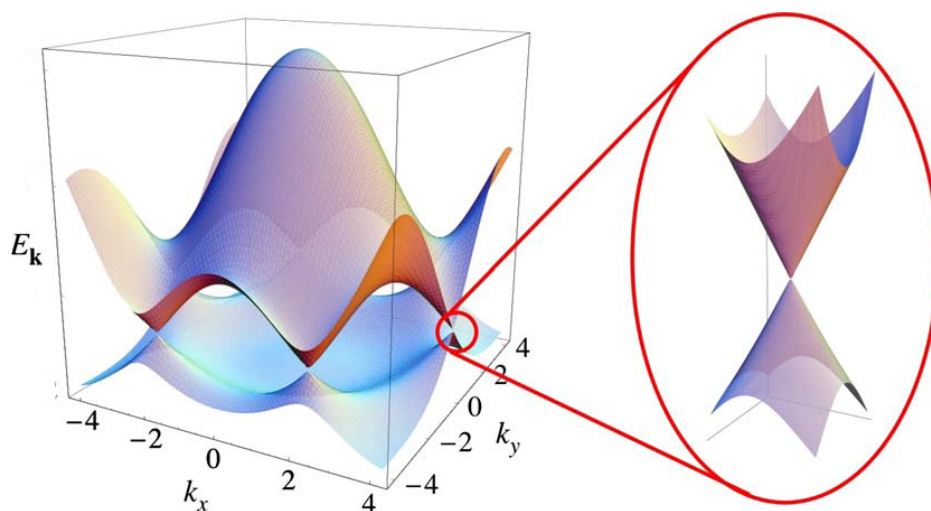


Figure 1: Electronic dispersion of graphene showing 6 Dirac points in the first Brillouin zone; on the right is a magnified image of the energy bands meeting at one of the Dirac points [image adapted from [22]]

this material [18]. Single layer graphene can be seen as a zero-gap semiconductor [20] or as a zero-overlap semimetal [19].

Further, graphene stands as the first representative of a new class of materials, the 2D crystals. Since 2004 the world of 2D crystals has begun to be explored and stable monolayers of other materials, such as boron nitride, molybdenum disulfide and niobium selenide have been produced [23]. These successes opened another interesting research field – hetero-structures made of different 2D material layers in which properties might be tailored to suit certain ends [24].

2.1.1. Properties of graphene

Graphene comes with an impressive set of properties. Being only one atom thick it is extremely thin and light but at the same time shows remarkable mechanical strength and high electrical and thermal conductivity, as well as being impermeable to gases [24].

Considering the extent of the π -orbitals out of plane, the thickness of graphene is 0.35 nm [25]. This monoatomic thin sheet absorbs only 2.3 % of white light and is therefore almost completely transparent [24]. In graphene of high crystallinity very little scattering of charge carriers occurs and they can travel several thousand interatomic distances without hindrance [19]. The charge carrier mobility is the readiness with which electrons and holes respond to an external electric field. Mobility measurements of graphene at room temperature exceeding $2 \cdot 10^5 \text{ cm}^2 \text{ V}^{-1} \text{ s}^{-1}$ have been reported [26]. As electrical and thermal conductivity are usually closely related it is hardly surprising that values above $3000 \text{ W m}^{-1} \text{ K}^{-1}$ were recorded for graphene [27]. Using nano-indentation on suspended monolayer graphene an intrinsic strength of 130 GPa and a Young's modulus of 1 TPa were measured [28]. It is important to note that these exceptional values can only be achieved in graphene samples of the highest quality - usually mechanically exfoliated graphene [24]. Other preparation methods still have to catch up in terms of graphene quality and some, by their very nature, never will, but their strength lies elsewhere.

Not only has graphene a distinctive set of interesting properties that makes it relevant for a great number of different applications, it also opened a way to observe quantum relativistic phenomena in reasonably simple experiments. As an example, even at room temperature, the Quantum Hall effect can be witnessed in graphene [19]. Graphene's charge carriers behave as relativistic particles and are easier described with the Dirac equation than with the Schrödinger equation. The interaction of the electrons with the periodic

honeycomb lattice gives rise to new quasi-particles – “... *electrons that have lost their rest mass m_0 or neutrinos that acquired the electron charge e .*”. These quasi-particles are called massless Dirac fermions and are, at low energies, described by the Dirac equation [19].

Graphene can easily be doped chemically or with an external electric field showing a distinct ambipolar field effect, as depicted in Figure 2 (a). The transition between electrons and holes as charge carriers is continuous [19] Both electrons and holes can be transported at very high carrier mobilities [19] making ballistic transport at room temperature [29] on the submicron scale possible [25]. Angle resolved photoemission spectroscopy (ARPES) can be used to make the linear electronic dispersion near the Dirac points visible (see Figure 2 (b)) [18].

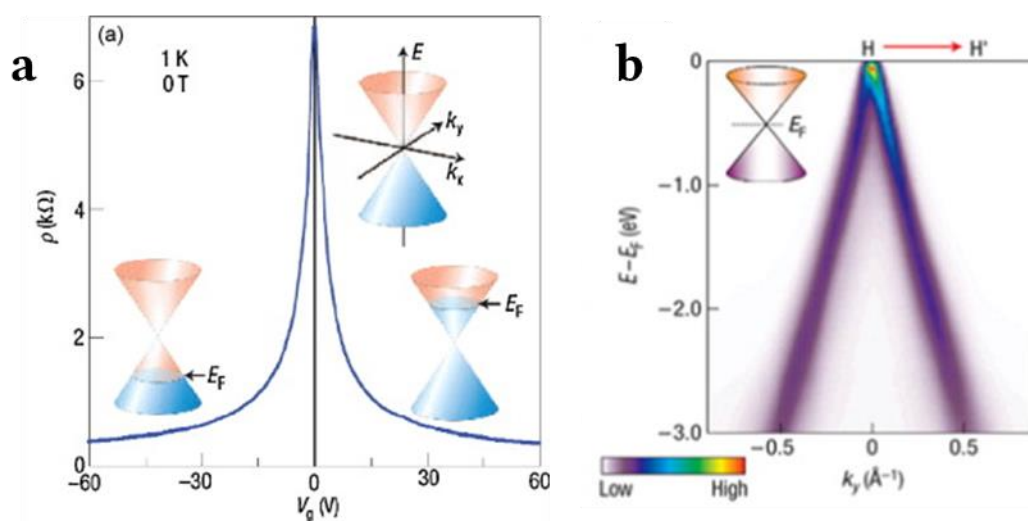


Figure 2: a) The ambipolar electric field effect of single-layer graphene; in the insets the change of the Fermi level E_F is depicted; b) ARPES spectrum of graphene (image adapted from [19] and [18])

2.1.2. Applications of graphene

From its extraordinary properties arise a vast number of potential uses for graphene, ranging from flexible, transparent electronics to DNA sequencing [24]. Many big companies, like Samsung [30], Intel and IBM [19], either have their own or fund graphene research groups.

Its electrical properties are especially promising and intensive research has been and continues to be put into the development of graphene electronics. Its high charge carrier mobility makes graphene a candidate for the channel material in integrated logic circuits. A big hindrance is the absence of a bandgap in graphene. Different advances such as graphene nanoribbons, single electron transistor formation, the control of bilayer and chemically modified graphene were able to open a bandgap but generally resulted in a decreased mobility. New transistor designs are currently being tested and it remains to be seen if and

when they will be suitable for mass production. Graphene does have its appeal not only as logic transistors but in high-frequency transistors as well. Again, there is still a long way to go until graphene based high-frequency transistors are ready to compete against today's semiconductor technology [24]. However, many other graphene based applications are developed presently using the currently available material, such as touch screens, solar cells, smart windows or rollable e-paper. The combination of graphene's transparency and its high electrical conductivity make transparent electronics possible. These days indium tin oxide (ITO) is widely used in transparent electronics and it still provides slightly better characteristics. However, ITO grows more and more expensive while graphene production improves constantly. In addition graphene also demonstrates the chemical durability and the mechanical flexibility that are absolutely necessary in flexible electronics [24].

Dispersions of graphene and graphene oxide (GO) flakes have been demonstrated as paints and inks and printed graphene electronics have been successfully fabricated [5]. Graphene can also be used to make conductive composite materials such as conductive plastics [19] and as graphene consists only of surface without bulk it is a logical step to use it in pressure sensors or highly sensitive gas sensors [18].

Another field of possible applications for graphene is photonics. Photo-detectors that work in a broad spectral range (between ultraviolet and infrared), possibly with very quick charge extraction due to graphene's high mobility, could be fabricated or optical losses in wireless communications could be minimised [24]. Graphene based optical modulators that are able to change phase, amplitude and polarisation of light as well as graphene based lasers were proposed. Compact optical polarisers were already demonstrated and their pending industrialisation is postponed only by the progress of high-quality graphene production technology [24].

High chemical stability and impermeability to gases make graphene barrier films possible. If it is grown on metals it provides a transparent water and oxygen corrosion protection [24].

In composite materials graphene could take over applications where traditionally carbon fibres are used. Especially in production routes where carbon fibres have proved difficult to handle, like injection-moulding, graphene can step up to reinforce materials [24].

A great many proposed uses remain unmentioned hereby, but generally speaking it is likely that applications that utilise the cheapest, lowest-grade graphene will become available earlier than those that need high quality sheets [24]. One of the few already commercially available graphene products are support grids for TEM analysis [31].

2.2. Synthesis of graphene

In the past few years a multitude of graphene production and processing techniques have been developed. The fabrication processes can be divided into two different categories – the top-down and the bottom-up approach.

The strengths of the following production methods are quite different and they provide graphene of greatly varying quality. A fabrication method has to be chosen that meets the specific requirements of the targeted product. Some applications require huge quantities of cheaply produced graphene flakes of relatively low quality; others need flat, mono crystalline graphene of only the highest quality. Graphene flakes or reduced graphene oxide flakes generally have low quality and are suited for conductive paints, composite materials and the like. Non-active or lower performance active devices require higher quality planar graphene. The highest quality, planar graphene is needed in high-performance electronics [24].

This section is aimed at giving a brief insight into the versatility of graphene production and is far from discussing all developed methods.

2.2.1. Top-down graphene synthesis

Top-down processes start with graphite and aim towards its delamination. They usually result in exfoliated graphene flakes. The challenge of this approach is to split the stacked graphite sheets without the destruction of the sheets themselves. Further, the re-agglomeration of the separated sheets has to be prevented. Top-down processes generally involve either multiple production steps and show low yields or produce great amounts of low-quality flakes. All these processes need the scarce raw material natural graphite as synthetically produced graphite does not show the needed level of graphitisation [1].

2.2.1.1. Mechanical exfoliation

Novoselov et al. were the first to demonstrate monolayer graphene. They used graphite and cleaved it with the aid of an adhesive tape [20]. This simple method still provides the highest quality graphene samples [24]. The downside of this technique is that it produces small isolated graphene flakes at a very low throughput and is virtually impossible to industrialise. Mechanical exfoliation will continue to be important in science, especially in fundamental studies [12].

2.2.1.2. *Liquid phase exfoliation*

Graphene can also be exfoliated in dispersions of graphite or graphite oxide via sonication [12]. The ideal surface tension for solvents in graphitic flake and graphene dispersions is ~ 40 mN/m. Organic solvents that fulfil this requirement (e.g. NMP, DMF, Benzyl benzoate) tend to have some disadvantages like toxicity or high boiling points. Surfactants are required to form aqueous dispersions. A cleaning step is usually necessary after the exfoliation to separate graphene flakes from bigger graphite particles, e.g. ultracentrifugation [12].

There are different procedures that partially oxidise graphite by introducing oxygen containing groups, e.g. epoxy, hydroxyl and carbonyl groups. Graphite- and graphene oxide (GO) are hydrophilic and readily form dispersions in pure water and organic solvents that are easier handled. GO does not have the same properties as graphene. Processes that aim toward the reduction of these GO flakes in order to re-establish graphene's properties succeed only partially, producing (highly) defective graphene -RGO [12].

Liquid phase exfoliation is an inexpensive technique that can be scaled up easily. Sonication and purification processes limit the size of the produced graphene flakes, but it is ideally suited for the production of inks and composites [12].

2.2.1.3. *Unzipping carbon nanotubes*

Unzipping carbon nanotubes may not be the simplest method but it can be convenient if graphene nanoribbons are desired. Strong oxidising chemicals or physical methods such as plasma etching or laser irradiation have been used to cut carbon nanotubes [1].

2.2.2. **Bottom-up graphene synthesis**

These techniques aim towards the synthesis of graphene from carbon containing sources. Graphene produced by some top-down approaches shows a lower level of defects than can currently be achieved by bottom-up methods. The advantage of bottom-up processes is that not only nanosheets but large graphene areas can be synthesised [1].

2.2.2.1. *Growth on silicon carbide*

Si can be sublimated from SiC wafers above 1000 °C, the excess carbon on the surface rearranges to form graphene layers. The Si(0001) as well as the C(000-1) surface are suited, though the latter tends to grow bigger graphene domains and generally shows films with higher mobility values. This graphene is of very high quality and domain sizes of up to 50 μm have been reported. The films can be decoupled from the surface via hydrogen intercalation. The major disadvantage of this technique is the high cost of SiC wafers.

New resistance standards using the Quantum Hall effect have been developed with graphene on SiC [12].

2.2.2.2. *Chemical synthesis*

The assembly of benzene based precursors seems to be a logical approach towards graphene synthesis. However, efforts with surface mediated reactions of polycyclic aromatic hydrocarbons have met with various obstacles and resulted in very small domains [12].

2.2.2.3. *Chemical vapour deposition on metals*

Metal surfaces are known for their ability to catalyse the decomposition of hydrocarbons and graphene of varying quality was grown on platinum, ruthenium, iridium, nickel and copper [18].

The growth on copper and nickel is most promising. Films grown on these metals differ substantially as the growth mechanisms are not the same. The solubility of carbon in nickel is low (see also phase diagram in Appendix Figure 67) but still a lot higher than in copper, where carbon is as good as insoluble, as can be seen in Figure 4. Graphene growth is usually conducted at elevated temperatures where the solubility of carbon is heightened. Upon cooling the dissolved carbon can segregate on the surface [1]. That is the reason why graphene growth on nickel usually yields multiple layers. The growth on copper is surface dependent [32]. It is almost a self-limiting process as once the copper is covered in graphene the growth stagnates [12].

Polycrystalline copper foils or thin copper films on a supporting substrate are typically used in CVD graphene production [24]. Most often methane and hydrogen are chosen as

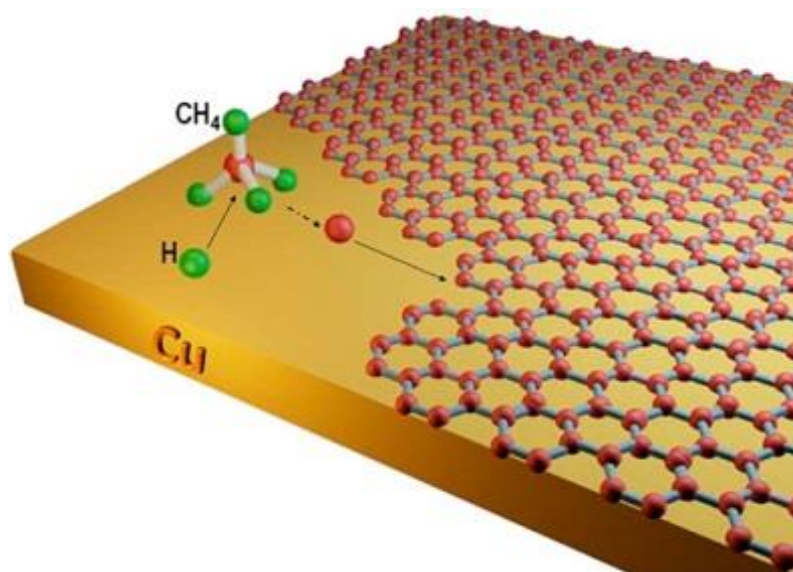


Figure 3: CVD growth of graphene on copper foil [reproduced from [33]]

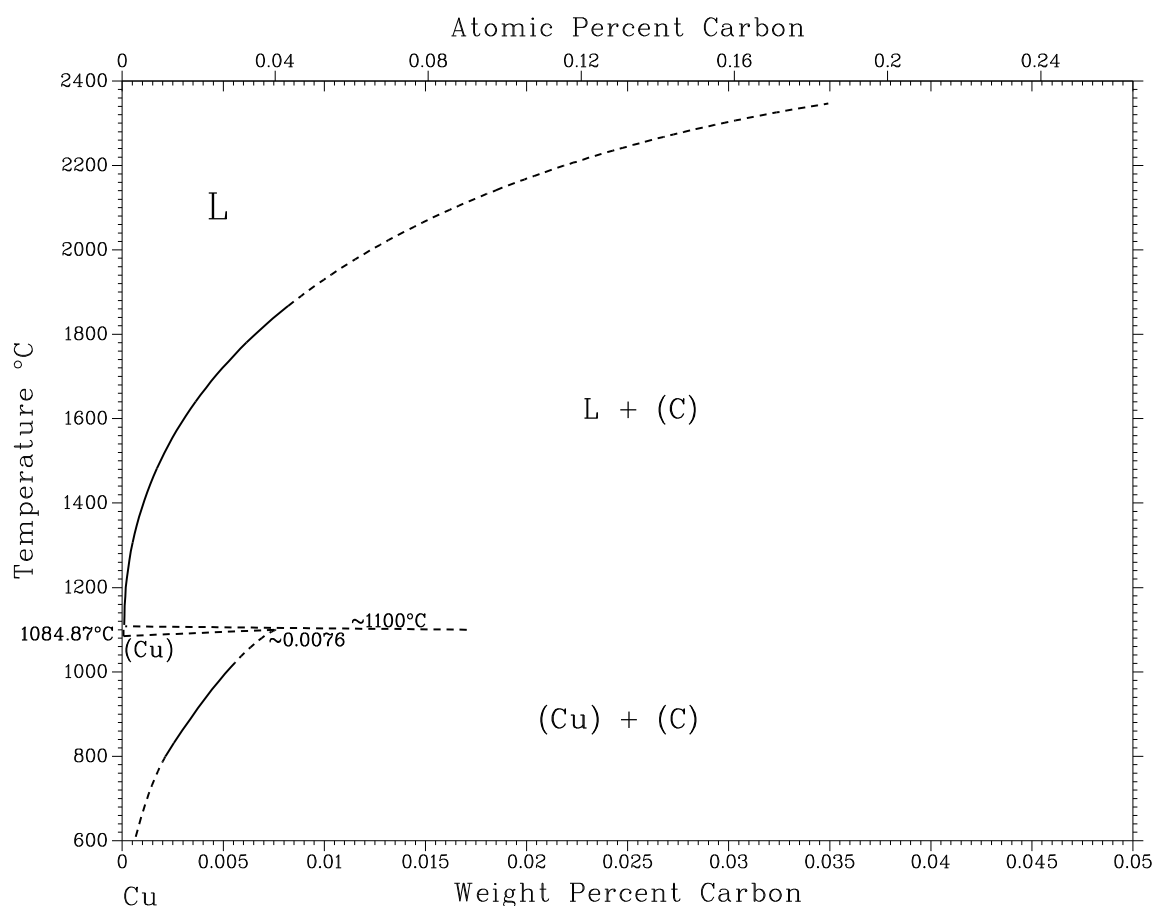


Figure 4: Phase diagram of carbon and copper [reproduced from [34]]

precursors (see also Figure 3). The best results are achieved at lowered pressures (often below 0.1 mbar) and temperatures above 1000 °C [12]. Depending on the growth parameters polycrystalline films, uniformly covering the growth substrate or isolated monocrystalline flakes can be produced. Square meters of polycrystalline graphene [24] and single crystals exceeding diameters of 2.3 mm have been grown on copper [35].

CVD growth depends on various factors, i.e. pressure, temperature, carbon source and concentration, the amount of hydrogen present and the quality of the metal substrate surface. The exact growth mechanism of graphene on copper is complex and only partially understood. It is assumed that hydrocarbons are thermally decomposed, aided by hydrogen. Thus formed thermodynamically unstable carbon species (e.g. $\text{CH}_{x<4}$) are adsorbed at the surface. They diffuse on the surface and may form larger clusters of carbon atoms. They can be desorbed if they do not come upon an active site (i.e. defects of the Cu surface). At the active sites graphene nuclei are formed that catch following carbon species. Gradually these domains grow until they touch and form a continuous graphene sheet of crystallographically mismatched domains [35].

Regulation of the process parameters is crucial in CVD graphene growth as many reactions happen simultaneously and are affected differently by changes. Only with tight control can the growth factors be held in balance. The higher the temperature the more effective the thermal decomposition of hydrocarbons and as more carbon is available the formation of nuclei is increased. This is counteracted by the fact that higher temperatures also make desorption of carbon from the surface more likely. Hydrogen plays another key role in graphene growth. On the one hand it aids in the decomposition of hydrocarbon on the other hand it etches already formed carbon structures from the surface [33]. According to the growth conditions graphene flakes of diverse shapes can be grown, i.e. hexagons, squares, snowflakes, etc. The terminal edges can have either zigzag or armchair configuration. These edges are etched at different rates by hydrogen, depending upon the H_2 partial pressure and the temperature [35].

Electrochemical polishing and high-pressure annealing was used to clean and smoothen the Cu growth substrate and was found to increase the graphene domain size, likely by the diminution of active sites at the surface [35]. Not only gaseous carbon sources can be used to grow graphene. Thermal decomposition of solid carbon sources such as amorphous carbon, polymers, as well as cookies, chocolate or grass have been successfully used to grow graphene [1].

Although CVD graphene is generally of high quality it does show lattice defects, grain boundaries and can even include areas of multilayer growth [24]. The difference in the thermal expansion coefficients of copper and graphene results in wrinkles in the later upon cooling [12]. Most applications necessitate the transfer from the copper growth substrate to an insulating material [24]. Therefore the graphene film usually needs to be protected with a polymer support and the metal is etched to release the graphene. After the transfer to the desired substrate the polymer film is dissolved [36]. Large areas of graphene can also be transferred to flexible substrates using other techniques such as roll-to-roll transfer or hot press lamination [12].

The disadvantages of CVD graphene growth are its energy intensity and the consumption of the metal catalyst [24]. However, the high quality, the possibility to grow large areas and its up-scalability make this technique very interesting for industry [12].

2.3. Graphene design

Many applications need precise graphene geometries. Different methods are currently used to bring graphene into the required shape. Either the graphene is produced and the desired geometry is formed afterwards or the graphene is already grown in the wanted pattern.

2.3.1. Post growth patterning

There are a number of processes to shape graphene after its synthesis. Some of them start from bigger graphene sheets or flakes and cut them into small features, others aim towards the assembly of small flakes to form bigger structures.

2.3.1.1. *Lithography*

Photolithography is a standard technique in microelectronic industry. Photo resist patterns are used to protect graphene designs. Uncovered areas are exposed to oxidative reactive ion etching. Subsequently the photoresist is dissolved. All of these steps pose the risk of damaging graphene, i.e. delamination, introduction of defects or contamination with polymer residues [14].

2.3.1.2. *Metal etch masks*

It has been shown that metal masks can be sputtered onto the graphene through metal hard masks. After the excess graphene is etched by oxygen plasma, the metal is removed by non-oxidising acids [14].

2.3.1.3. *Focused ion beam*

Focused ion beams can be used to cut graphene, especially if very small features are needed [18].

2.3.1.4. *Solution processing*

In solution based graphene processing dispersions of graphene flakes are produced, usually by liquid phase exfoliation (see also Section 2.2.1.2). These dispersions can be printed, spray coated, dip casted, rod coated, etc. to form graphene shapes on various materials [12].

2.3.2. Pre growth patterning

The opposite route is to grow graphene only where it is needed. This can either be accomplished by shaping the growth substrate itself or by blocking areas on the growth substrate.

2.3.2.1. *Growth substrate template*

The method of shaping the growth substrate, e.g. copper, is limited by the fact that the growth is usually carried out at temperatures that allow the growth substrate to restructure. The reshaping during this restructuring prevents the growth of precise geometries [17].

2.3.2.2. *Masking the growth substrate*

Masking the surface of the growth substrate is an elegant way to grow defined graphene patterns. It was shown that aluminium oxide put down with electron-beam evaporation [17] or ALD provides a good growth barrier. In this work chromium containing inks were successfully used to prepattern copper foils with inkjet printing.

2.4. Analysis of graphene

The most commonly used analytical techniques in graphene research are optical-, atomic force- (AFM) and electron microscopy (SEM and TEM) and Raman spectroscopy. Angle-resolved photoemission spectroscopy (ARPES) can be used to observe the electronic structure in graphene [18]. As graphene is widely considered for electrical applications its electrical properties are especially interesting and measuring them can, to some extent, be used as quality control.

2.4.1. Optical microscopy

Some substrates are able to maximise the optical contrast of the monoatomic carbon layer and therefore enable its visualisation with optical microscopy. An example of a suitable substrate is a silicon wafer with a 300 nm SiO₂ layer. On these wafers the interference of visible light can be observed due to the Fabry-Pérot cavity of their silica layer. If a thin graphene flake is added to this optical path a slight shift in the interference colour is observed. For certain SiO₂ thicknesses, such as 300 nm, even single graphene layers give sufficient contrast to be distinguished by the human eye [25].

2.4.2. Raman spectroscopy

One of the most important methods in graphene analysis is Raman spectroscopy. It is a non-destructive method that is ideally suited to probe sp²-hybridised carbon allotropes. It cannot only be used to determine the number of layers and structural damage of graphene. It also provides information about the type of edges, crystallite size, strain, doping, functional groups and the orientation of layers. Raman spectroscopy is sensitive to many factors and is therefore a very powerful tool but the interpretation of these spectra is not always trivial. Parameters such as the laser wavelength used (see also Figure 8 and Figure 9), the focus, the temperature, magnetic fields and the isotope distribution can also have an effect on the measured spectrum [37]. In Raman spectroscopy the wavelength shift of inelastically scattered monochromatic light is measured. The vibrational modes of samples are probed. The majority of the scattering processes taking place are elastic, where the incident light is equal in frequency to the scattered and the system returns to its initial ground state – so called Rayleigh scattering. There is the possibility that the material absorbs a fraction of the photon's energy in this process and the final stationary state is of different energy than the initial state. This inelastic scattering is called Stokes scattering. The absorbed energy has to correspond with a phonon and the resulting states are usually vibrational modes. If the energy of the incident wave is between the UV and the IR spectral

range the interaction is not directly between photon and phonon. The excited intermediate state is that of an excited electron. Therefore Raman spectroscopy is also able to give some information about the behaviour of electrons [37]. By rastering the surface with a small laser spot Raman scan maps can be created. Especially for large polycrystalline sheets, as produced via CVD, these maps can provide valuable information.

The two most intense peaks in the Raman spectrum of monolayer graphene are the so called G peak at $\sim 1580\text{ cm}^{-1}$ and the 2D peak at $\sim 2700\text{ cm}^{-1}$ (sometimes the 2D peak is also referred to as G'). Defects in the crystalline structure of graphene give rise to another peak at $\sim 1350\text{ cm}^{-1}$, the D peak. In the Raman spectrum of perfectly crystalline, undoped, single-layer graphene the intensity ratio between the 2D and the G peak is approximately 4 and the D peak only appears at the sample edges [29]. In Figure 5 Raman spectra of graphene and graphite are depicted.

The G peak is the result of a one-phonon process that is correlated to the in-plane vibration depicted in Figure 6 (a). The D peak corresponds to the breathing mode of the carbon hexagons, seen in Figure 6 (b). A lattice defect is needed to activate this scattering mode [37].

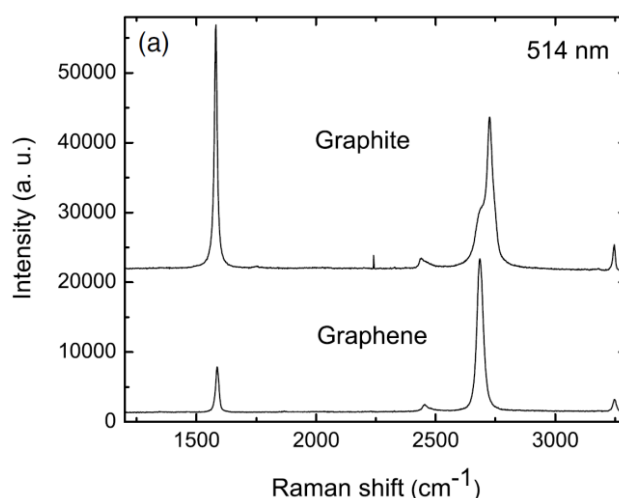


Figure 5: Raman spectra of graphite and graphene [adapted from [29]]

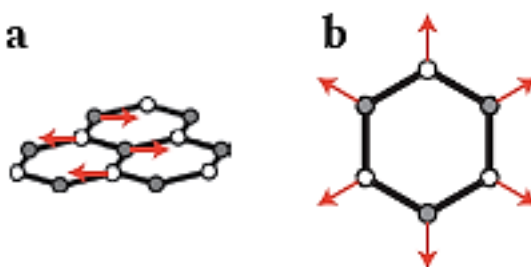


Figure 6: Vibrational modes in graphene; a) in-plane mode that corresponds to the Raman G peak; b) hexagonal breathing mode related to the Raman D peak [adapted from [37]]

The 2D peak is a D peak overtone. In this scattering process an electron hole pair is created, after the emission of two phonons of opposite wave vectors the pair is recombined and the scattered photon is emitted (see also Figure 7). The 2D peak does not need a defect for activation [37].

The spectrum is altered noticeably if more layers are added to the graphene until it merges with the spectrum of graphite. In particular, the 2D peak appearance changes with the number of layers as can be seen in Figure 8. Raman spectroscopy is able to differentiate between monolayer, bilayer and few layer graphene [29].

In bilayer graphene the 2D peak is split into four components because the two carbon layers interact in a way that splits the π and π^* electronic bands into four (see also Figure 9) [29]. It was reported that any random orientation of stacked graphene sheets can be fabricated and different orientations lead to different electronic structures. Extended study of the 2D peak in multilayer samples can give information about the relative orientation of the layers [37].

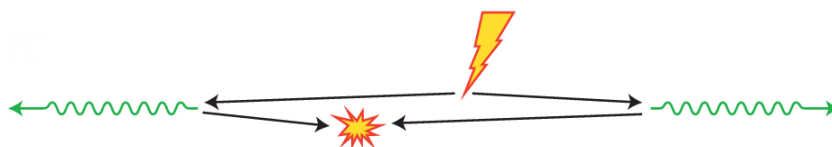


Figure 7: Two phonon scattering process resulting in the Raman 2D peak; the incident light (lightning) excites an electron into the π^* band, leaving a hole in the π band; both move and at some point emit phonons (green waves); if electron and hole meet at one point of space after having travelled the same period of time they can recombine if they have opposite momenta; in the recombination a photon of different frequency from the incident frequency is emitted [adapted from [37]]

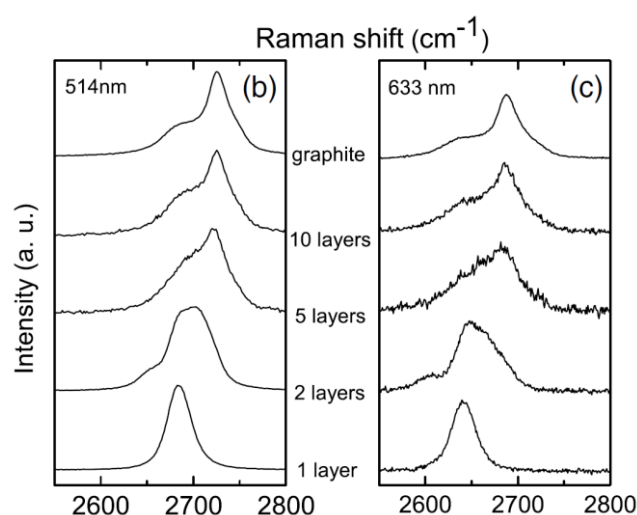


Figure 8: 2D peak in the Raman spectrum of graphene changing with number of layers; a slight difference in the spectra taken with two different lasers can be observed (514 nm laser on the left and a 633 nm on the right) [adapted from [29]]

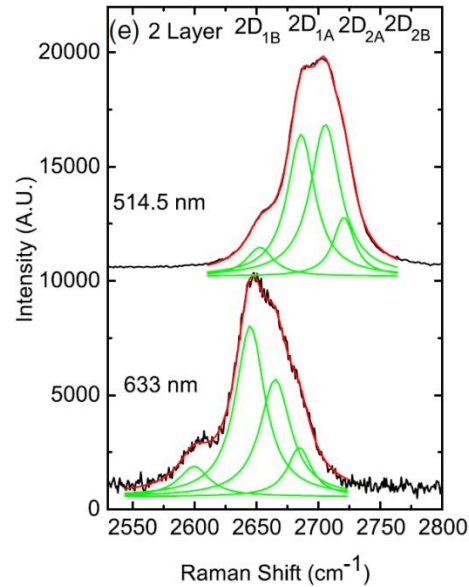


Figure 9: 2D peak of bilayer graphene (reproduced from [38])

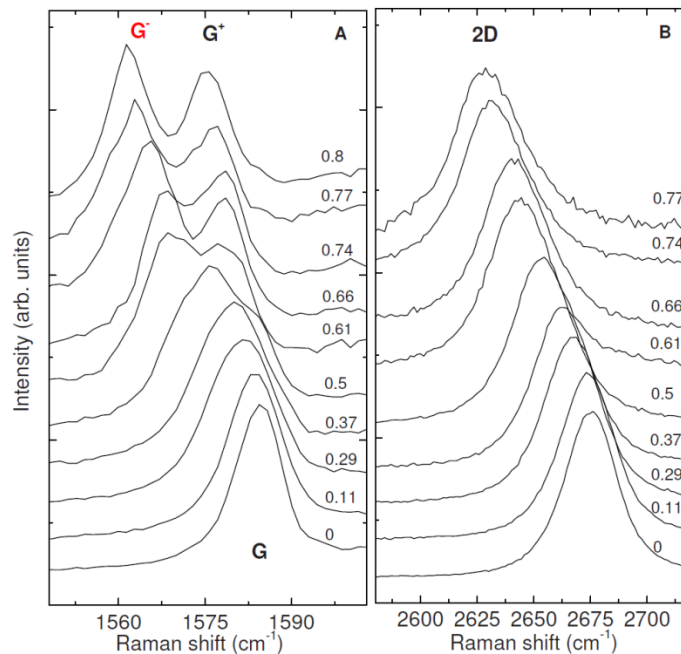


Figure 10: Strain dependence of graphene's Raman spectrum, the spectra are measured between 0% and 0,8% strain; A) G peak position is redshifted and split into two subbands G^+ and G^- ; B) 2D peak is redshifted [reproduced from [39]]

In unstrained graphene the vibrations resulting in the G peak are symmetric. If uniaxial strain is applied this symmetry is broken, resulting in a redshift and strain dependent splitting of the G peak. The two peaks that can be seen in Figure 10 are called G^+ and G^- . The 2D peak does not split with applied strain but is redshifted. Even strains smaller than 1 % have a remarkable effect [39].

It was reported that doping shifts the peak positions slightly and also has a major effect on the 2D to G peak intensity [40]. The edge of a graphene film can have either a zig-zag or

an armchair configuration or, of course, mixed types. The fact that the Raman spectrum of these configurations is dependent on the polarisation of the incident light can be used to determine the edge type [37].

2.4.3. AFM

Atomic force microscopy is rather slow and the size of the probed samples is usually limited making it unsuitable as the primary identification tool for graphene samples. Despite these drawbacks it is the best method to measure the topology of graphene. Typically soft imaging modes (non-contact mode) are used [18]. AFM tools can also be used to probe the elastic properties and the intrinsic strength of graphene, where suspended graphene is punctuated with an AFM tip [28].

2.4.4. SEM

As optical microscopy is limited by the wavelength of visible light, electron microscopy is the method of choice if images of higher resolution are required. Taking images of a one-atom thick material is not trivial and the right instrumentation has to be used to make graphene films visible. Electron beams with low acceleration voltages do not penetrate the sample as deeply as those with more energy. Therefore the information obtained with a low energy electron beam contains more surface related data. It was reported that acceleration voltages between 0.5 kV and 2 kV are especially suited because the contrast between substrate and graphene and between monolayer and multilayer graphene is at its maximum [41]. In-lens (in-column) secondary electron detectors are superior to conventional SE or BSE detectors at imaging graphene [42]. In-lens detectors are located in the electron column of field-emission-SEMs and are known to collect low energy secondary electrons [43].

2.4.5. TEM

Transmission electron microscopy is not only used as a reference method to distinguish between single and multilayer graphene. With its atomic resolution it is possible to visualise individual defect sites (or the absence of them) [18]. In Figure 11 a TEM image of graphene is displayed.

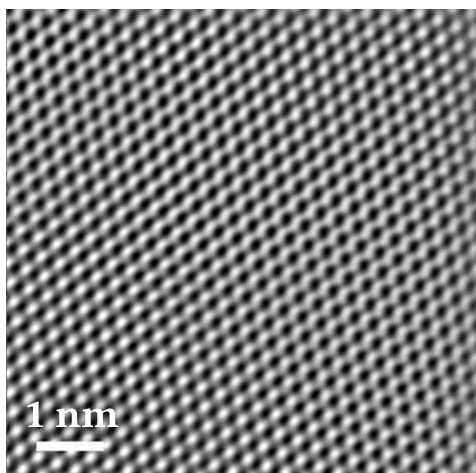


Figure 11: TEM image of CVD grown graphene fabricated by the ASIN research group [adapted from [44]]

2.4.6. Electrical Measurements

Graphene's electrical properties are a huge research field these days and plenty of data is available and can be used as reference material. Parameters like conductivity, sheet resistance, charge carrier mobility and charge neutrality point are closely related to the quality of the graphene sample. To carry out measurements graphene is often incorporated into devices such as field effect transistors (FETs).

As an example, the charge neutrality point (Dirac point) of graphene can be shifted by chemical doping. It was shown that vacuum annealing can be used to minimise doping residues and therefore move the Dirac point towards 0 V (gate voltage) where it is expected to be in graphene [45].

2.5. Inkjet printing

Inkjet printing is based on the ejection of droplet sequences. The first inkjet printers were produced in the middle of the twentieth century. Some major inventions have made this technique one of the most attractive deposition methods today. In the nineteen eighties printing of conductive materials started to be investigated and from then onwards it has been integrated in the production of numerous applications [4].

Most commonly used in manufacturing are drop on demand (DOD) printers where droplets are only ejected when they are needed. Five steps characterise the DOD inkjet printing process: droplet ejection, droplet flight, droplet impact, droplet spreading and droplet solidification. The droplet volume, the accuracy of the droplet placement, the droplet spacing and the interactions between substrate and ink are responsible for the minimum feature size. The resolution of inkjet printing cannot compete with conventional silicon micro-fabrication methods (e.g. lithography). The smallest reported line widths in inkjet printing are about 20 μm , whereas features in the order of tens of nanometres are being fabricated with micro-fabrication techniques [4]. The strengths of inkjet printing lie elsewhere. It is a technique that uses minimum amounts of materials. Something that is especially useful when it comes to handling expensive materials. It is very flexible – it usually takes just a few mouse clicks to set up completely different printing patterns. Inkjet printing is compatible with a wide variety of substrates as high temperatures or harsh chemicals can be avoided. On top of that it is easily incorporated in roll-to-roll processes.

2.5.1. Inkjet printer

The majority of inkjet printers use DOD piezo-electric printheads. These printheads can have various designs but their basic principle is the same. From a reservoir the ink can flow into a chamber that has at least one wall that can be flexed with a piezo-actuator (see also Figure 12) [46]. To eject a droplet an electric driving waveform has to be generated that matches the fluid dynamics of the ink. This waveform moves the piezo-crystal and thus creates a transient pressure wave in the capillary of the nozzle. The pressure wave has to provide enough energy to push the fluid out of the nozzle, break the surface tension and accelerate the droplet to a velocity of between 1-30 ms^{-1} [4].

The success and stability of the droplet ejection depends on the waveform design, the fluid properties and the nozzle geometry. If these parameters do not fulfil the requirements or are not perfectly matched the printing result will not be satisfactory. Ideally the process is optimised towards one spherical drop per electrical impulse. Major difficulties can lead to

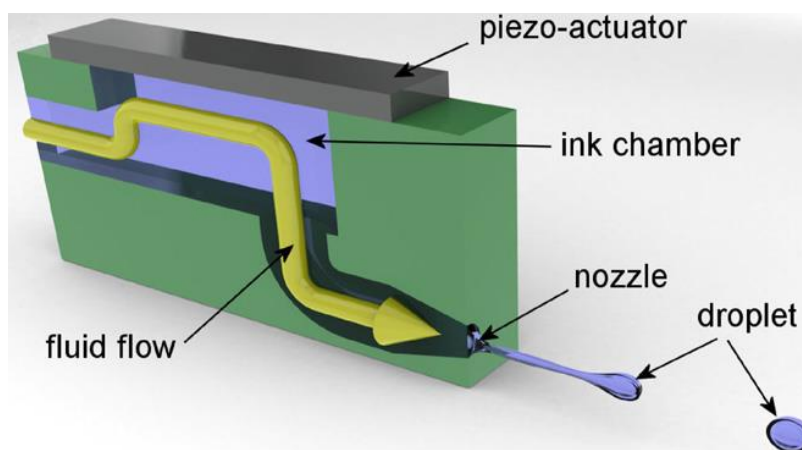


Figure 12: Design of a DOD piezoelectric inkjet printhead [image adapted from [47]]

the formation of satellite droplets that impair the quality of the print, or the droplets don't fly straight towards the substrate or the droplets are not even formed and do not leave the nozzle. To avoid these problems inks have to be designed and chosen carefully [4].

The printed patterns are fabricated by precise computer-controlled movements of the printhead stage and/or the substrate platen, while the droplets are fired [46].

2.5.2. Inks for inkjet printing

The performance of an ink in inkjet printing is dictated by its fluid properties, i.e. surface tension, viscosity, density, and particle size and loading. The surface tension has to be low enough to allow a drop to be formed upon ejection, but at the same time has to be high enough to prevent uncontrolled dripping from the nozzle. The surface tension also has to be in accord with the substrate surface to get optimum wettability. In order to refill the reservoir in about 100 ms and to make the expulsion of a drop by a pressure pulse possible the viscosity has to be in a given range [4]. To improve the jettability the viscosity as well as surface tension can be manipulated to a certain extent by regulating the ink and nozzle temperature.

Conductive inks usually contain metal nanoparticles, conductive polymers, organometallics or carbon allotropes, e.g. carbon nanotubes, graphene flakes or graphene oxide. Most commonly used in metal nanoparticle loaded inks are silver and gold. Inks with copper [48] and nickel are also produced but tend to have oxidising issues and require special treatment. To avoid clogging the particle size should not be greater than a 100th of the nozzle diameter as a general rule. Further, the more homogeneous the dispersion and the less distribution in particle size, the better [4].

2.5.3. Sintering of Ag nanoparticle ink

Printing nanoparticle dispersions produces loose networks of metal particles. A curing step is necessary to increase the conductivity and stability of these features. Any organic layer between the particles has to be removed and the formation of sintering necks should take place. Ideally a dense metallic crystal structure is formed. Often the sintering temperature is restricted by the substrate. Polymeric materials or papers cannot withstand harsh sintering conditions. As grain coarsening starts, as a rule of thumb, at a temperature that is half the melting point, extensive grain coarsening of silver is not expected at low temperatures. Very small particle sizes (nanoscale) have a large surface-to-volume ratio. These systems strive towards surface energy reduction via Ostwald ripening [3]. Therefore sintering takes place at significantly reduced temperatures. This makes the formation of semisolid metal films at temperatures below 300 °C possible. The conductance behaviour of such a particle network is known as percolation [49].

It cannot be assumed that extended sintering times result in lower resistivity. On the contrary, it was reported that the resistivity of silver nanoparticles sintered for 24 h was higher than the resistivity of lines sintered for 1 h (at 250 °C). It is reasoned that this behaviour is the result of oxidation during curing in air [49].

II. Experimental

3. Materials and methods

CVD graphene was grown on copper substrates. To achieve well defined graphene structures the substrate foils were prepatterned with inkjet printing. The produced graphene features were subsequently assembled into GFETs and their electronic properties were analysed.

3.1. Production of CVD grown graphene

A standard CVD graphene growth process involved the growth substrate preparation, the graphene growth itself, a quick check with the “hotplate test” and the transfer of graphene from the growth substrate to a wafer. All graphene samples presented in this work were grown with the same growth conditions.

3.1.1. Growth substrate preparation

18 μm thick electrodeposited *Gould* copper foils were used as the substrate for CVD graphene growth.

3.1.1.1. Polishing of Cu-foil

To increase the flatness of the copper foil and thus improve the quality of the grown graphene an optional electropolishing step of the copper foil substrate was carried out for all growth experiments if not stated otherwise. Only graphene grown on polished copper foils was turned into electrical devices.

The foil was clamped into a homemade frame and submerged in aqueous 75 % H_3PO_4 . The foil worked as the anode in this electrochemical system. To polish the copper ~ 2.3 V were applied for 15 min while the acid was kept in motion with a magnetic stirrer. Subsequently the foil was rinsed in water and isopropanol and blow dyed.

The polishing of the foils used in this work was carried out by *Riley Gatensby*. The quality of the polishing step was monitored using AFM. AFM data presented here was acquired by *Sinéad Winters* with an *Asylum MFP-3D* AFM in tapping mode.

3.1.1.2. Cleaning the copper foil

To clean the copper foil (polished or unpolished) directly before the growth a 5 min immersion in concentrated acetic acid, followed by a 5 min bath in 10 % HCl, a dip in millipore water (produced in a *Barnstead Nanopure* system) and an acetone and IPA rinse was carried out. Afterwards it was blow-dried with a nitrogen gun using dry, filtered

nitrogen. To minimise impurities introduced by the solvents, acetone and isopropanol were purchased from *Sigma-Aldrich* in HPLC grade quality.

3.1.2. CVD graphene growth

Graphene was produced by high temperature CVD. The growth took place in a *Carbolite* furnace (see Figure 13). The reaction chamber in this furnace was a 150 cm long quartz tube with a diameter of 3.8 cm that was heated by resistive coils. The gas inlet was regulated by digitally controlled mass flow controllers. The pressure in the tube was kept at desired level with an *Edwards* rotary vane vacuum pump that was attached to the outlet of the tube. Through a sample loading port a quartz shovel carrying the copper foil was introduced to the furnace.



Figure 13: Carbolite furnace for high temperature CVD growth

The growth of graphene was accomplished by a four step process:

Ramp – The furnace was heated at 850 °C/h with 50 sccm H₂ to 1035 °C.

Annealing – The copper foil was annealed for 1 h at 1035 °C under 50 sccm H₂. The pressure in the tube was kept at 0.53 mbar.

Growth – For 20 min the inflowing gases were changed to 10 sccm CH₄ and 2.5 sccm H₂ at 1035 °C. The pressure in the reaction chamber was 0.23 mbar.

Cooling – The gas flow was changed to 0.5 sccm CH₄ and 2.5 sccm H₂ and the furnace was pushed along its rails so the quartz shovel holding the sample was no longer in the hottest zone of the furnace.

The hydrogen used was produced by a *Schmidlin DBS PG-H₂ 250* hydrogen generator. The Methane was purchased from *BOC*.

3.1.3. Graphene growth control - “hotplate test”

The graphene is firmly attached to the copper growth substrate and is able to prevent the oxidation of copper in air. To perform a quick check to see if the graphene growth was successful a piece of copper foil was placed on a hotplate at about 200 °C for 5 min. Copper areas that remained uncovered after the CVD growth oxidised and were visible with an optical microscope (see Figure 14). Only samples that showed no signs of oxidation were used in the following steps.

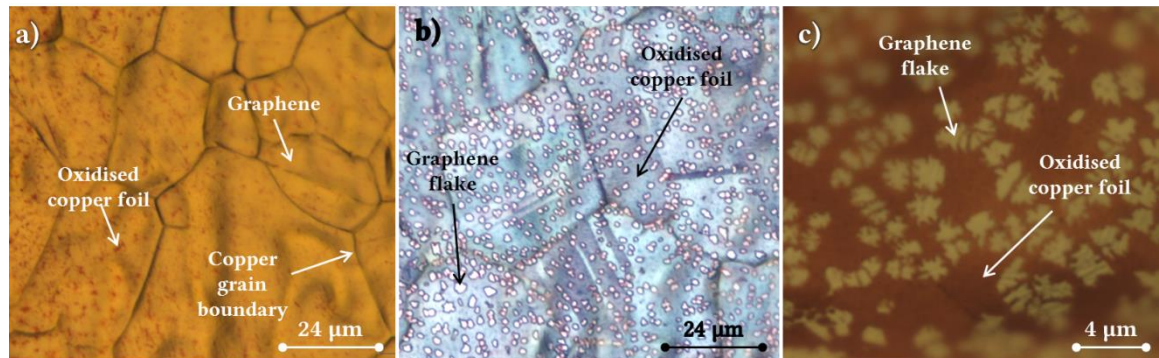


Figure 14: Copper foils with incomplete graphene growth after the “hotplate test”; a) almost complete graphene coverage; b+c) only small graphene flakes

3.1.4. Graphene transfer from copper foil to wafer

After the growth on copper foils the graphene had to be transferred to other substrates for further use (see also Figure 15). All transfer steps had to be carried out with as little handling and bending as possible.

3.1.4.1. Adding a PMMA transfer handling layer to graphene

First the copper foil/graphene was mildly sonicated in HPLC grade acetone for 2 min. Afterwards it was rinsed with IPA and blow-dried with a nitrogen gun. A solution of 2 % 950K A2 PMMA (purchased from *MicroChem*) in anisole was applied on top of the graphene with a spin coater (3000 rpm for 60 sec followed by 1000 rpm for 60 sec). Then the foils were heated for 5 min on a 150 °C hotplate and cut into sample size.

3.1.4.2. Removal of copper-foil

The copper foil was removed by etching it in a 0.2 M aqueous ammonium persulfate solution (APS, purchased from *Sigma Aldrich*). The samples were placed floating in the etchant with the copper foil facing down. Graphene growth can also take place on the backside of the copper growth substrate. The liquid graphene interaction can be used to lift this unwanted backside graphene layer off. Therefore the samples were floated for 4-5 min in the etchant and afterwards rinsed in a millipore water bath. In this bath the samples were submerged and lifted out of water several times so the surface tension was able to pull loose

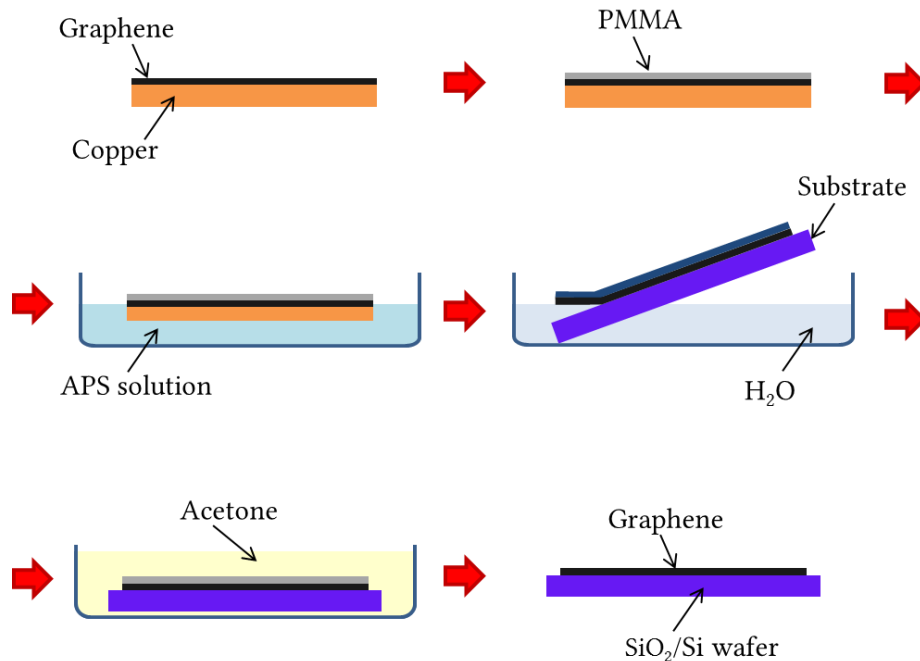


Figure 15: Graphene transfer process; graphene is protected by a PMMA layer and the underlying copper foil is etched away with an ammonium persulfate solution; the floating graphene/PMMA film is lifted from the etching bath with an arbitrary substrate (in this work a SiO₂/Si wafer), the protective PMMA layer is dissolved in acetone

the backside graphene. After a further 1-2 min of etching in the APS solution, the dipping procedure was repeated. To fully remove the copper foil the samples were placed in a fresh APS solution for at least 40 min.

3.1.4.3. Transferring graphene to a wafer

To fabricate devices graphene had to be transferred to a wafer with an insulating top-layer. As substrates two different Si wafer types were utilised: As standard wafers polished, p-doped (Boron) prime grade Si wafers with a 300 nm thermally grown, dry SiO₂ layer on the Si (100) surface from *QL* were used. Because they showed a high rate of electrical gate leakage through the insulating SiO₂ layer, *Si-Mat* wafers were used for the production of GFETs. These wafers were N-doped with arsenic and had a thermally grown, polished SiO₂ layer on the Si (100) surface. The backside of these wafers was covered in gold that acted as the back gate in the GFETs. These wafers will further be referred to as “device wafers”. For the graphene transfer the wafers were cut into pieces of approximately 1.5 cm to 1.5 cm. These pieces were cleaned by a 5 min acetone sonication followed by an IPA rinse and blow-drying.

To rinse the graphene, the samples were fished out of the etchant with a glass slide and floated on millipore water. Then the samples were transferred onto a clean substrate using the same fishing technique. The film on SiO₂ was dried in a desiccator for at least 2 hours.

To improve the adhesion of the graphene layer on the SiO₂ the sample was heated for 5 min on a 200 °C hotplate.

3.1.4.4. *PMMA removal*

To remove the PMMA layer the samples were soaked in acetone for at least 20 min at room temperature, followed by an IPA rinse and blow drying.

3.2. Inkjet printed graphene device fabrication

An inkjet printer was used to define the geometry of graphene features on the growth substrate (copper foil) prior to CVD growth. After the transfer of graphene to SiO₂/Si wafers the graphene was electrically contacted with silver nanoparticle ink using the same inkjet printer to put down the electrodes. With the fabrication route depicted in Figure 16 graphene field effect transistors (GFETs) were successfully produced.

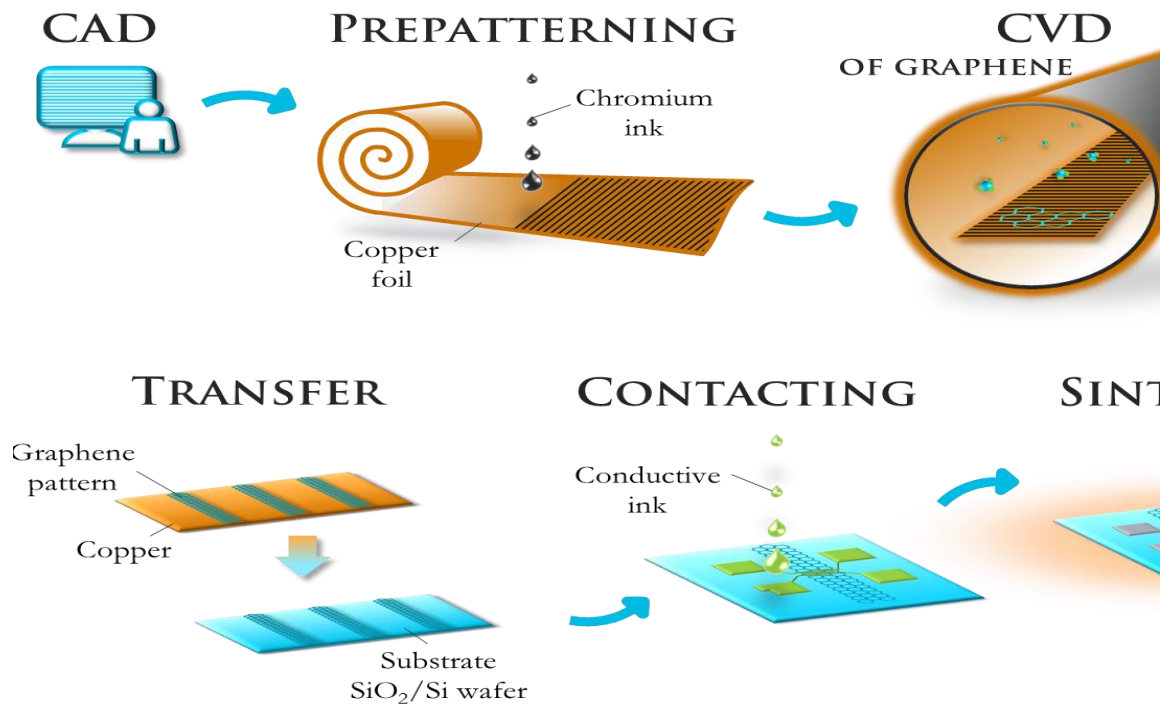


Figure 16: Flow chart of the fabrication of GFETs - the inverse pattern is designed on a computer, the pattern is printed on copper foil with an inkjet printer, graphene is grown via CVD on the patterned foil, the graphene features are transferred to an arbitrary substrate, contact leads are inkjet printed onto the graphene with silver nanoparticle ink, the ink is sintered at 180 °C to improve its conductivity

All printing was carried out using a drop on demand piezoelectric *Fujifilm Dimatix DMP 2831 materials* inkjet printer with *DMC-11610 polypropylene* cartridges and 10 pl printheads (see Figure 17 and Figure 18). The cartridges were designed to hold 1.5 ml ink. The printheads held 16 individually addressable nozzles with 21.5 μm diameters and a spacing of 254 μm. The driving voltage of the piezo-system was modifiable in duration, amplitude and slew rate to optimally adjust the printer to the fluid dynamics of the desired ink.

3.2.1. Prepatterned graphene growth

To limit the size of the graphene to the desired geometry *Staedtler Lumocolor® permanent marker 385 + 388 (black)* ink was used to mask the copper foils in areas where graphene growth was not desired prior to the graphene growth in the high temperature

CVD process described above. The ink was printed onto electropolished and unpolished *Gould* copper foils. Before the printing the foils were cleaned as reported in Section 3.1.1.2.

A waveform was developed to jet the ink. The printhead was set 1.2 mm above the printer platen. The platen was heated to 40 °C, the ink to 45 °C. Using one nozzle and a droplet spacing of 35 μm gave the most even printing results.

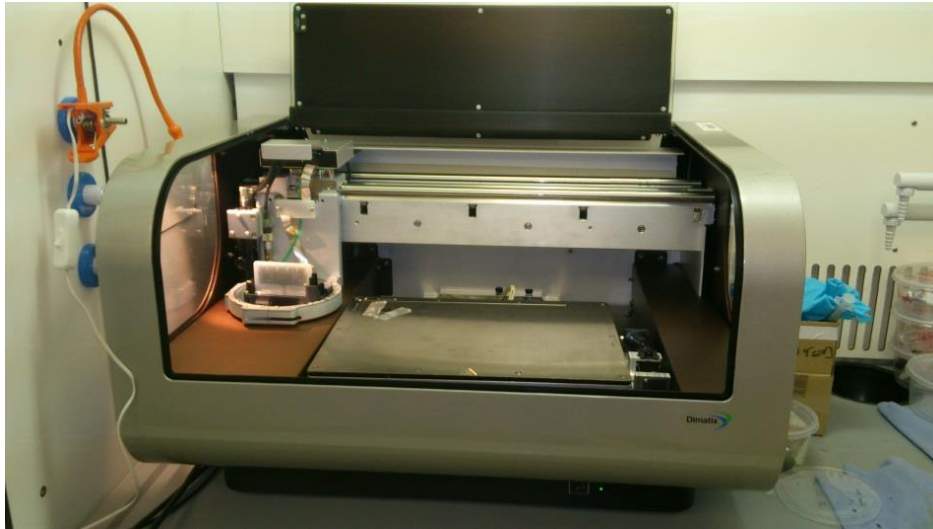


Figure 17: FUJIFILM Dimatix DMP 2831 materials inkjet printer

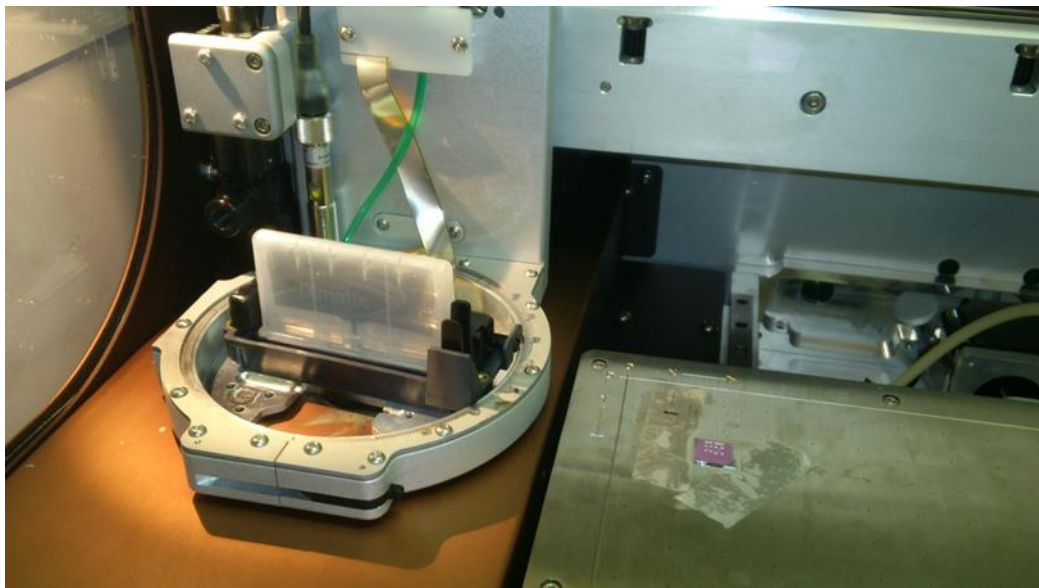


Figure 18: DMC-11610 polypropylene cartridges and 10pl print heads in a FUJIFILM Dimatix DMP 2831 materials inkjet printer

3.2.2. Inkjet printing of silver electrodes

Silver electrodes were printed onto graphene using *SunTronic*[®] Silver nanoparticle ink. This ink is an ethanol and ethandiol based dispersion that contains 20 wt.% *Cabot* silver nanoparticles. The properties of the ink (as stated by the supplier *Sigma-Aldrich*) are listed in Table 1. To ensure that the nozzles in the printhead were not clogged by oversized

Table 1: SunTronic® Silver Ink Properties [50]

Silver solid loading	20 wt.%
Density at 25°C	1,22 g/ml
Viscosity	11.6-13.0 cP
Surface Tension at 25°C	28.0-31.0 dynes/cm
Particle size	< 150 nm (DLS)
Annealing temperature	150-300 °C
Volume resistivity	5-30 $\mu\Omega$

particles or agglomerates, the ink was filtered through a *Whatman® GD/X PVDF membrane* 0.2 μm syringe filter prior to loading into the cartridge.

A waveform to jet the ink was developed. The spacing between the printhead and the platen was set at 1.2 mm or 1.55 mm, respectively. The platen and the ink were heated to 40 °C. The inbuilt magnifying camera of the inkjet printer was used to locate the desired printing area. A droplet spacing of 30 μm printed with one nozzle gave the best printing results. A nominal printing pattern for the printing of 4-point-probe contacts is depicted in Figure 19.

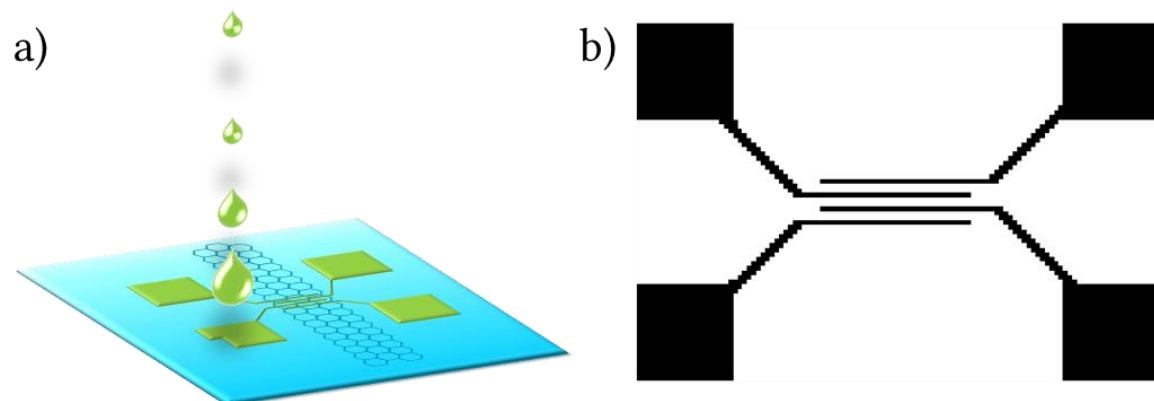


Figure 19: 4-point-probe contacts print; a) illustration of the printing geometry; b) nominal printing pattern, printed feature size was about 5 mm at 30 μm droplet spacing

3.2.3. Sintering of Ag nanoparticle ink

To increase the conductivity, the printed silver nanoparticle features had to be cured. The sintering took place in an oven at 180 °C for 10 min. Because the specifications of the ink allowed it and to keep this step as simple as possible the curing was carried out in air and not in an inert atmosphere.

Due to problems, that are described in more detail in Section 4.3.1.4, with the fabrication of graphene/silver devices the ink had to be dried slowly before being sintered. This though, did result in silver features of lowered conductivity compared to directly sintered ones. The ink was dried in an oven at 45 °C for about 12 h.

3.3. Analysis

Graphene grown via CVD, the permanent marker ink, the sintering process of the silver nanoparticle ink and the electrical properties of the produced devices was analysed.

3.3.1. Analysis of CVD grown graphene

The quality of the grown graphene was analysed using the following methods.

3.3.1.1. Raman spectroscopy

All Raman spectroscopy data presented in this work was obtained using a *Witec Alpha 300 R* with a 532 nm laser. This system was able to generate Raman spectroscopy maps. All shown graphene Raman spectroscopy graphs were normalised to the G-peak intensity.

3.3.1.2. Optical microscopy

Optical analysis of the samples were carried out using a *Reichert* microscope, with 2.5x, 5x, 10x, 20x, 50x, 100x and 150x magnification objectives. Images were taken using a *Motic* CCD camera attached to the microscope. Some of the optical pictures were acquired with the Raman spectroscopy tool described above.

3.3.1.3. SEM

To visualise graphene a *Zeiss Ultra* field emission SEM with an in-lens secondary electron detector was used at an acceleration voltage of 1-2 kV.

3.3.2. Influence of marker ink/chromium on the graphene growth

To gain more information about the nature of the ink and its interaction with the graphene growth the following analysis was carried out.

3.3.2.1. Analysis of *Staedtler Lumocolor® permanent marker 385 + 388 ink black*

Drops of ink on Si/SiO₂ wafers were baked at 1035 °C in oxidising and reducing atmospheres. Yet another drop of ink that was dried for 72 h at 80 °C in a vacuum oven and XPS spectra were measured by *Dr. Nina Berner*. SEM images and EDX scans of the ink at various stages were taken with a *Zeiss Ultra* FE-SEM. To inquire the nature of the ink residue after graphene transfer, Raman scans were carried out.

3.3.2.2. Sputtering chromium on substrate

To investigate the effect of chromium on CVD graphene growth, chromium was sputtered on electropolished copper foils prior to the growth. The argon ion beam sputtering of a chromium target took place in a *Gatan PECS* instrument. A metal hard mask ensured that only parts of the copper foil were coated in chromium. The thickness of the

deposited chromium film was regulated with the inbuilt quartz crystal microbalance of the *Gatan* and was approximately 1 nm, 2.5 nm or 5 nm. The copper foils were introduced into the *Carbolite* furnace and a standard graphene growth run was carried out. The resulting films were analysed using SEM, optical microscopy and Raman spectroscopy.

3.3.3. Analysis of *SunTronic*[®] silver ink

3.3.3.1. SEM

SEM images of dried and sintered *SunTronic*[®] silver ink were taken using a *Zeiss Ultra* FE-SEM with an acceleration voltage of 10 kV.

3.3.3.2. Sheet resistance

To control the quality of the sintering parameters the sheet resistance of the cured silver was measured. Therefore silver ink was spin-coated (10 s at 1000 r/min) onto a Si wafers with 300 nm thermally grown SiO₂. The ink was allowed to settle for 30 min before curing.

The sheet resistance of the sintered silver was measured with a *Jandel* 4-point probe and a *Keithley 2400 Source Meter*. The needle probes were arranged in a straight line and had a fixed distance of 1 mm. Using a four point probe measurement, the effects caused by the probe contact resistance, the probe resistance and the spreading resistance can be eliminated but a correction factor for finite sample geometries has to be considered. For very thin samples with probes positioned far from the edges this correction factor only has to consider the finite sample thickness and can be assumed as $\frac{\pi}{\ln 2}$. Equation 1 is the final expression used to calculate the sheet resistance [51]. Equation 2 shows the relationship between the sheet resistance and the bulk resistivity. To determine the thickness of the silver coating a scratch was made upon the surface and the resulting gap depth was measured with a *Veeco Dektak 6M Stylus Profiler*.

$$R_s = \frac{\pi}{\ln 2} \frac{V}{I} \quad \text{Equation 1}$$

$$\rho = R_s * d \quad \text{Equation 2}$$

R_s ... Sheet resistance at defined sheet thickness [Ω]

V ... Voltage [V]

I ... Current [A]

ρ ... Bulk resistivity [$\Omega \cdot \text{m}$]

d ... Thickness of sheet [m]

3.3.3.3. Resistance

The same electrode geometry as used in the GFETs (see Figure 20), but with connected instead of interdigitated wires, was printed onto SiO₂/Si wafers to measure the resistance of these features with needle probes and a *Keithley Source Meter*.

3.3.4. Characterisation of fabricated GFETs

Charge carrier mobility and the sheet resistance are values that are highly linked with the quality of the produced graphene. To determine the field effect mobility graphene field effect transistors (GFETs) were produced. The electrical measurements of the fabricated GFETs were carried out on two different needle probe test stands – one under ambient conditions and one in a vacuum annealing chamber. Both test stands were attached to a *Keithley Source Meter* that was connected with a computer. In the ambient test stand the samples were measured without a preceding temperature treatment. The devices measured in the vacuum chamber were annealed in the chamber at 500 K for 1 hour and later for 12 hours. Annealing and measurements took place at about 10⁻⁶ mbar.

3.3.4.1. 4-point-probe geometry

To eliminate the influence of the contact resistance, the method of choice for the electrical characterisation of the produced graphene was the 4-point-probe measurement of the fabricated back gated GFETs. The architecture used for these electrical measurements is depicted in Figure 20. A constant current of 10 μA, 50 μA or 100 μA was applied at the outer two electrodes while the changing voltage at the inner two electrodes during a sweep of the gate voltage was measured.

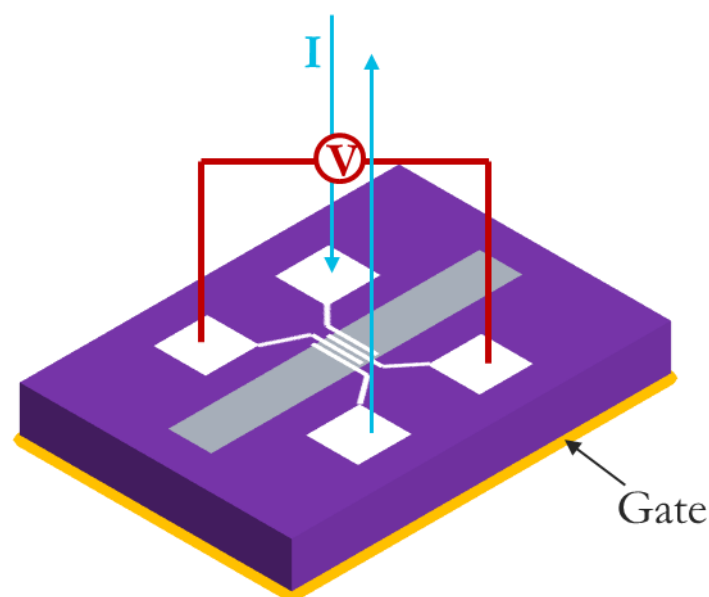


Figure 20: 4-point-probe GFET measurement architecture

With these measurements it was possible to determine the changing sheet resistances of graphene at different gate voltages and to calculate the charge carrier mobilities out of the acquired data using Equation 3 - Equation 6.

$$\frac{V_{sd}}{I_{sd}} = R \quad \text{Equation 3}$$

$$\rho = R \frac{w}{l} \quad \text{Equation 4}$$

$$g_m = \frac{d \frac{1}{\rho}}{dV_g} \quad \text{Equation 5}$$

$$\mu = \frac{-g_m}{C_i} \quad \text{Equation 6}$$

V_{sd} ... Voltage [V]

I_{sd} ... Current [A]

R ... Resistance [Ω]

ρ ... Sheet resistance [Ω/square]

w ... Channel width [μm]

l ... Channel length [μm]

g_m ... Transconductance [S]

V_g ... Gate voltage [V]

μ ... Field effect mobility [$\text{cm}^2\text{V}^{-1}\text{s}^{-1}$]

C_i ... Capacitance of 300 nm $\text{SiO}_2 = 11.6 \cdot 10^{-9} \text{ Fcm}^{-2}$

3.3.4.2. 4-point-probe geometry without a gate sweep

As mentioned in Section 3.1.4.3, some of the wafers used showed excessive gate leakage. As a result it was not possible to apply a gate voltage to these “GFETs”. Therefore only the sheet resistance at zero gate voltage was determinable. These samples were analysed by applying a sweep of either current or voltage on the outer two electrodes and the measurement of voltage or current, respectively, at the inner two electrodes (see Figure 20).

3.3.4.3. 2-point-probe geometry

To calculate the current on-off ratio of the GFETs, measurements had to be carried out in a 2-point-probe geometry. A gate voltage sweep was applied and the changing current between the probes was measured. The devices were of the same design as depicted in Figure 20 but only two neighbouring electrodes were probed.

4. Results

The CVD growth yielded continuous graphene films. A pre patterning method using inkjet printed marker ink was successfully developed and defined graphene structures were grown. This pre patterning technique was used to form graphene strips that were further used to fabricate GFETs. The electrical properties of these GFETs were measured.

4.1. Production of graphene

As described in Section 3.1.1.1 CVD graphene was grown both on electropolished and on unpolished copper foils. The graphene was grown as described in Section 3.1.

4.1.1. Graphene growth on unpolished copper foils

The result of AFM measurements, that were taken to characterise the roughness of unpolished *Gould* copper foils, showed a RMS roughness of 177.6 nm and an average roughness of 137.1 nm (see also Figure 21).

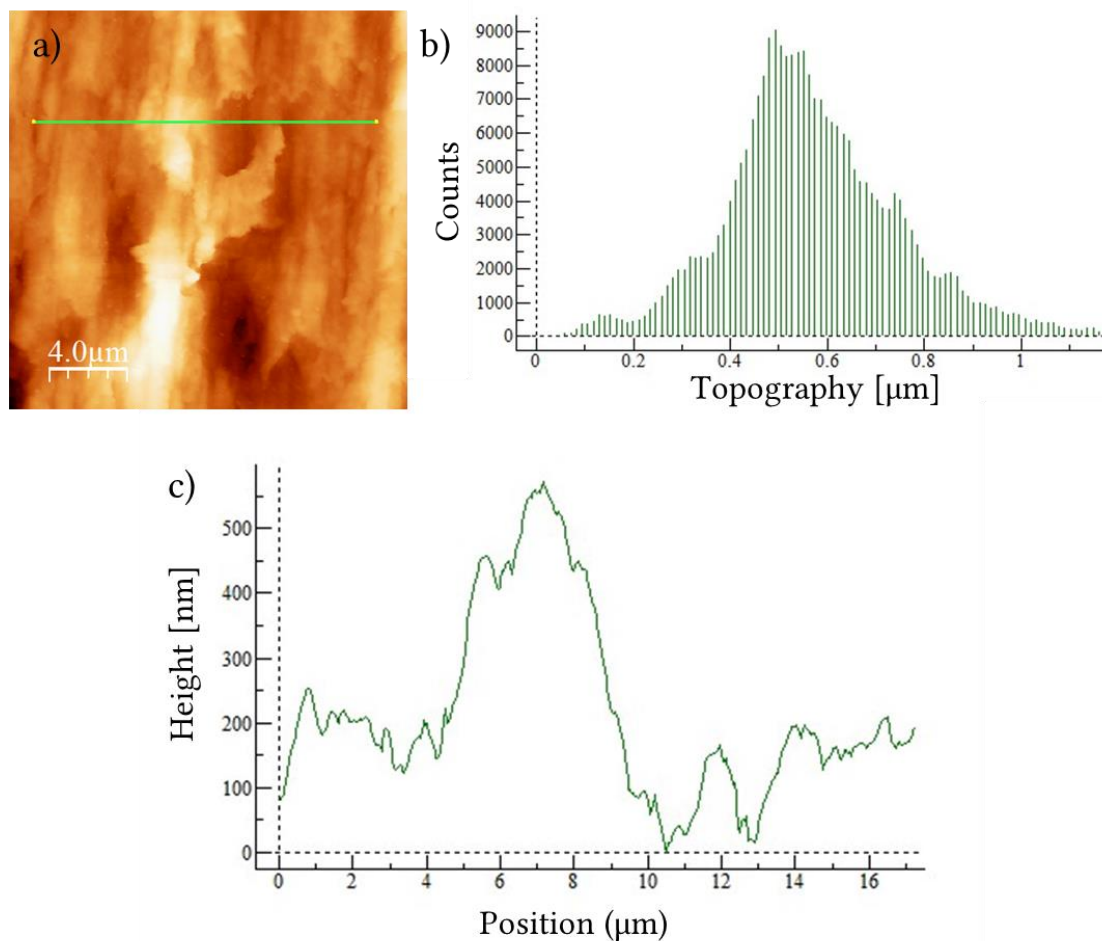


Figure 21: AFM measurement of unpolished Gould copper foil; a) topographic image; b) distribution of sample height; c) height profile along the green line in a)

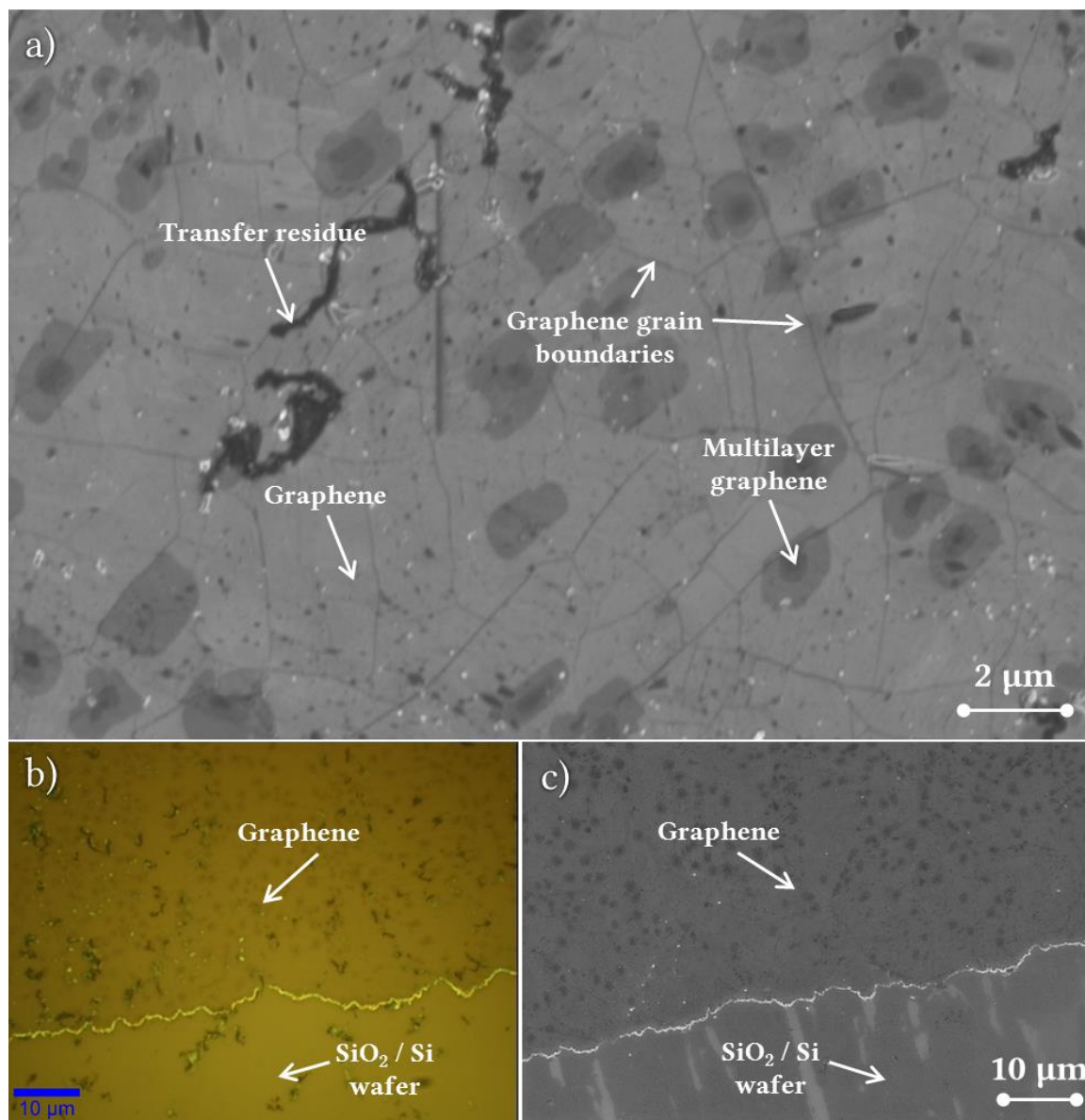


Figure 22: Graphene grown on prepatterned, unpolished Gould copper foils, transferred to a SiO₂/Si wafer substrate; a) SEM image of graphene; b) optical microscopy image of prepatterned graphene edge; c) SEM image of prepatterned graphene edge

In Figure 22 optical microscopy (b) and SEM images (a + c) of graphene grown on unpolished Gould foil are presented. Figure 22 (a) shows a continuous graphene sheet that is rich in defects, such as graphene multilayers, transfer residues and lines that might be graphene grain boundaries. Figure 22 (b + c) displays edges of graphene films created by prepatterned growth as described in Section 3.2.1.

The average spectrum of a large area of graphene, that was grown on unpolished foils and subsequently transferred to SiO₂/Si wafers, is shown in Figure 23 (a). The highest intensity of the G peak lies at 1581 cm⁻¹ and is markedly more intense than the 2D peak at 2673 cm⁻¹. The 2D signal shows a small shoulder on the left (at about 2664 cm⁻¹). A D peak is also visible at 1342 cm⁻¹. This Raman spectrum can be seen as the spectrum of monolayer

graphene with a lot of multilayer growth and is in accordance with the obtained SEM images.

In Figure 23 (b +c) scanning Raman maps of a prepatterned graphene sample are visible. The scans show the edge of a graphene pattern. The inhomogeneity in the map colour reflects the distribution of single and multi-layer areas.

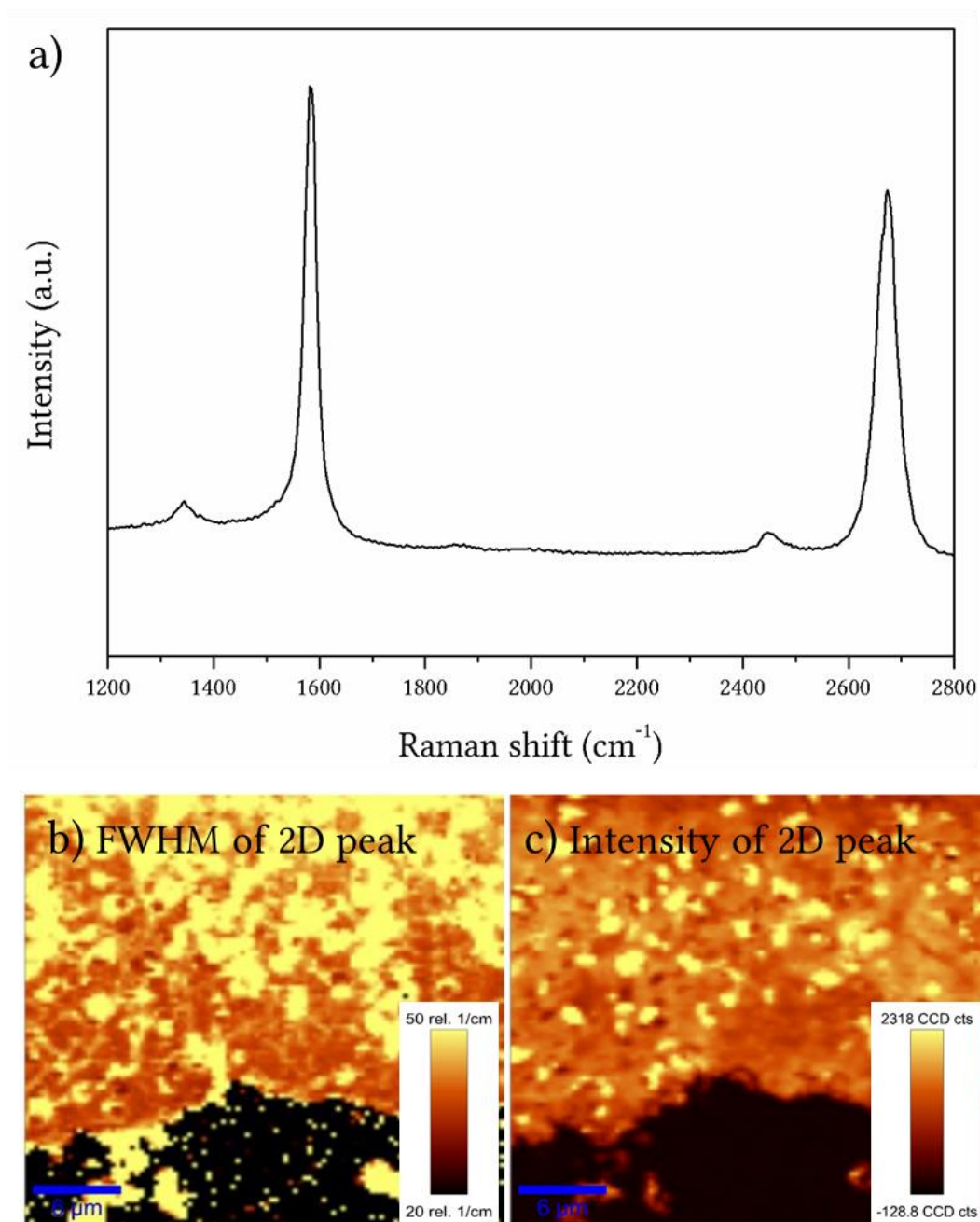


Figure 23: a) Raman spectrum and b) + c) Raman maps of graphene grown on unpolished foils

4.1.2. Graphene growth on electropolished copper foils

To measure the effect of the electropolishing step AFM scans of polished *Gould* copper foils were carried out prior to the graphene growth. Figure 24 summarises one of these scans. Typical electropolished foils showed a RMS roughness of about 30 nm and an average roughness of about 25 nm.

Figure 25 depicts SEM (a+c) and optical microscopy (b) images of graphene samples grown on electropolished copper foils and transferred to SiO₂/Si wafers. With the CVD growth conditions described in Section 3.1 continuous graphene films with small bilayer islands were produced. In Figure 25 (b+c) the edges of prepatterned graphene films are shown.

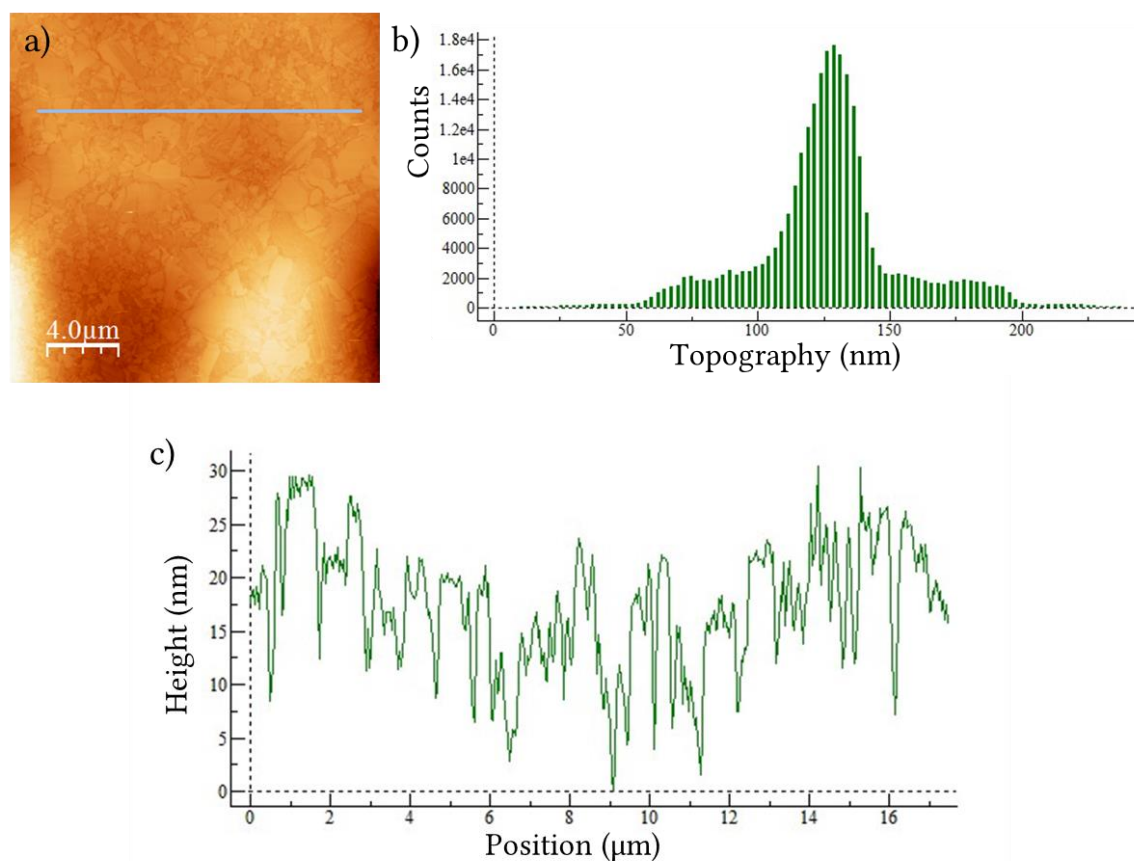


Figure 24: AFM measurement of electropolished *Gould* copper foil; a) topographic image; b) distribution of sample height; c) height profile along the blue line in a)

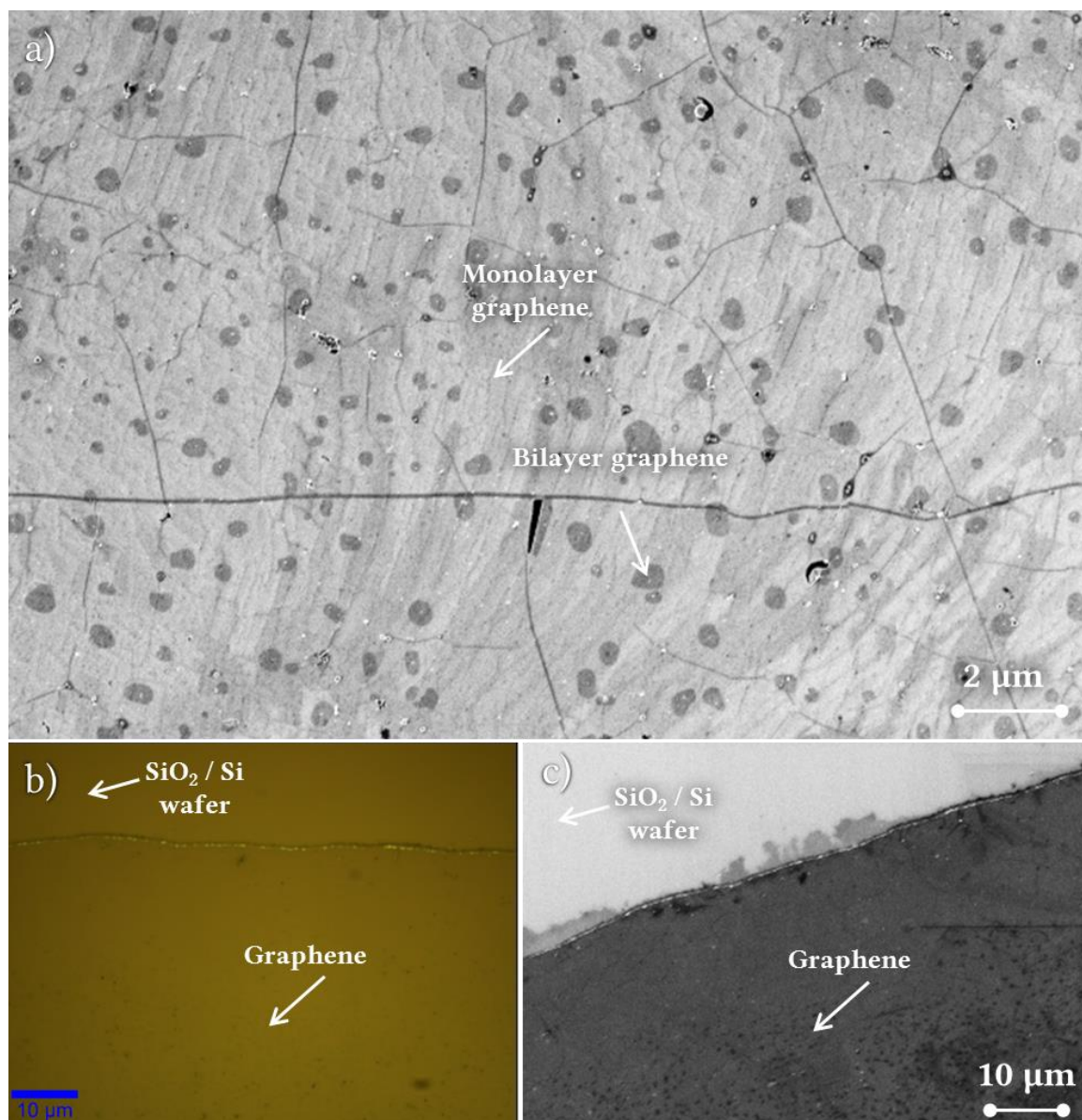


Figure 25: Prepatterned graphene grown on electropolished *Gould* copper foils, transferred to a SiO₂/Si wafer substrate; a) SEM image of graphene; b) optical microscopy image of prepatterned graphene edge; c) SEM image of prepatterned graphene edge

Raman scans of graphene films shown in Figure 25 are displayed in Figure 26. Figure 26 (b+c) also shows Raman maps of the edges of a prepatterned graphene film. The Raman spectrum indicates mostly monolayer graphene of high quality. The 2D peak (at about 2688 cm⁻¹) leans a little to the right towards higher wavenumbers, indicating a very small amount of multi-layer growth. The tiny D peak at 1356 cm⁻¹, the 2D peak FWHM and the fact that the intensity of the 2D peak is not 4 times higher than the G peak (at 1601 cm⁻¹) signals that the growth is not perfectly crystalline, but that is not to be expected in polycrystalline graphene.

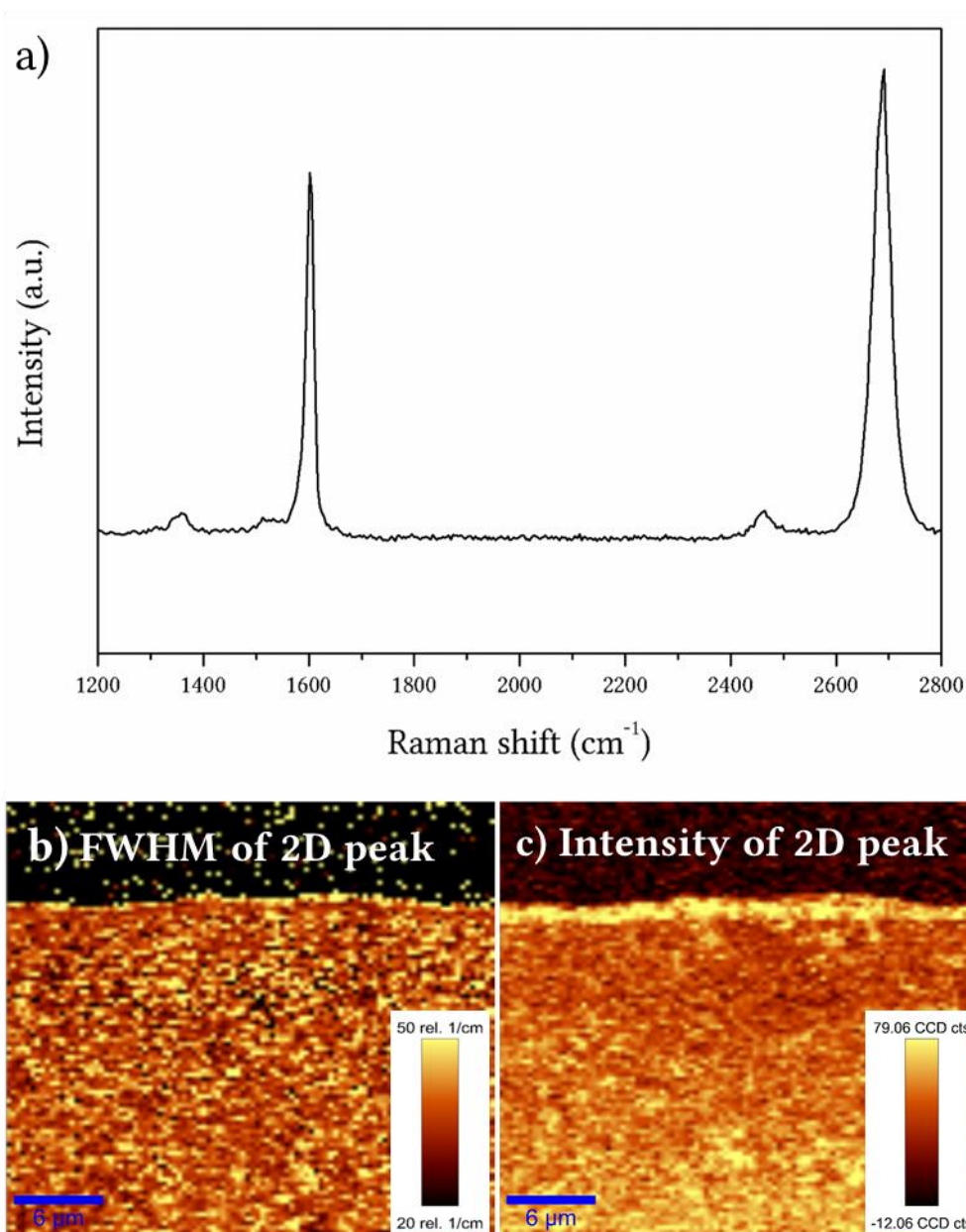


Figure 26: a) Raman spectrum and b) + c) Raman maps of graphene grown on polished foils

Figure 27 shows a spectrum of the sum of areas that were identified as multilayer growth on polished copper foils. The G peak at 1588 cm^{-1} is notably higher than the 2D peak at 2689 cm^{-1} . A tiny D peak is visible at 1352 cm^{-1} . A close look on the 2D peak reveals a peak that cannot be fitted with a single Lorentzian function (as would be expected in monolayer graphene). Figure 28 shows the 2D peak of these multilayer areas. It reflects the 2D band expected in bilayer graphene, consisting of 4 merged peaks (called $2D_{1B}$, $2D_{1A}$, $2D_{2A}$, and $2D_{2B}$) [29].

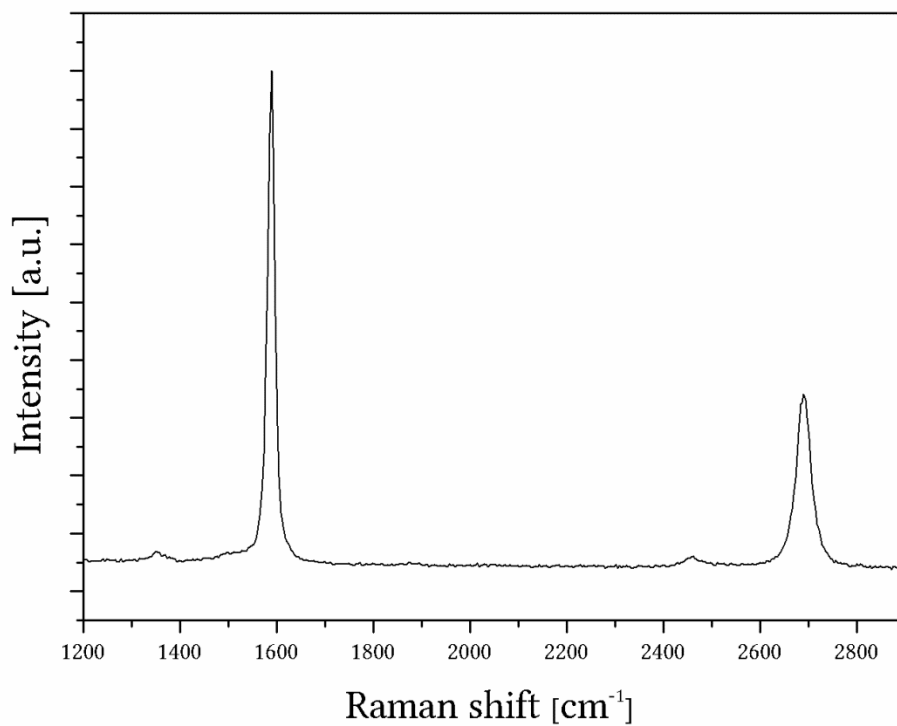


Figure 27: Raman spectrum of multilayer islands on a continuous graphene sheet grown on polished copper foil

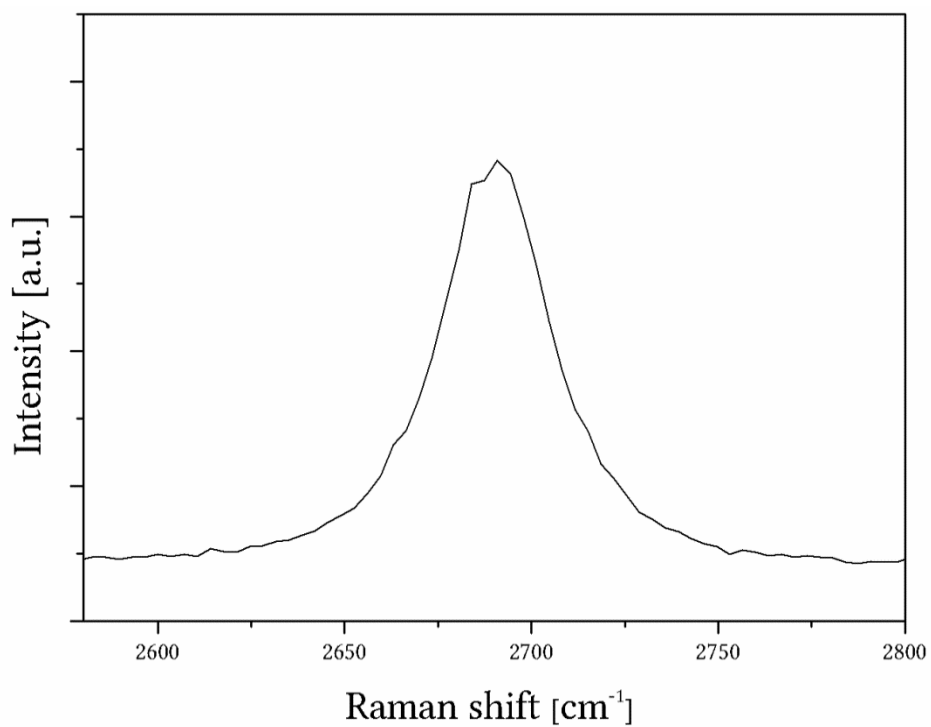


Figure 28: 2D peak in Raman spectrum of multilayer islands on a continuous graphene sheet grown on polished copper foil

4.2. Patterned graphene growth

As described in Section 3.2.1 graphene patterns were created by masking the copper growth substrate prior to the CVD growth.

4.2.1. Ink masking the growth substrate prior to graphene growth

Staedtler Lumocolor[®] permanent marker ink was printed onto copper foils to successfully block the CVD graphene growth.

This ink was designed to come on in very thin layers and wetted the copper foils very well. A skin, that protects the ink from drying quickly, was built immediately on the surface of bigger drops. Dried ink lines showed a thicker outer edge (see Figure 29). This resulted in an ink coating of varying thickness.

Figure 30 follows a sample through the prepatterning process. As shown in Figure 29 inked areas appeared black on the copper foil. During the CVD growth the inverse ink pattern vanished partially (see Figure 30 (b)). Nonetheless, graphene growth took place only in areas that were bare from the start. Bare copper foils sagged slightly during the growth procedure. Prepatterened foils behaved in a way that areas that held no ink were raised, embossing the pattern on the foil as seen in Figure 30 (b+c). This though was of no further consequence to the quality of the transferred graphene. The PMMA transfer handling layer was spun onto the copper foil covering areas that held graphene and areas that did not. After the copper was etched away completely it was perceivable that the floating PMMA layer was more stable where graphene supported it. Small as well as big graphene features were successfully fabricated and transferred to SiO₂/Si wafers with this technique (shown in Figure 30 (d)).

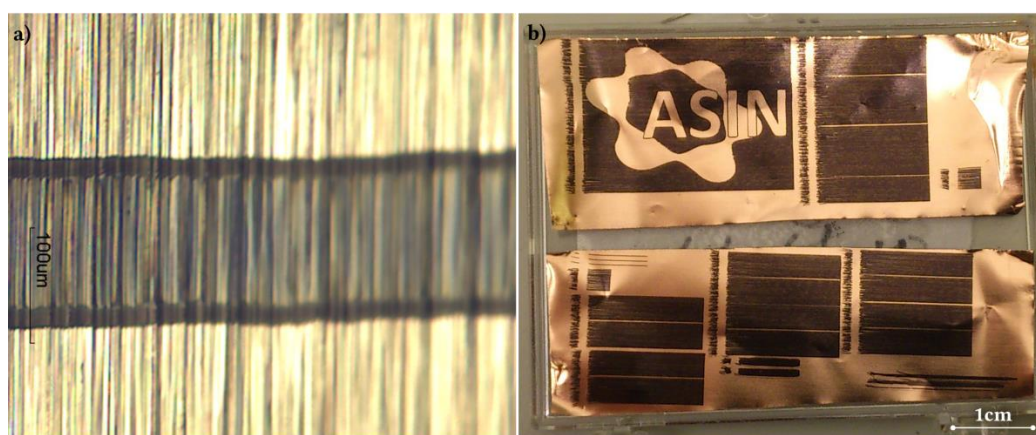


Figure 29: *Staedtler Lumocolor*[®] permanent marker ink prepatterning on copper foils; a) optical microscopy image of one ink line printed on copper with two nozzles at a time, the thicker edges of the printed line are visible; b) picture of two copper foils that were prepatterened by inkjet printing



Figure 30: Prepatterned graphene; a) an inverse pattern that is printed in marker ink on a copper foil; dark (inked) areas will not grow graphene, bare copper will; b) the same foil after CVD growth; c) after mild sonication and d) graphene pattern transferred to SiO₂/Si wafer

Unfortunately not all ink residues came off during the cleaning step and further work has to be put into this area to get flawless graphene patterns. Although the ink residue was found to be electrically conductive, its conductivity was orders of magnitude lower than that of the produced graphene and therefore did not prove a hindrance for the production of GFETs as described in this work. In Figure 30 (d) the ink residue lights up in the flash of the camera. The dark blue areas in this picture are completely covered in graphene.

4.2.2. Quality of prepatterned graphene

The quality of the graphene patterns was analysed with optical and electron microscopy and with Raman spectroscopy. Figure 22 and Figure 25 depict microscopy images of such prepatterned graphene. For predominant parts of the patterns the quality of the patterned graphene was found to be equal to that of the unpatterned one. The only difference found was that the border of the patterns showed less second layer graphene growth. This phenomenon is dealt with in more detail in Section 4.2.4. In Figure 26 (b+c) scanning Raman maps of graphene patterns are displayed. The Raman scans that are summarised in Figure 31 show not only the quality of the patterned graphene versus the unpatterned one but also the defective nature of this outermost part of the patterns. That the edge of a graphene structure behaves as defects is to be expected [38].

Others have shown that graphene can be produced by conversion of solid precursors. It is likely that in this work the carbon of the marker ink slightly increased the carbon content of the vapour phase. This, however, did not seem to affect the graphene growth considerably.

The size of the fabricated features is limited by the size of the droplets formed by the inkjet printer. A single marker ink drop on a copper foil had a diameter of about 70 μm. Therefore the average ink line on copper printed with one nozzle had a width of ~70 μm. As mentioned previously, the graphene pattern was formed on uninked areas, i.e. gaps between printed lines. Therefore it was possible to produce graphene ribbons thinner than 70 μm by controlling the ink line spacing. For the production of GFETs prepatterned

graphene strips of $\sim 50\ \mu\text{m}$ were reliably produced, but strips of widths down to $10\ \mu\text{m}$ were also possible with this technique (see Figure 32).

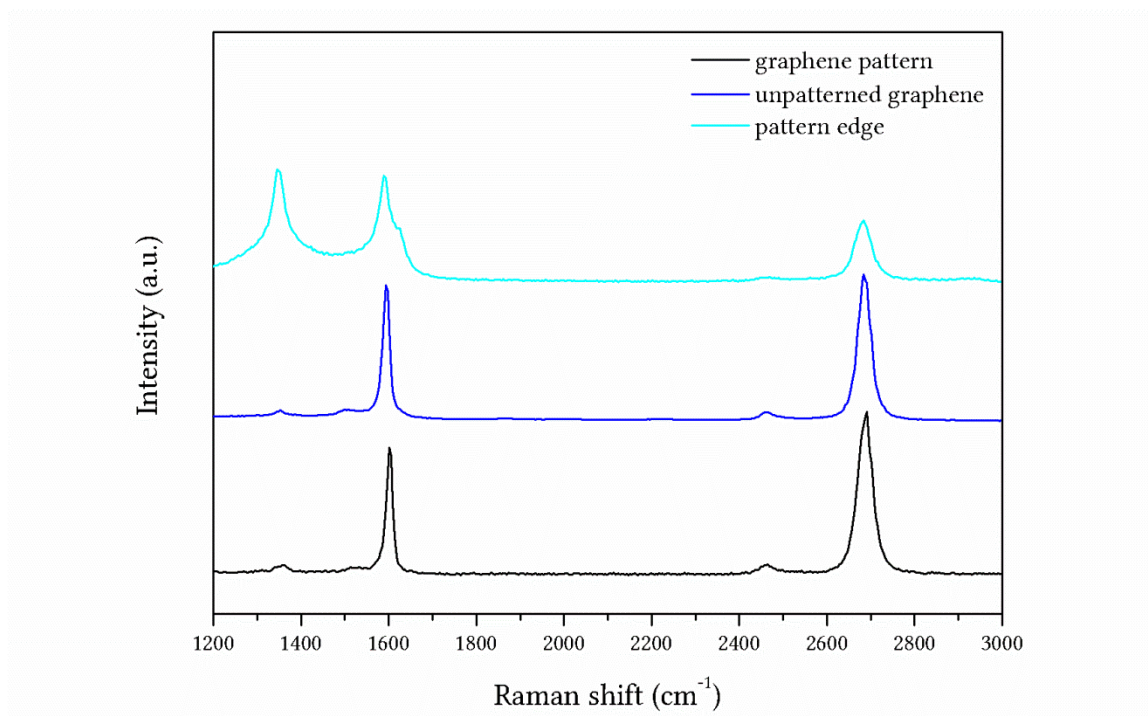


Figure 31: Raman spectra of a graphene pattern edge [turquoise], graphene pattern [black] and unpatterned graphene [blue]

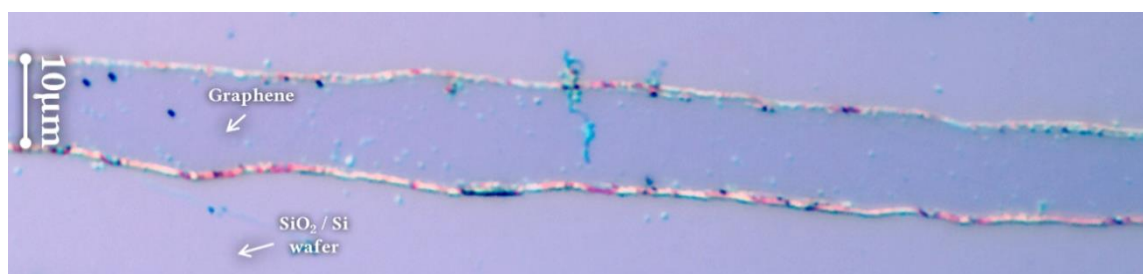


Figure 32: $10\ \mu\text{m}$ strip of prepatterned graphene on a SiO_2/Si wafer

4.2.3. Analysis of *Staedtler Lumocolor*[®] permanent marker black ink

Baking a drop of ink on a Si/SiO_2 wafer at $1035\ ^\circ\text{C}$ in reducing atmosphere resulted in silver/blue crystals. The same experiment carried out in oxidising atmosphere produced pale green crystals (see Figure 33). This gave rise to the assumption that the ink is not solely organic.

XPS scans on dried ink revealed the presence of chromium (see Figure 34). In addition carbon, oxygen, nitrogen and silicon were found. Silicon and oxygen can be attributed to the wafer that held the ink, carbon, nitrogen and oxygen derive presumably from organic parts of the ink. A carbon to chromium atom ratio in the dried ink of 10:1 was calculated.

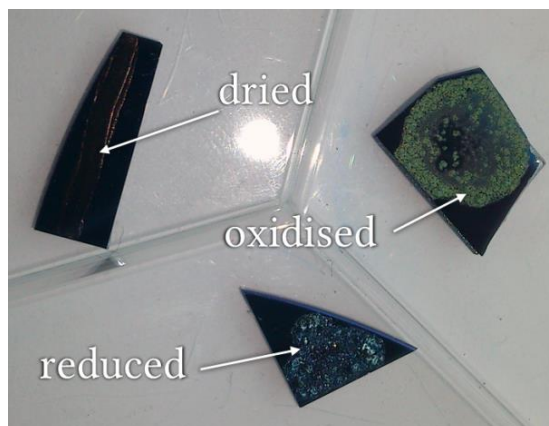


Figure 33: *Staedtler Lumocolor*® permanent marker ink dried, oxidised and reduced on SiO₂ wafers

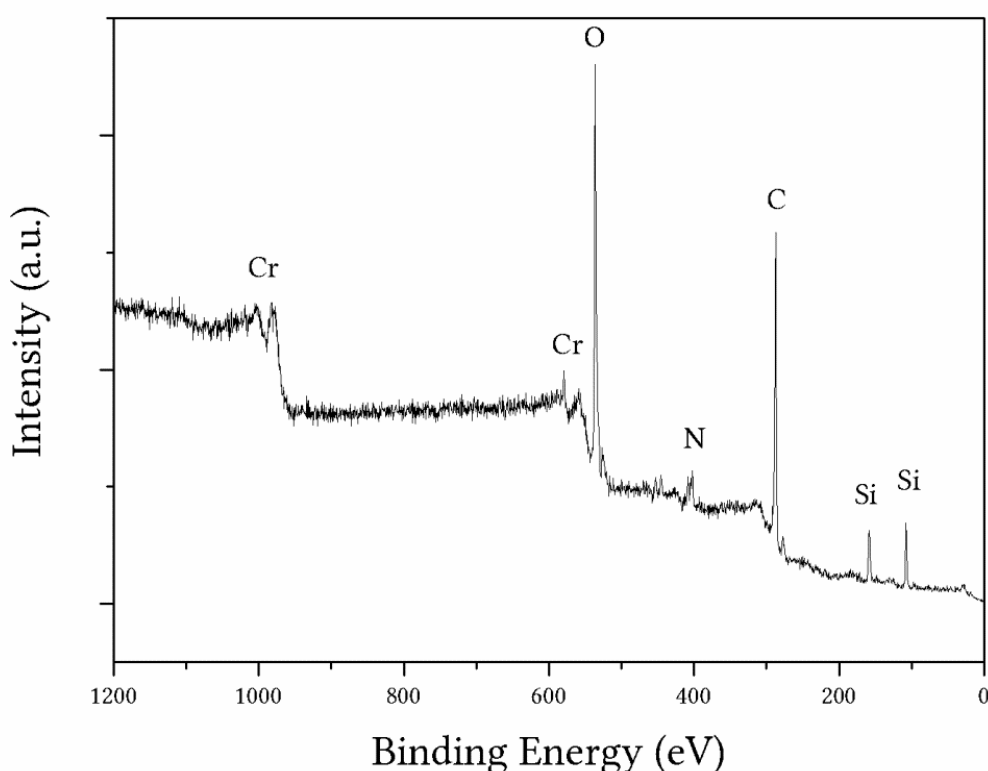


Figure 34: XPS data of dried *Staedtler Lumocolor*® permanent marker black ink on SiO₂ [by *Dr. Nina Berner*]

To further analyse the marker ink SEM images and EDX scans were made. Areas on the copper foils, which had been inked before the graphene growth, were studied after the growth. The edges of the inkjet printed ink lines are still discernible in the ink residue (Figure 35 (a)) and small crystals on the copper surface can be observed (Figure 35 (b)). EDX spectra of these crystals confirm the presence of chromium (Figure 38).

Some of the ink residue was transferred to the wafer substrates, as can be seen in Figure 30 (d) and Figure 36. It has been reported that organic resins can pyrolyse under similar conditions, as the growth conditions used in this study, to form glassy carbon layers [52].

The ink residue on SiO_2/Si wafers was also analysed with Raman spectroscopy. Most areas showed no signal in the carbon characteristic wavelengths, but some gave signals that can be linked to highly disordered graphitic carbon (Figure 37).

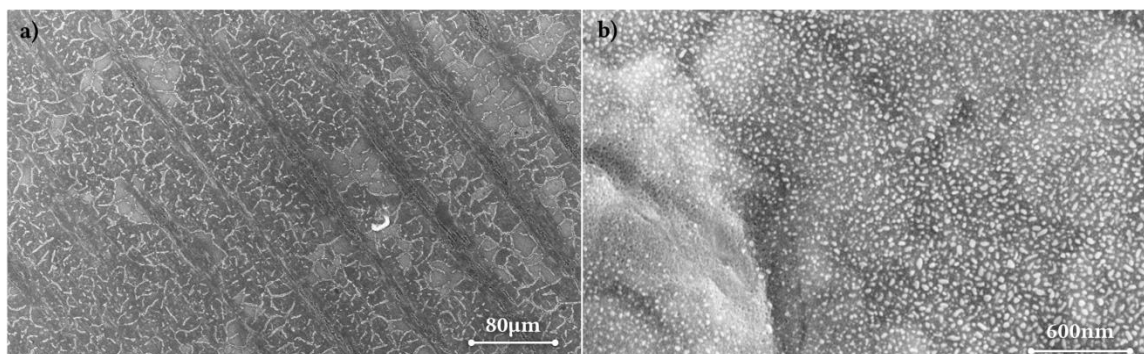


Figure 35: SEM images of marker ink residue on copper foils after CVD graphene growth

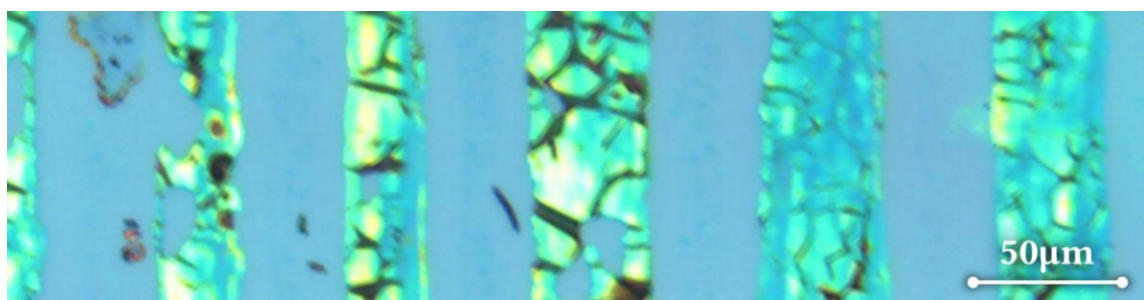


Figure 36: Ink residue on SiO_2/Si wafer

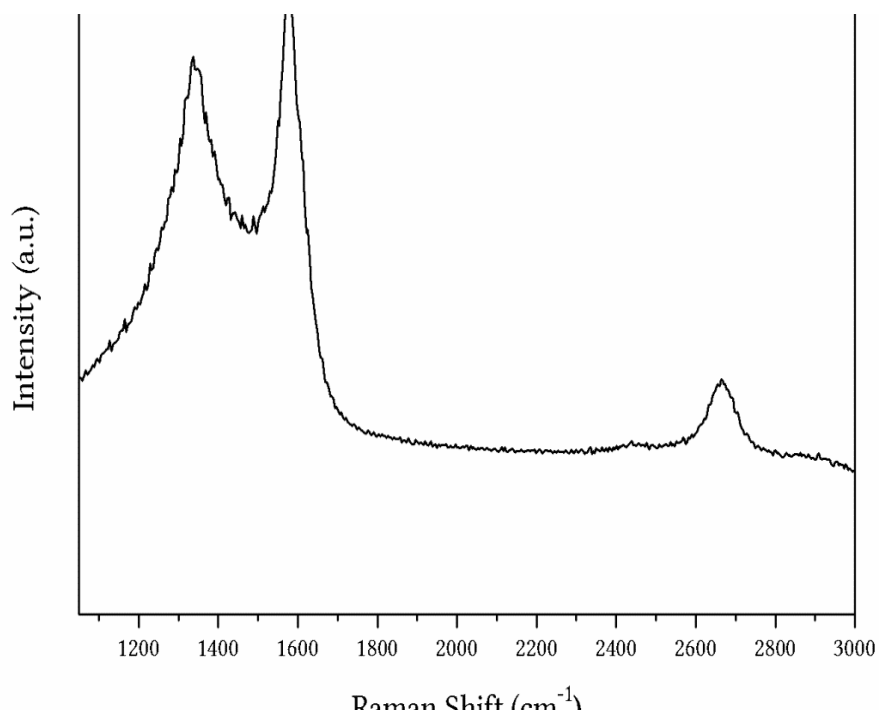


Figure 37: Raman spectrum of to SiO_2/Si wafer transferred marker ink residue

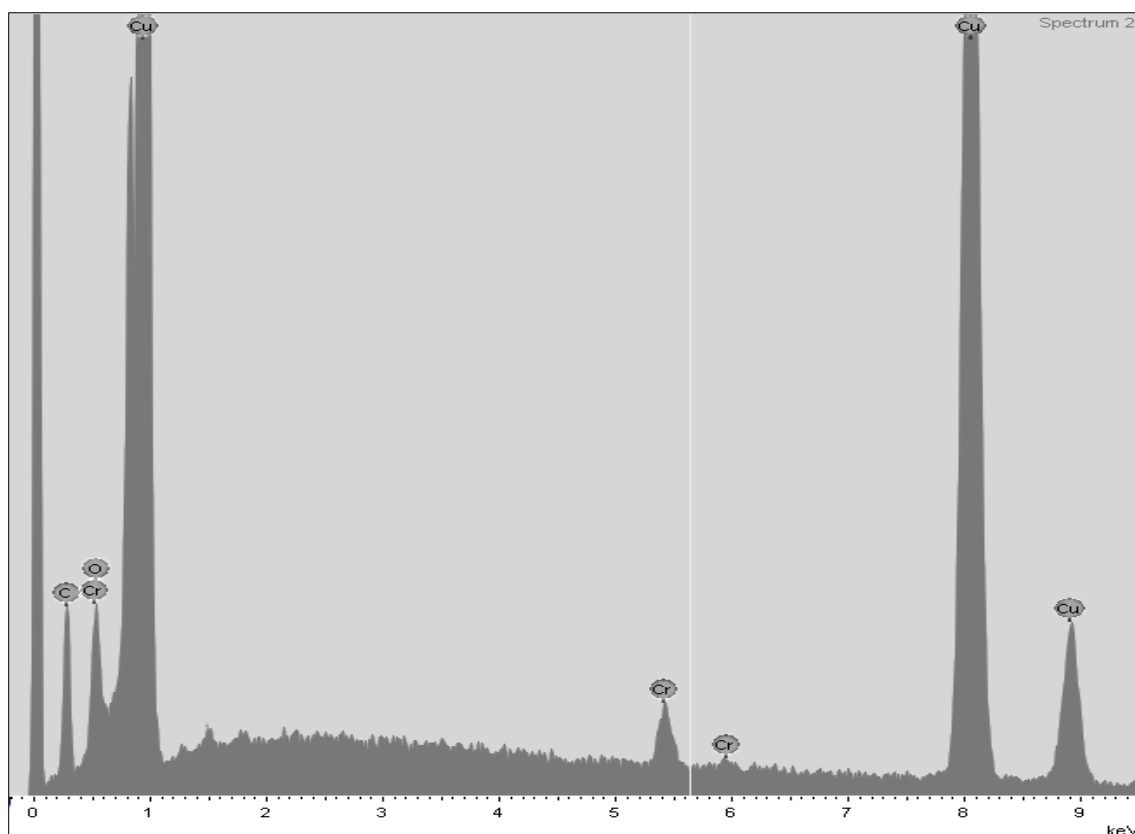


Figure 38: EDX scan of marker ink residue on copper foil after CVD graphene growth

4.2.4. Influence of chromium on graphene growth

It was noticed that chromium seems to have an influence on graphene growth beyond simply masking the growth substrate.

4.2.4.1. *Border of ink-prepatterned features*

Graphene that was grown on copper foils prepatterned with ink containing chromium showed a gradient of multilayer islands from the edge (see Figure 39). At the border of the graphene features was a $\sim 20\mu\text{m}$ wide zone where no multilayer growth seemed to take place. Adjoining this zone the multilayer island size increased until they had the same size and distribution as seen in unpatterned graphene films. This phenomenon was also observed on unpolished foils but was far more obvious on electropolished ones.

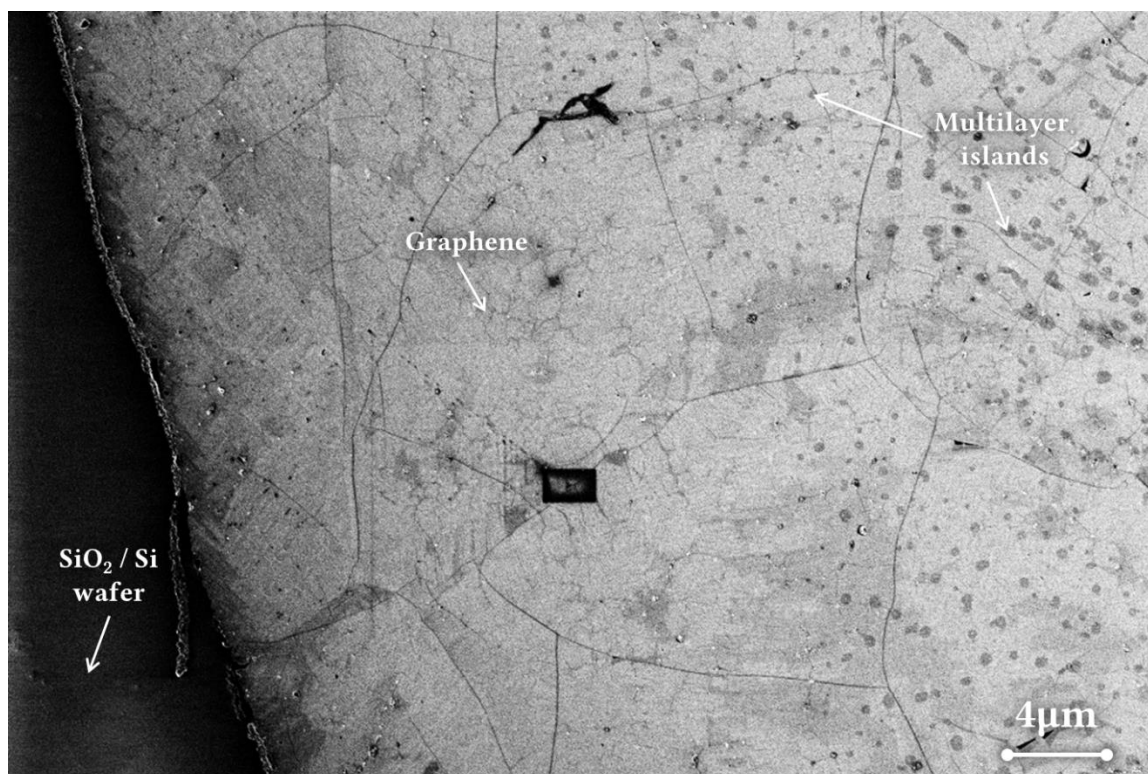


Figure 39: SEM image of an ink prepatterned graphene feature border; a gradient of multilayer islands from the edge of the feature (left) can be observed

4.2.4.2. Sputter deposited chromium

To discern information about the mechanism by which chromium affects the graphene growth experiments with sputtered chromium were carried out. The quality of the grown graphene depended greatly on the thickness of the chromium film deposited.

4.2.4.2.1. 1 nm chromium layer

In the Figures 40 and 41 SEM images of transferred graphene that was grown on a copper foil with a ~1 nm thick layer of chromium are displayed. The border between the area that held chromium and the area that didn't is clearly visible. Areas where chromium was present do not show multilayer graphene growth. EDX confirmed that the tiny dots visible in Figure 41 and Figure 41 (a) are small particles consisting of chromium (see also Figure 38).

Figure 42 (a) shows an optical microscopy image of the film displayed in Figure 41 (a). A Raman spectrum of this graphene is displayed in Figure 43 and Figure 42 (b-d) shows Raman maps. The Raman spectrum shows a defined 2D peak at 2684 cm^{-1} , a G peak at 1593 cm^{-1} and a very small D peak at 1348 cm^{-1} . This is a spectrum of graphene of good quality, though its perfection is tarnished by the G to 2D intensity ratio and the unexpected peak at 1500 cm^{-1} that cannot be identified.

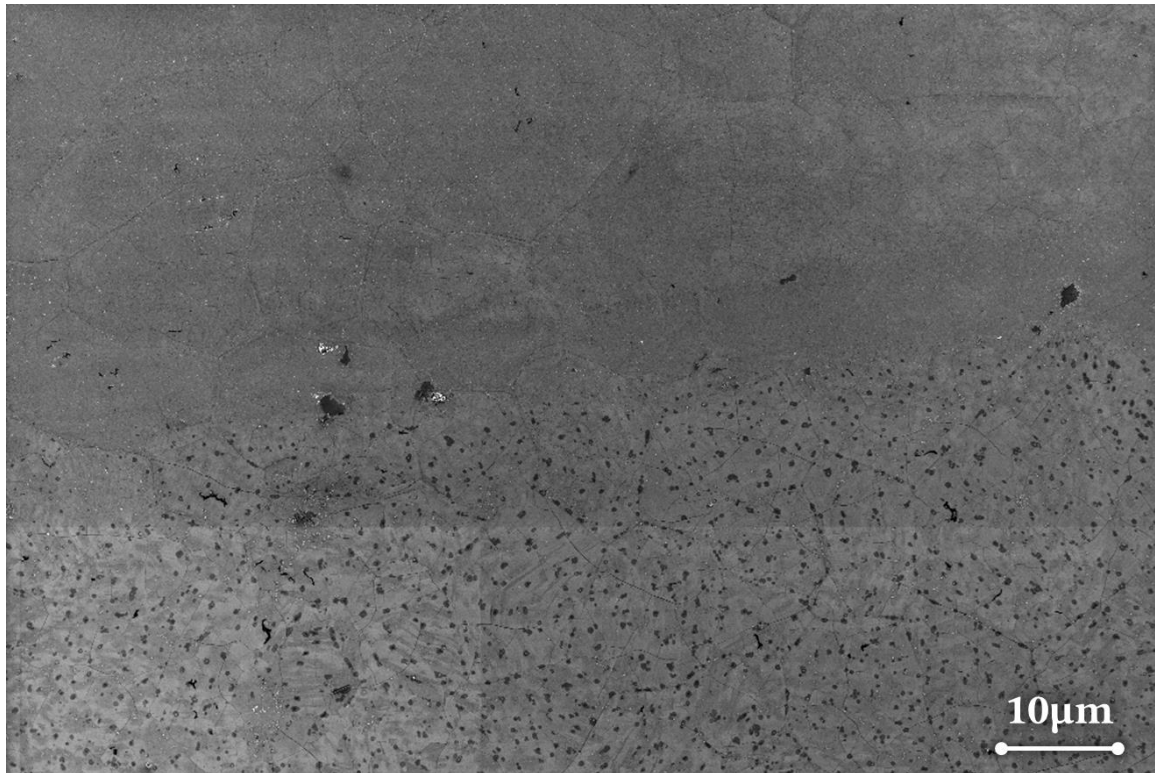


Figure 40: SEM image of graphene grown on a copper foil with a 1 nm chromium layer, transferred to a SiO₂/Si wafer; in the upper part of the picture shows an area where chromium was sputtered on; the lower part bore no chromium

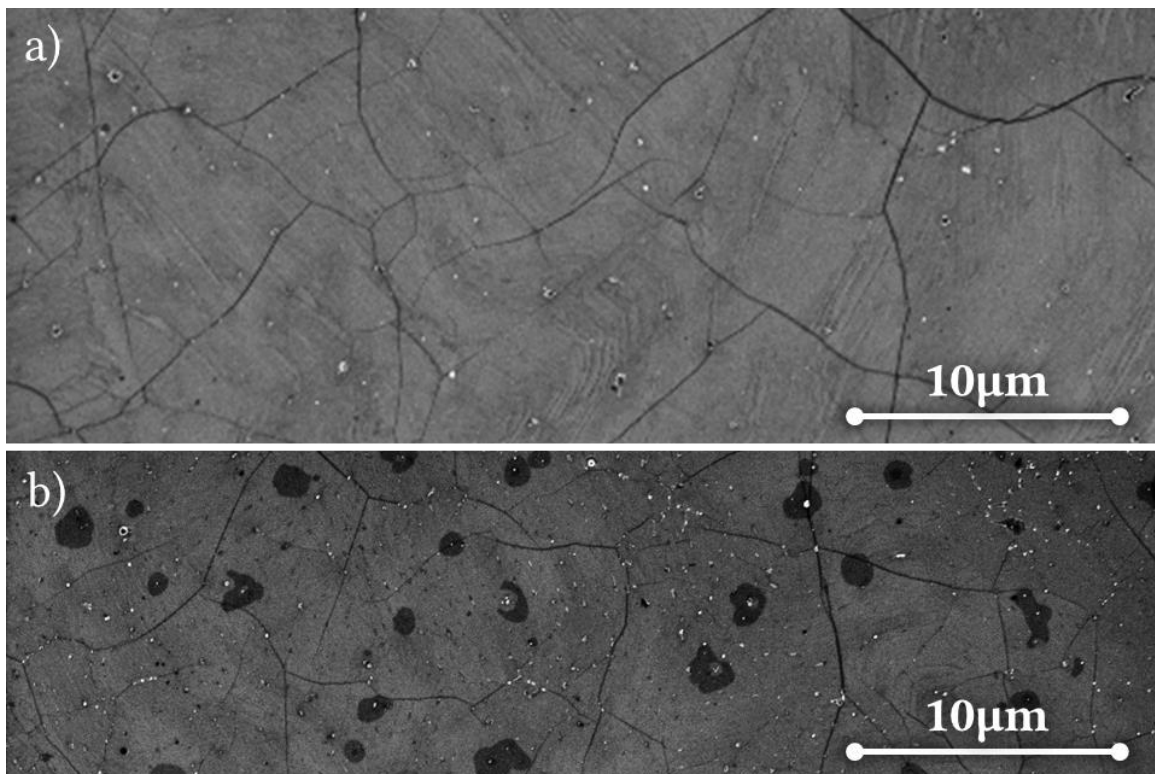


Figure 41: SEM image of graphene grown on a copper foil with a 1 nm chromium layer; a) area where chromium was sputtered on; b) area on the same copper foil but without a chromium layer

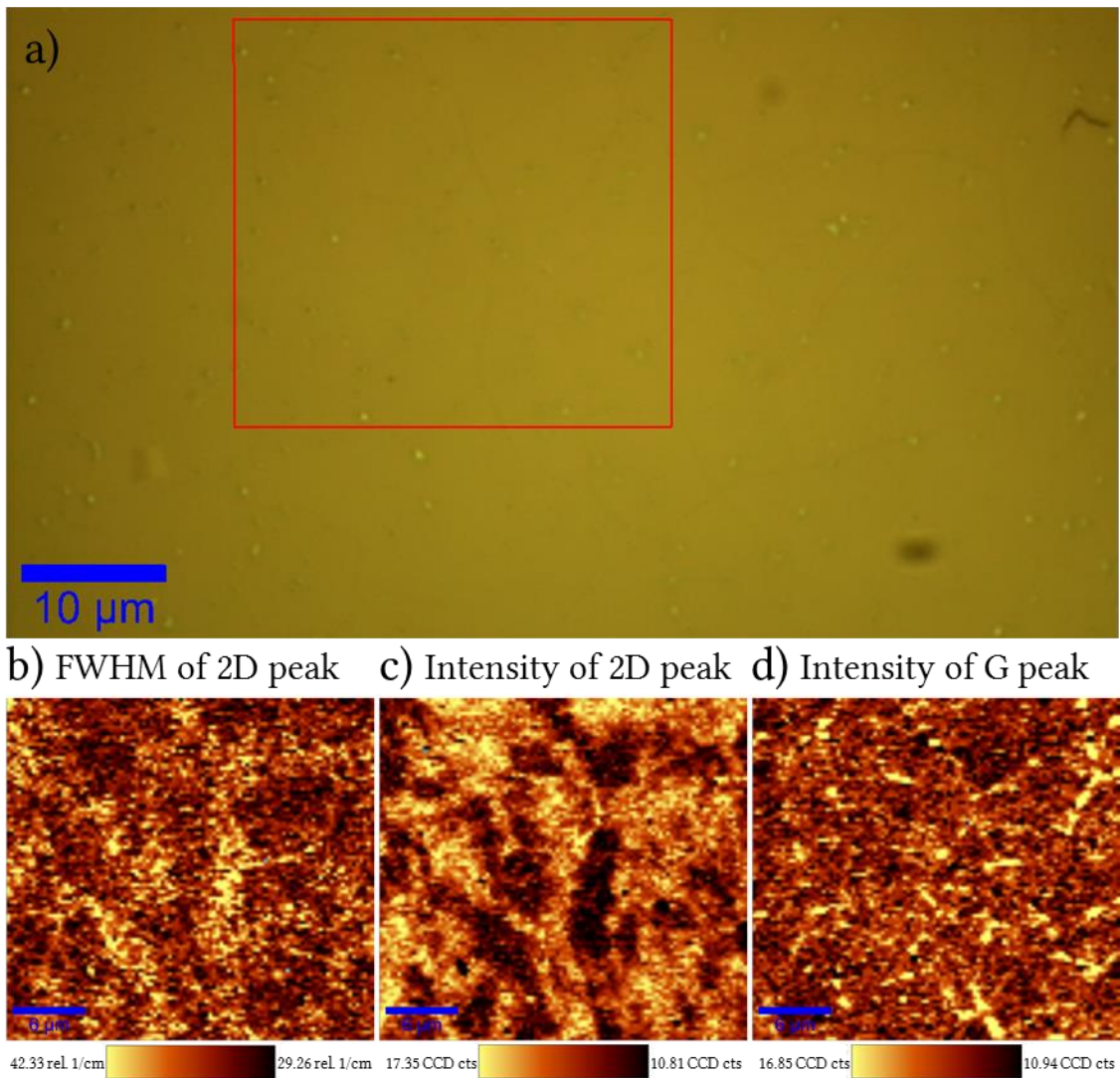


Figure 42: Graphene grown on a copper foil with a 1 nm thick chromium layer; a) optical microscopy image; b-d) maps of Raman scans of the area in the red square in (a)

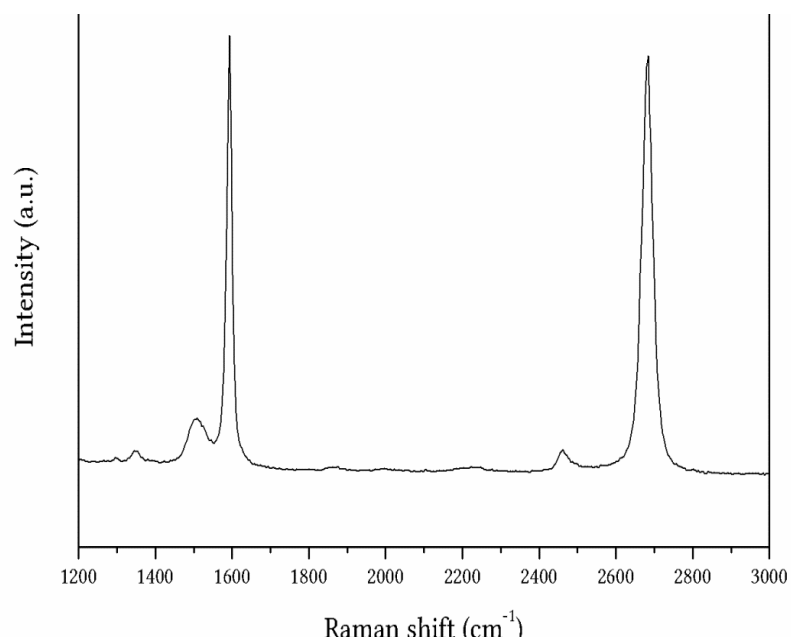


Figure 43: Raman spectrum of graphene grown on a copper foil that held a 1 nm thick chromium layer

4.2.4.2.2. 5 nm chromium layer

As the graphene growth with a 1 nm chromium layer, the graphene growth with an approximately 5 nm chromium layer showed no multilayer growth in areas where chromium was present (see Figure 44). As can be seen in Figure 44 and Figure 45 a lot more chromium containing particles were found than in the 1 nm chromium sample and generally no graphene was found in the immediate vicinity of chromium containing particles. Figure 46 displays an EDX scan of one particle in Figure 45. Figure 45 also makes the superiority of an In-Lens over an SE2 detector visible when it comes to imaging graphene. The difference between the growth with chromium and the growth without chromium was not only observed in SEM (Figure 44) but also in optical microscopy (Figure 47 (a)).

Figure 47 (a) shows an optical microscopy image of the film shown on the left in Figure 44 (a + b). A Raman spectrum is depicted in Figure 48 and Figure 47 (b-d) presents Raman maps of this film. The Raman spectrum shows a 2D peak at 2688 cm^{-1} that can be fitted with a single Lorentzian function indicating solely mono-layer growth. The G peak appears at 1597 cm^{-1} and a small D peak at 1347 cm^{-1} . The FWHM of the 2D peak lies close to 30 cm^{-1} further underlining the mono-layer character of this growth. The fact that the G peak intensity is larger than the 2D peak intensity and the existence of a D peak expresses the imperfection of this growth.

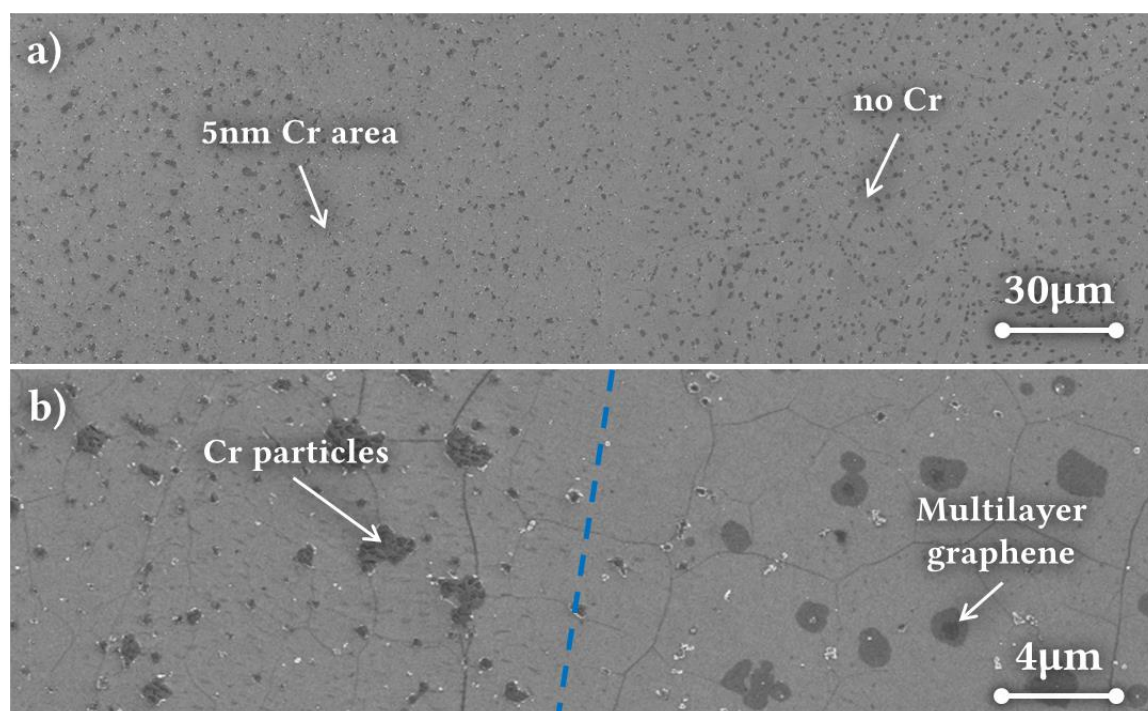


Figure 44: SEM images of transferred graphene grown on a copper foil with a 5 nm chromium layer; left half had chromium sputtered on, right half did not

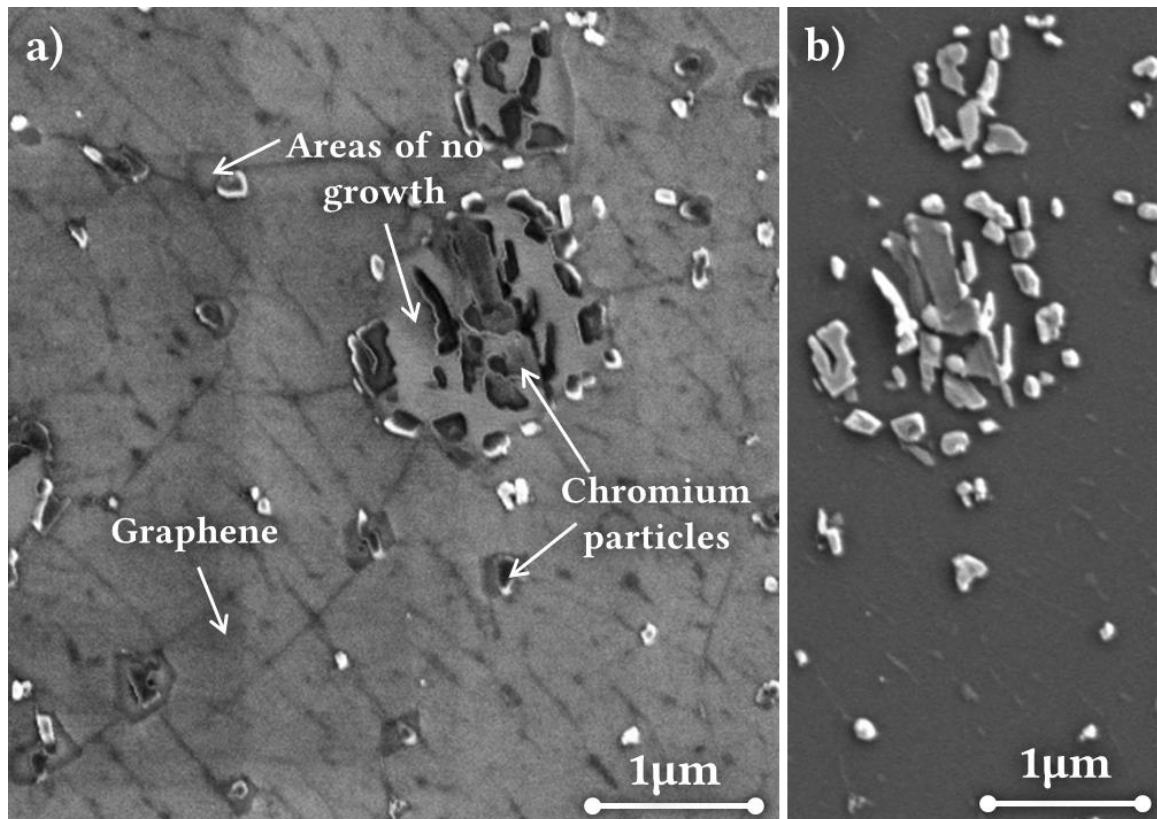


Figure 45: Graphene grown on a copper foil with a 5 nm chromium layer, transferred to a SiO₂/Si wafer; a) SEM image taken with an in-lens detector; b) SEM image of the same area taken with a secondary electron detector

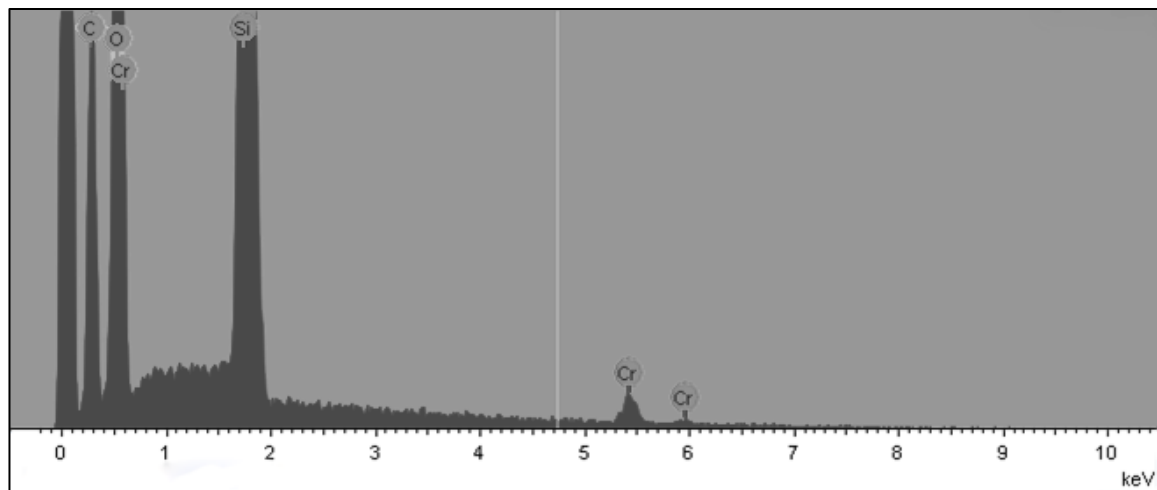


Figure 46: EDX spot scan of a chromium containing particle as shown in Figure 45

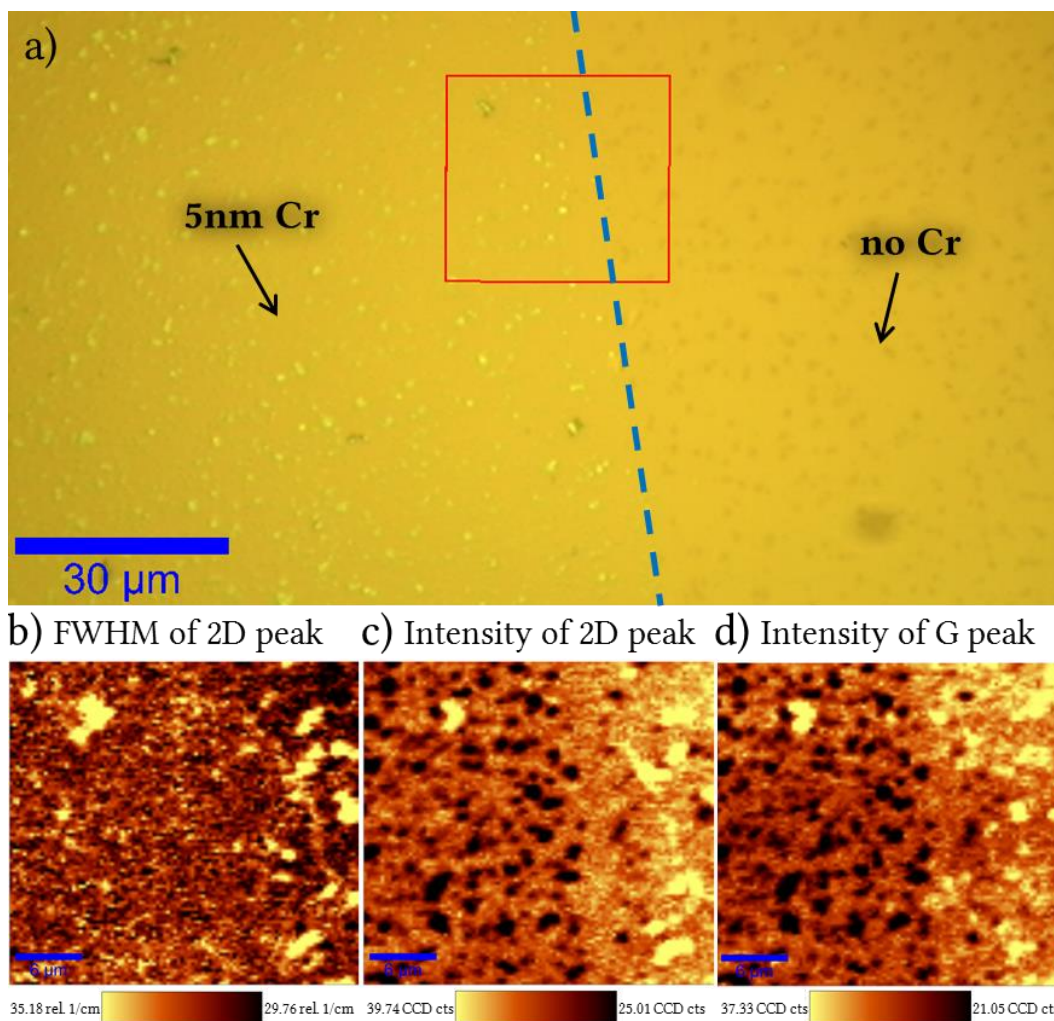


Figure 47: Graphene grown on a copper foil with a 5 nm thick chromium layer; a) optical microscopy image; the blue dashed line indicates the border between the area on the copper foil where chromium was sputtered on (left) and where no chromium was present (right); b-d) maps of Raman scans of the area in the red square in (a)

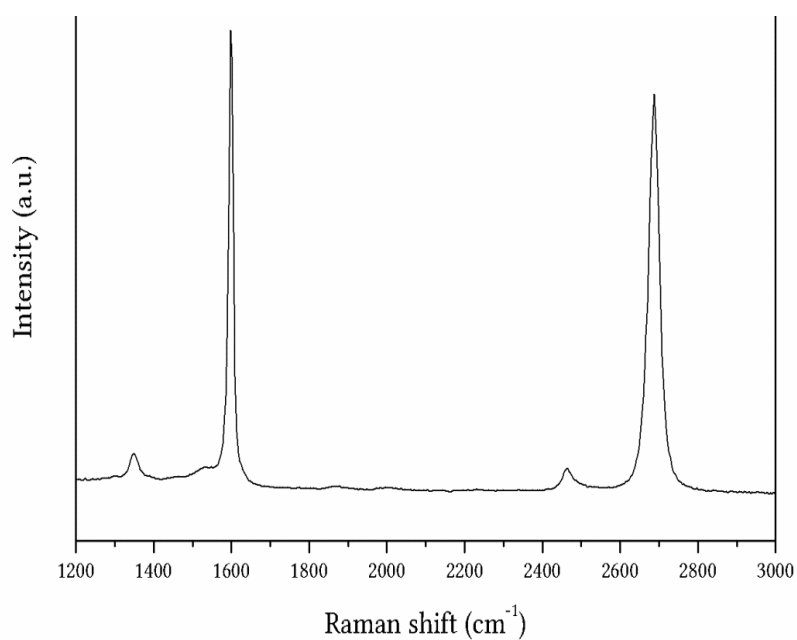


Figure 48: Raman spectrum of graphene grown on a copper foil with a 5 nm chromium layer

4.3. Production and characterisation of GFETs

After the transfer of produced graphene to SiO₂/Si wafers, electrical contacts had to be added to create GFETs. Prepatterned graphene stripes as well as full sheets of graphene were used.

4.3.1. Printing electrical contacts onto graphene

In this work contact leads were inkjet printed on the graphene with a commercially available silver nanoparticle ink, i.e. *SunTronic® Silver*.

4.3.1.1. Inkjet printing silver nanoparticle ink

The calibration of the silver inkjet printing on graphene and SiO₂/Si wafers was aimed at reaching the smallest reliably reproducible resolution of 4-point-probe contacts printed as depicted in Figure 19. A droplet spacing of 30 µm gave the most satisfactory results. The wettability of the silver nanoparticle ink was found to be different on graphene transferred to SiO₂/Si wafers and bare SiO₂/Si wafers. This resulted in printed silver line widths of about 40 µm on graphene and of about 50 µm on bare wafers (see Figure 64).

4.3.1.2. Sintering of silver nanoparticle ink

To enhance the electrical conductivity of the printed silver features a sintering step was carried out. Test runs at 150 °C, 200 °C and 250 °C in air in an oven showed that a brownish colourisation of the silver features took place, starting at temperatures of about 200 °C and getting more pronounced at higher the temperatures. Therefore all further samples were sintered at 180 °C for 10 min in air. As can be seen in the comparison of Figure 49 (a) and (b), this was sufficient to increase the average particle size and the contact between the particles. The sintering was not observed to have an influence on the line width of printed lines, but due to drying phenomena the resulting lines did not have a defined edge (see Figure 49 (c)).

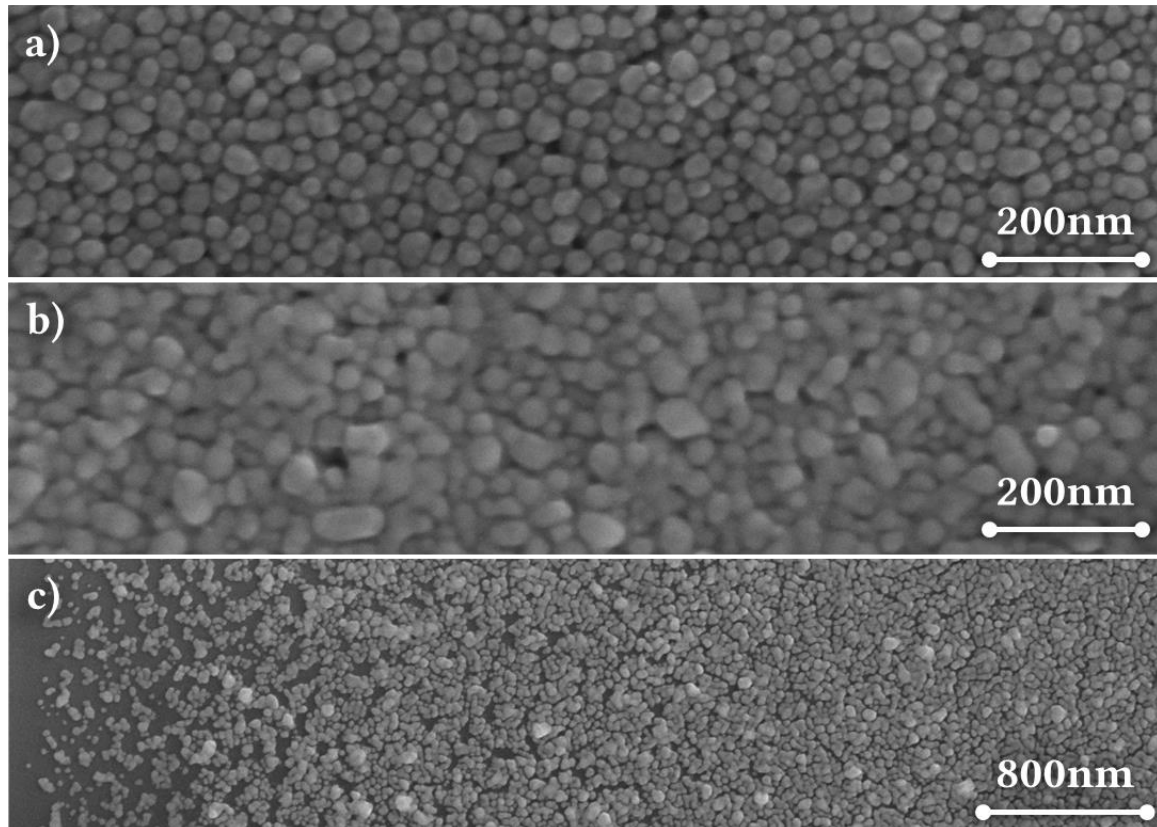


Figure 49: SEM images of SunTronic® Silver ink on SiO₂/Si wafers; a) slowly dried in air after printing; b) printed and sintered while the ink was still wet; c) edge of a printed line that was sintered while wet

4.3.1.3. Electrical characterisation of silver contacts

The electrical conductivity of the sintered silver ink was analysed with the following two methods.

4.3.1.3.1. Sheet resistance measurement

A thin film of ink was spin coated onto a SiO₂/Si wafer. In Table 2 the results of the sheet resistance measurements are summarised. These values assure that the sintered silver is of high conductivity, but cannot be seen in absolute numbers because the *Keithley SourceMeter* used was not accurate enough for a resistance range that low.

Table 2: Spin coated and sintered SunTronic® Silver ink

Curing @180°C	Resistance	Thickness	Sheet resistance	Bulk resistivity
10 min	0.0844 [Ω]	460 [nm]	0.3827 [Ω]	1.76*10 ⁻⁷ [Ω.m]

4.3.1.3.2. Resistance of printed contact lines

To directly characterise the resistance of silver features as outlined in Figure 19 (b) the electrodes were not printed interdigitated but touching each other. The length of the measured straight silver “wires” was 0.5 mm. After sintering the silver the contact pads were touched with needle probes. To see possible changes the measurement was repeated

55 days later. The resistance of the features increased, as can be seen from the data presented in Table 3.

Table 3: Resistance of silver contacts

Days after sintering	Resistance
1	50 Ω
56	77 Ω

4.3.1.4. Sintering of silver nanoparticle ink printed on graphene

In Figure 50 silver features printed on a graphene sheet are visible. On the top the ink is still wet, on the bottom the same lines are depicted after sintering.

It was observed that while the wet ink was sitting on the graphene an appreciable amount of liquid was able to migrate between the graphene sheet and the wafer (seen in Figure 51 (a)). This, in itself, would not have been a problem, but during sintering the solvent evaporated abruptly and ripped holes into the graphene sheet (see Figure 51 (b)). Not all graphene samples showed the same extent of liquid migration and therefore the same degree of damage. The cleaner and more flawless the graphene sheets were and the quicker the sintering followed the printing the less destruction took place. A short annealing (180 °C

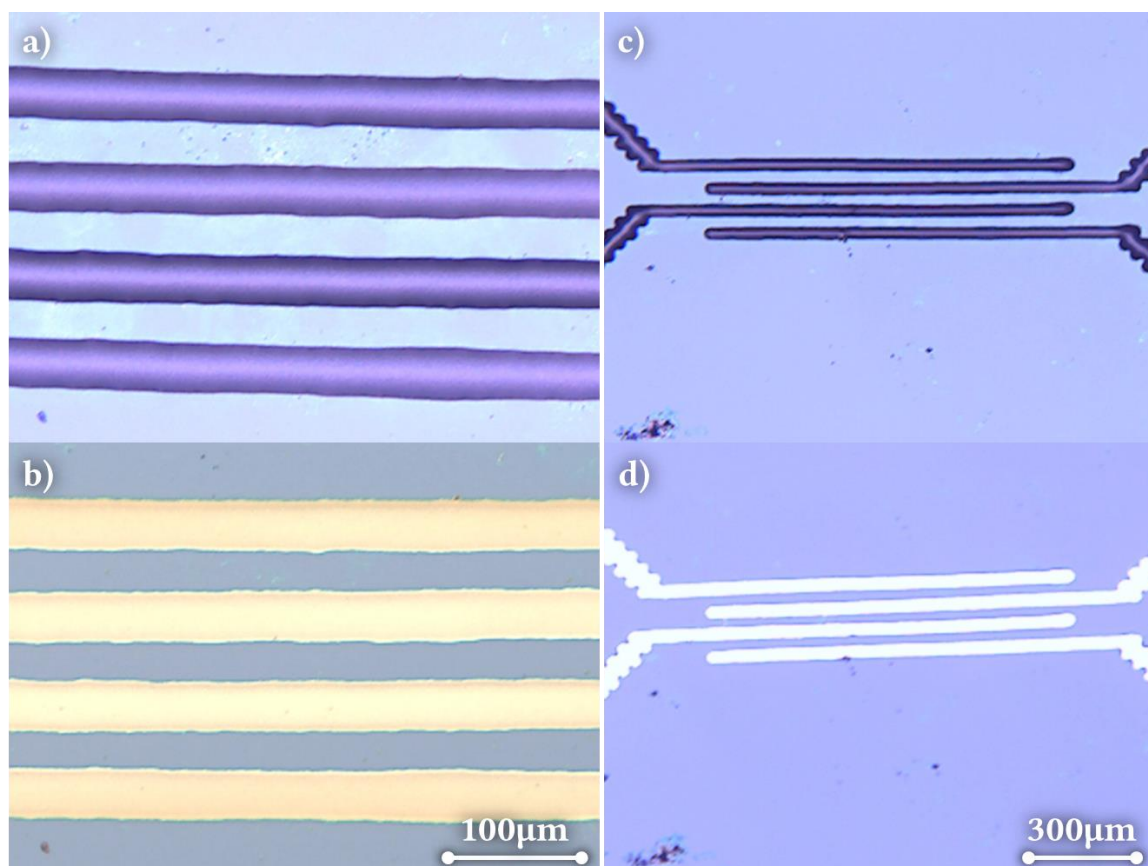


Figure 50: Optical microscopy images of silver nanoparticle ink printed on a graphene sheet on a SiO₂/Si wafer; a+c) wet ink on graphene; b+d) the same lines as in (a+c) after sintering

for 10 min in an oven in air) prior to printing also helped to limit the damage but was unable to completely prevent it (see Figure 51 (c+d)). Very clean, preannealed samples showed almost no tears. To prevent the deterioration of the graphene completely the ink had to be dried slowly over several hours at 45 °C. In device fabrication the ink was dried prior to the sintering step. This decreased the conductivity of the sintered lines. In this work all samples were fabricated in a 4-point-probe architecture where probe resistances do not affect the measurement.

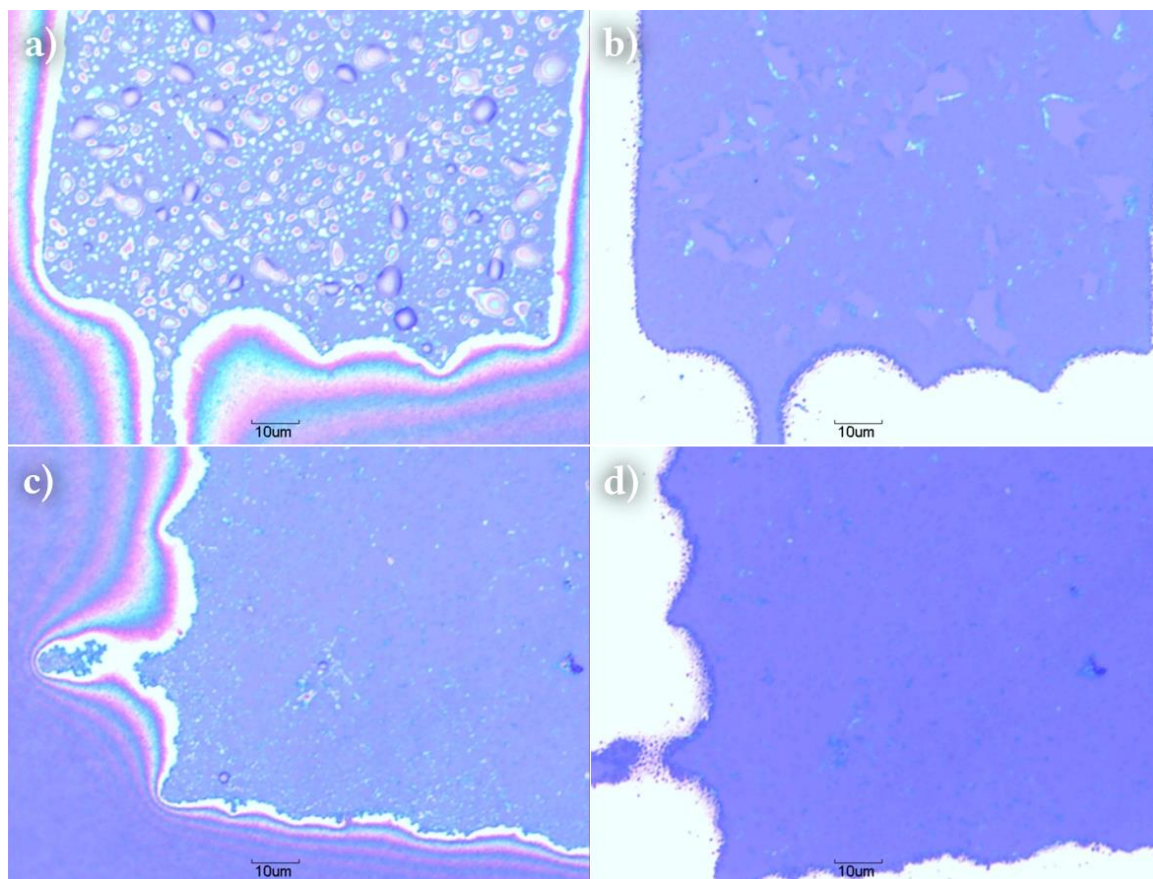


Figure 51: Sintering silver nanoparticle ink on graphene; a) 16h wet ink on a full graphene sheet; b) sample (a) after sintering; c) 16h wet ink on a full graphene sheet that was preannealed; d) sample (c) after sintering

4.3.2. Device characterisation

Graphene field effect transistors have been fabricated as described in Section 3.2. Figure 52 depicts optical microscopy images of a GFET. The vertical graphene channel is a slightly darker blue than the SiO₂/Si wafer. The silver electrodes show up white. A close up photograph of such a device is shown in Figure 53.

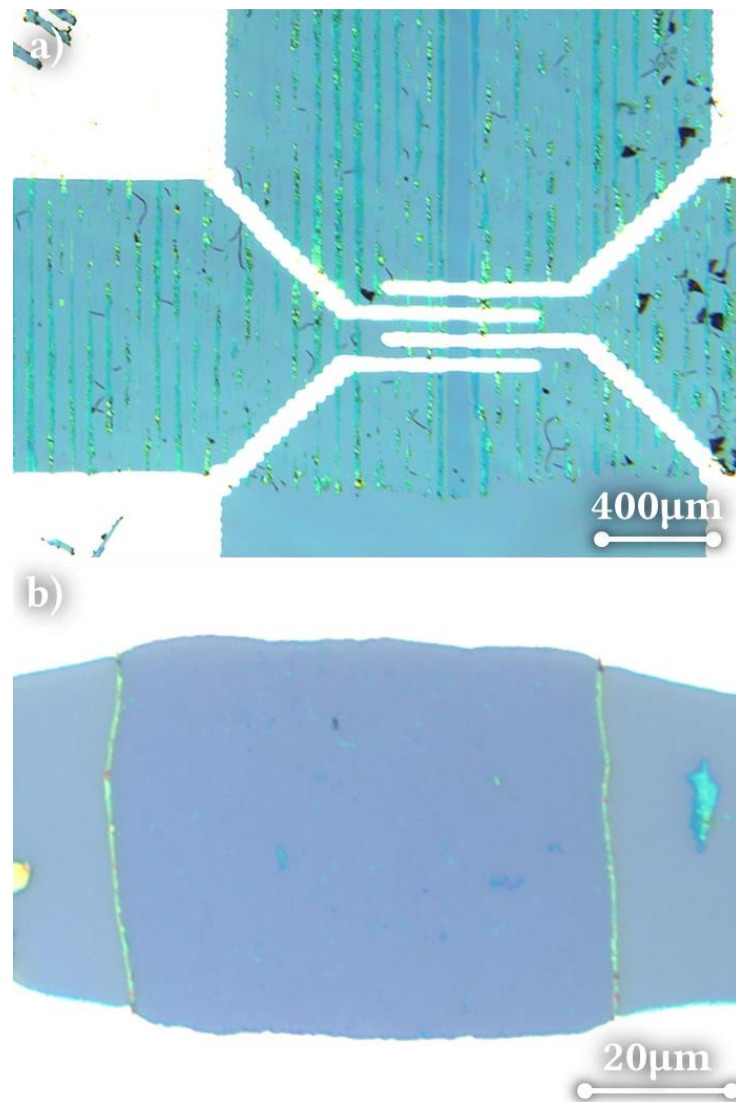


Figure 52: a) Microscopy image of a GFET; b) channel of the GFET depicted in (a) [Sample 21.2. I L]

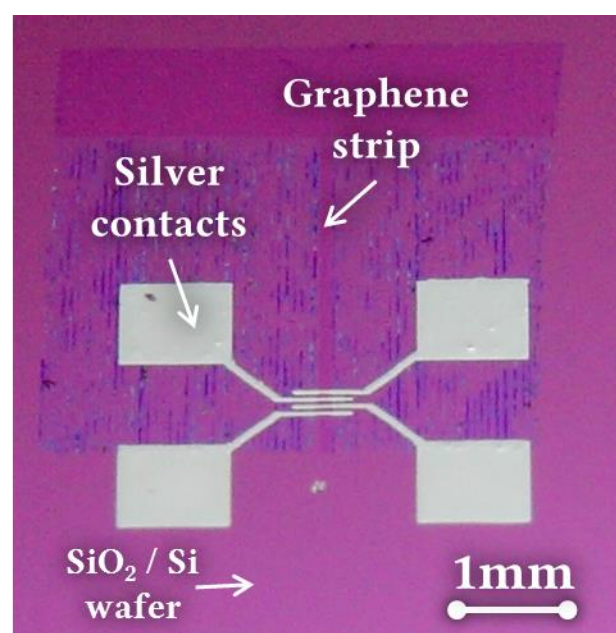


Figure 53: Photography of a GFET, ready for characterisation

Table 4 lists the channel dimensions of the devices that were investigated for their sheet resistance and charge carrier mobilities.

Table 4: Channel dimensions of analysed devices

Sample	Channel width [μm]	Channel length [μm]
D21.2. I L	69	54
D21.2. I U	38	50
D21.2. II L	112	51
D21.2. II U	110	50
N21.2. III	83	45
N21.2. I	107	50
N15.1. T2 VII L	353	53

4.3.2.1. *Sheet resistance and charge carrier mobility*

The sheet resistance measurements took place in ambient conditions and in a vacuum chamber at room temperature. The day after a first analysis in ambient conditions some of the devices were annealed for one hour at 500 K and were subsequently measured in the vacuum annealing chamber at about 10^{-6} mbar. The samples were stored in ambient conditions for 17 days before being annealed for another 12 hours and measured in vacuum. 31 days after the production one of the samples was measured again in ambient conditions.

As described in more detail in Section 3.3.4, the changing voltage between the inner two of four electrodes was recorded during a gate voltage sweep while a fixed current was applied at the outer two electrodes. The collected data was used to calculate the sheet resistance and the charge carrier mobilities using Equation 3 to Equation 6.

Graphs of sheet resistance vs. gate voltage that are not included in this chapter can be found in the appendix (Figure 68 to Figure 76) for all samples.

4.3.2.1.1. Measurements in ambient conditions

The results of the measurements that took place in ambient conditions are listed in Table 5. Due to the fact that the charge neutrality point for all samples was out of the applied gate voltage range it was not possible to assess it and the electron mobility. Figure 54 shows the sheet resistance of one device changing with the gate voltage. The maximum in the field effect mobility curve is the electron hole mobility. The charge neutrality point would show as a maximum in the sheet resistance, but lies above a gate voltage of 70 V in this sample. Beyond the charge neutrality point a minimum in the field effect mobility curve would appear. This minimum would indicate the electron mobility, but is also out of the range of this measurement.

Table 5: Results of gated 4-point-probe measurements in ambient conditions

Sample	Charge neutrality point [V]	Sheet resistance [Ω /square]	Hole mobility [$\text{cm}^2\text{V}^{-1}\text{s}^{-1}$]	Electron mobility [$\text{cm}^2\text{V}^{-1}\text{s}^{-1}$]
D21.2. I L	n/a	435 - 1372	1376	n/a
D21.2. I U	n/a	321 - 594	1338	n/a
D21.2. II L	n/a	594 - 2580	1184	n/a
D21.2. II U	n/a	640 - 1679	864	n/a

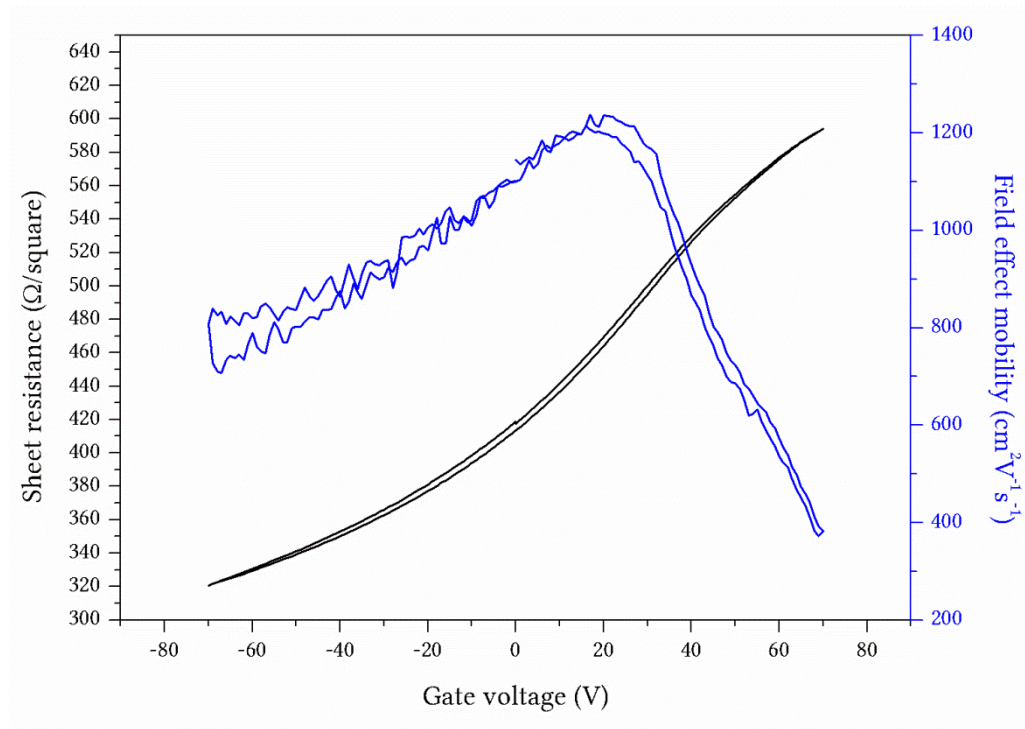


Figure 54: Sheet resistance and the calculated field effect mobility curve of which the maximum gives the hole mobility, of sample D21.2. I U in ambient conditions

Table 6: Results of 4-point-probe measurements in ambient conditions without an applied gate voltage

Sample	Sheet resistance [Ω /square] at gate voltage 0V
N15.1. I2 VII L	940
N21.2. I	1037
N21.2. III	1008

Table 6 contains the evaluated sheet resistances of samples that were fabricated on wafers that showed leakage in the insulating oxide layer and were therefore not fit for the application of a gate voltage. Figure 55 depicts the sheet resistance of such a measurement.

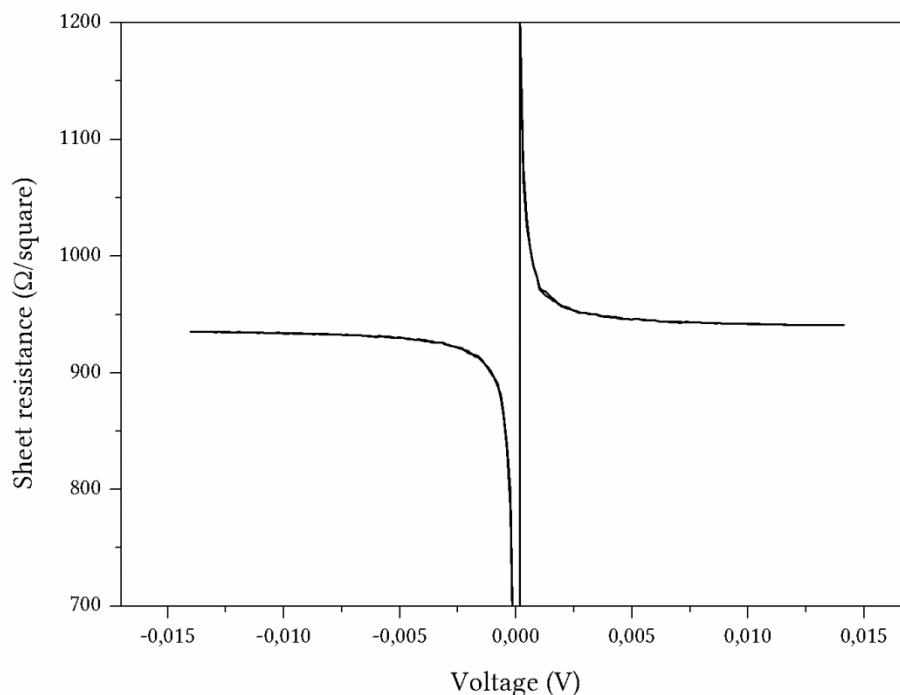


Figure 55: N15.1 T2 VII ambient conditions, no gate voltage was applied

4.3.2.1.2. Measurements after one hour of vacuum annealing

In order to remove residues some of the samples were annealed for one hour at 500 K at 10^{-6} mbar. The measurements took place in vacuum at room temperature. The results are listed in Table 7 and Figure 56 shows the sheet resistance curve of one device. The charge neutrality point is visible, the electron mobility still out of the measurement range.

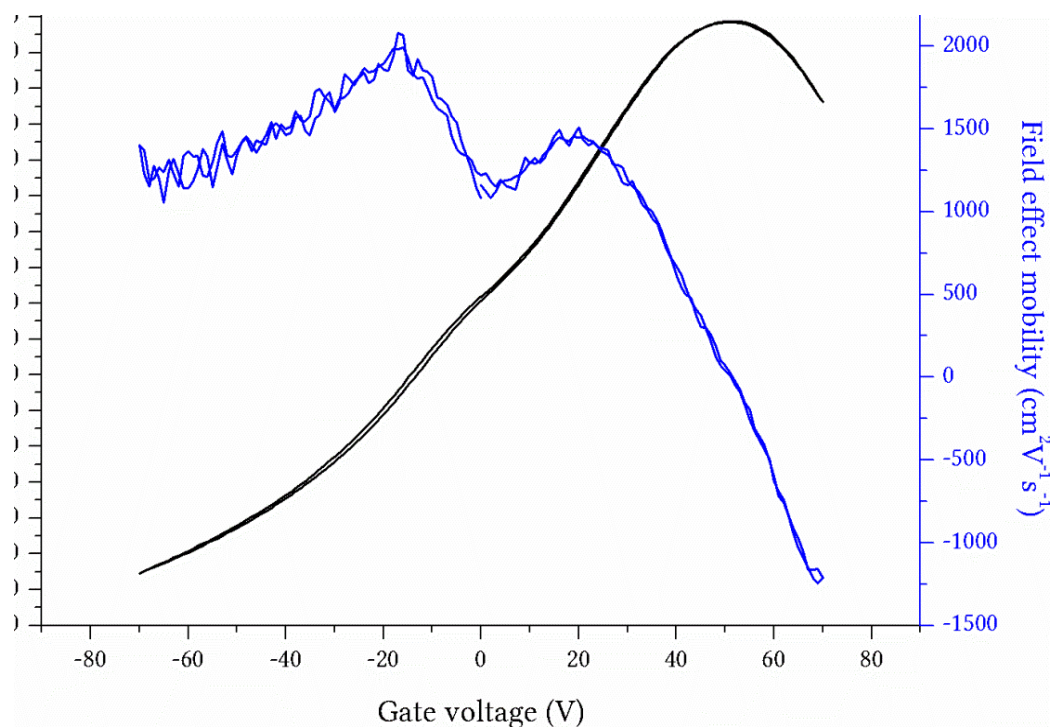


Figure 56: Sheet resistance and the calculated field effect mobility curve of which the maximum gives the hole mobility, of sample D21.2. I U in vacuum after a 1 h vacuum anneal

Table 7: Results of gated 4-point-probe measurements after a one hour vacuum anneal

Sample	Charge neutrality point [V]	Sheet resistance [Ω /square]	Hole mobility [$\text{cm}^2\text{V}^{-1}\text{s}^{-1}$]	Electron mobility [$\text{cm}^2\text{V}^{-1}\text{s}^{-1}$]
D21.2. I L	50	39 - 1438	2056	> 1687
D21.2. I U	51	289 - 598	2078	> 1248
D21.2. II L	n/a	460 - 2528	1781	n/a

4.3.2.1.3. Measurements 18 days after production and another 12 hour vacuum anneal

Seventeen days after the 1 hour vacuum anneal the samples were annealed for another 12 hours to remove more of the doping residues. The results of this measurement are shown in Table 8 and Figure 57 which show the considerable downshift of the charge neutrality point and the minimum in the field effect mobility curve that indicates the electron mobility.

Table 8: Results of gated 4-point-probe measurements after a twelve hour vacuum anneal

Sample	Charge neutrality point [V]	Sheet resistance [Ω /square]	Hole mobility [$\text{cm}^2\text{V}^{-1}\text{s}^{-1}$]	Electron mobility [$\text{cm}^2\text{V}^{-1}\text{s}^{-1}$]
D21.2. I U	10	337 - 569	1681	2155
D21.2. II L	26	572 - 2300	1625	1822
D21.2. II U	33	681 - 1515	1224	1213

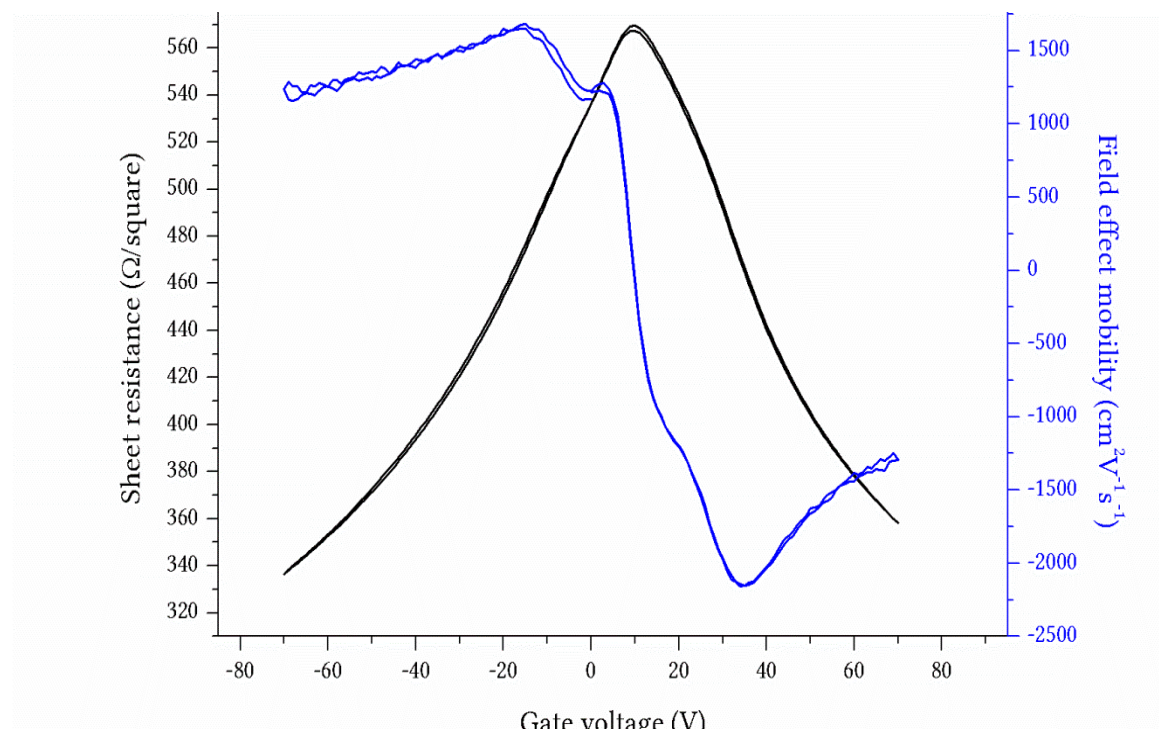


Figure 57: Sheet resistance and the calculated field effect mobility curve of which the maximum gives the hole mobility and the minimum the electron mobility, of sample 21.2. I U in vacuum after a 12h anneal

4.3.2.1.4. Measurements in ambient conditions 31 days after production

31 days after the production one of the samples was measured again in ambient conditions. The results are shown in Table 9. The measured curve was quite jagged. To obtain mobility values it was fitted as can be seen in Figure 76 (appendix).

Table 9: Results of a gated 4-point-probe measurement in ambient conditions, 31 days after the production of the device

Sample	Charge neutrality point [V]	Sheet resistance [Ω /square]	Hole mobility [$\text{cm}^2\text{V}^{-1}\text{s}^{-1}$]	Electron mobility [$\text{cm}^2\text{V}^{-1}\text{s}^{-1}$]
D21.2. II L	n/a	695 - 1703	716	n/a

4.3.2.2. Current on-off ratio

A transistor has to have a current on-off ratio. To investigate devices for it they have to be analysed in a 2-point electrode configuration. This measurement architecture has the disadvantage of not being independent of the probe conductivity.

After a one hour anneal sample D21.2. I L was tested for its on-off ratio. Figure 58 shows the results of this measurement. Graphene does generally not show a complete current-off state. The saturation of the current is not reached within the gate voltage range. Therefore the $I_{\text{on}}/I_{\text{off}}$ ratio can only be named as bigger than 3. 31 days after the production a current on-off ratio of bigger than 2 was measured in sample 21.2. II L in ambient conditions.

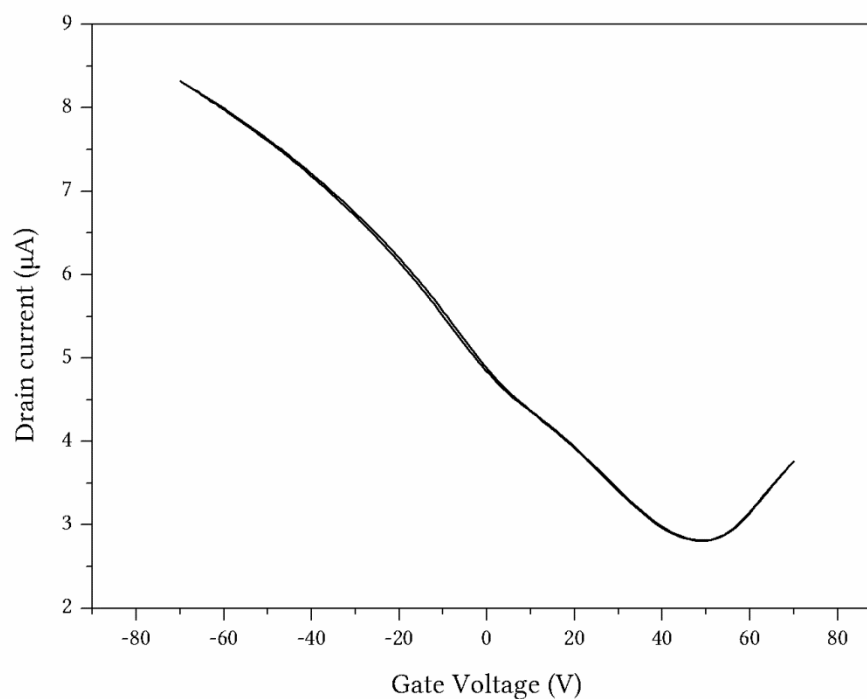


Figure 58: Drain current vs. gate voltage of sample D21.2 I L for the determination of the current on-off ratio

5. Discussion of results

In this work many closely related yet different subjects were investigated. Graphene sheets and patterns were grown, the influence of chromium on graphene growth was scrutinised, silver electrodes were inkjet printed and GFETs were fabricated and their electrical performance was tested.

5.1. Graphene growth on unpolished vs. growth on polished copper foils

As can be seen in Figure 59, the roughness of the growth substrate - copper foil - was vastly diminished by the preceding electropolishing step.

This had a major influence on the subsequent graphene growth. Figure 60 shows graphene sheets grown on (a) unpolished and (b) polished copper. It is evident that the multilayer growth is especially affected by the polishing procedure. On unpolished copper the size of multilayer islands is bigger and many of them show areas of more than two layers, whereas on polished foils only small dots of bilayer growth are observed. Figure 60 (a) shows debris on the graphene whereas the graphene in Figure 60 (b) does not. It was observed on various samples that the less defective the graphene growth the cleaner the transfers. Further, the images depicted in Figure 60 (c+d) illustrate the fact that edges of prepatterned graphene structures are a lot smoother when grown on polished copper foils.

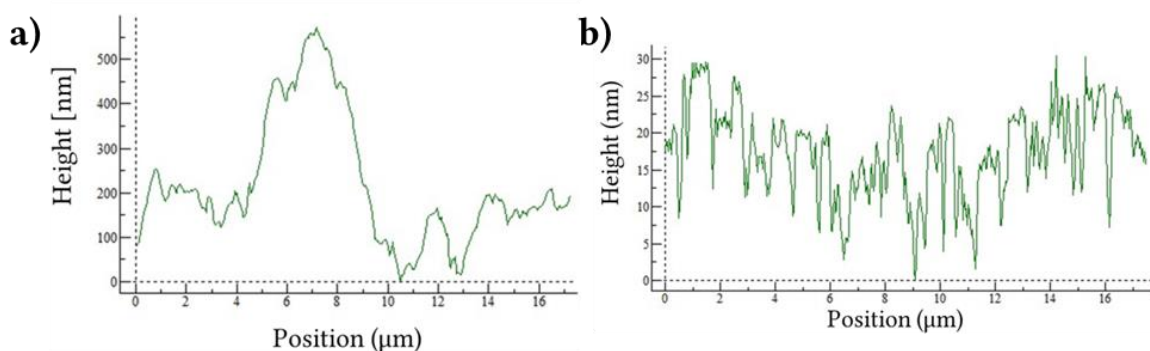


Figure 59: AFM profiles of an a) unpolished and a b) polished Gould copper foil

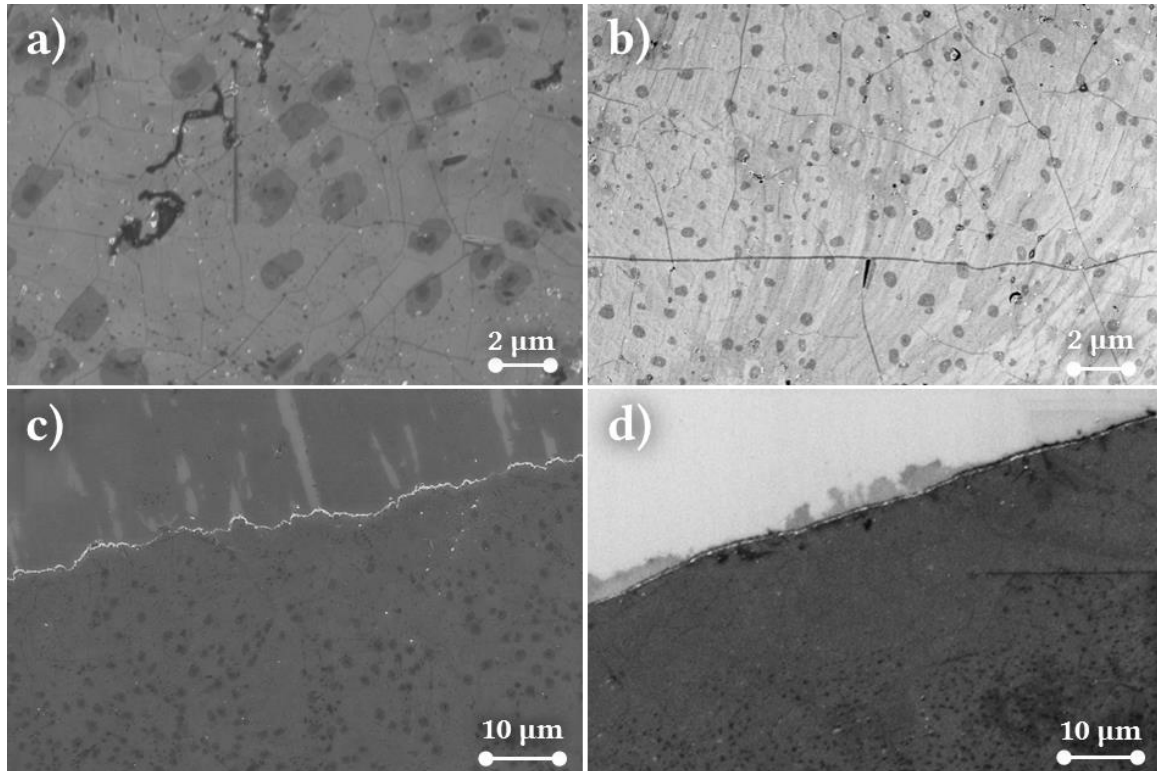


Figure 60: SEM images of graphene; a+c) grown on unpolished copper foils; b+d) grown on polished foils; c+d) show the edges of prepatterned graphene films

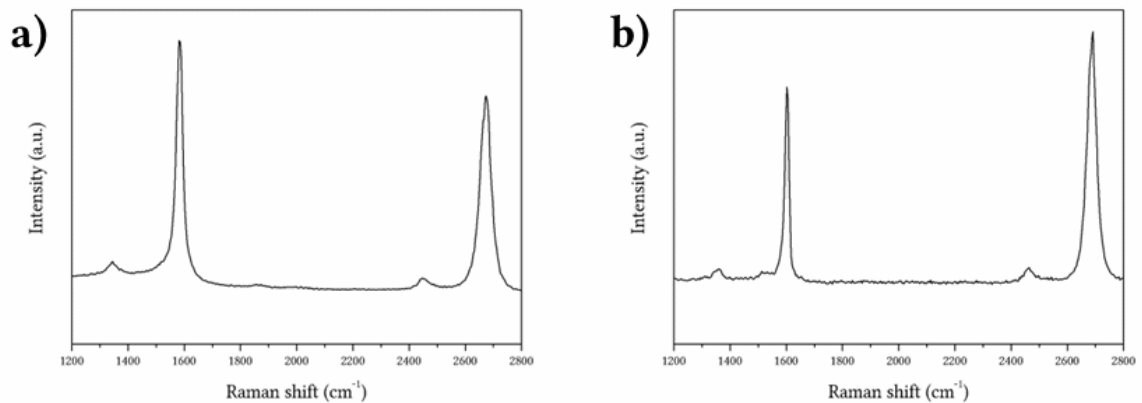


Figure 61: Raman spectra of graphene films grown on a) unpolished copper foil and b) polished foil

Figure 61 compares Raman spectra of graphene films grown on unpolished and polished copper foils. The intensity ratio of the 2D to G peak is bigger in the graphene grown on the polished substrate, underlining its superior quality.

It was also observed that the lift-off of ink residue was easier on polished foils. Resulting in cleaner samples on which less unwanted ink residues remained after the transfer to a wafer substrate.

5.2. *Staedtler Lumocolor*[®] permanent marker ink

The wettability and coverage of copper foils with this ink was satisfying and the ink successfully prevented the graphene growth. Yet, some problems did arise from the ink's drying behaviour. The ink was equipped with the so called "dry safe" technology to prevent the quick drying up of a pen. This is accomplished by a skin that forms rapidly on the surface of an ink drop and protects the liquid from evaporation. With inkjet printing it has an extremely unwanted effect – it clogs the nozzles. The printing results were not always flawless because of missing drops and askew printing lines.

The information published by *Staedtler* specifies the ink as a combination of pigment material, alcohol based solvent and organic resin binder. The presence of chromium, which was confirmed by EDX and XRD analysis, was ascribed to the pigment material. Unfortunately not all ink residues came off the samples during the cleaning steps and the graphene transfer. This did not prove to be a problem in this study but could be an issue in future works. However, prepatterning the CVD growth substrate with this ink resulted in defined graphene features. Raman spectroscopy was used to analyse the produced films and the graphene quality was found to be comparable with unpatterned graphene (see Figure 31).

5.3. Chromium influenced graphene growth

The oxidising/reducing treatment of the *Staedtler Lumocolor*[®] permanent marker ink gave rise to the idea that the ink contained an inorganic component. EDX and XRD affirmed the presence of chromium. To further investigate the mechanism that prevents the graphene growth experiments with sputtered chromium were carried out. SEM images of these samples showed that no graphene grew in the vicinity of chromium containing particles (see also Figure 45). This indicates that the chromium did not only mask the copper foils but also poisoned the growth. The presence of chromium also reduced the number, size and thickness of multilayer islands, further hinting toward an influence in the growth mechanism beyond simple blockage of the substrate.

Additional studies are needed to discern the way in which chromium affects the growth but two mechanisms are thought to be possibly responsible. One is that chromium blocks reactive sites of the catalytic copper substrate. The other is that carbon is consumed by the formation of chromium carbides.

Detailed analysis of the chromium containing particles is needed to prove the likely presence of chromium carbides. The chromium was sputtered on the copper surface and the

process of the generation of the chromium containing particles is not clarified. It might be that the thin chromium layer restructures during the one hour annealing at 1035 °C prior to the graphene growth or that the particles form during the graphene growth as chromium carbide is generated.

The comparison of Figure 62 (a) and (b) shows that multilayer growth can be suppressed by sputtering small quantities of chromium onto the growth substrate. Too much chromium, though, results in an incomplete chromium sheet, as depicted in Figure 62 (c).

The comparison of Raman spectra of growth without chromium, growth under the influence of 1 nm chromium and growth with 5 nm chromium is displayed in Figure 63. The G to 2D ratios suggest that the growth without chromium provided the best graphene growth. A close look at the shape of the 2D peaks reveal that the growth without chromium showed multilayer growth whereas no hints towards multilayer growth can be found in the Raman spectrum with 5 nm chromium. A growth with less chromium may result in suppressed bilayers without disruption of the graphene film.

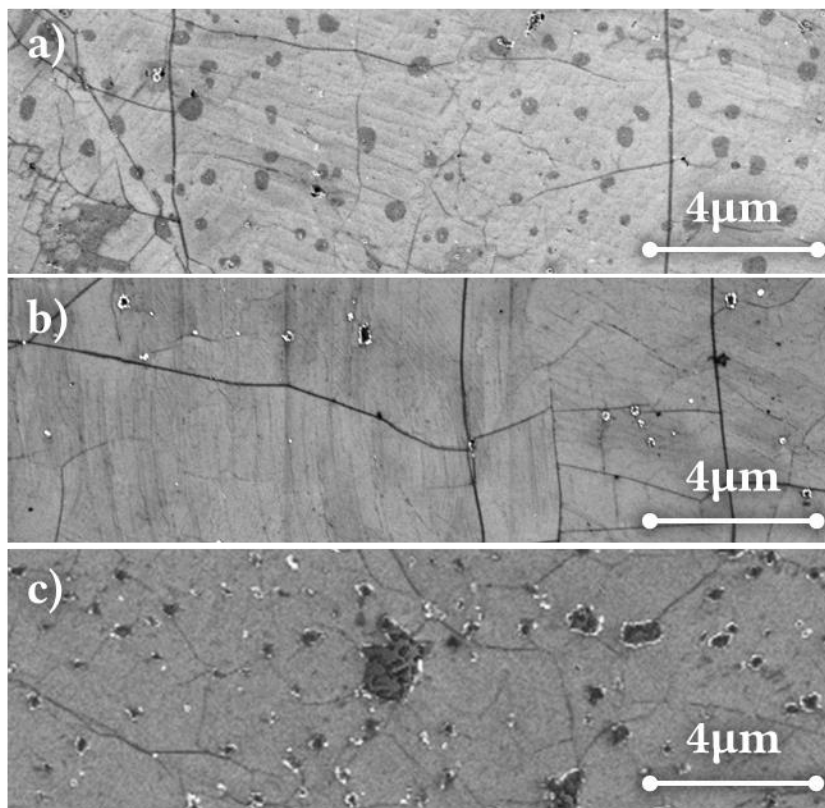


Figure 62: SEM images of graphene on SiO₂/Si wafers; the growth on copper foils was carried out with varying amounts of chromium; a) no chromium, b) 1 nm sputtered chromium, c) 5 nm sputtered chromium

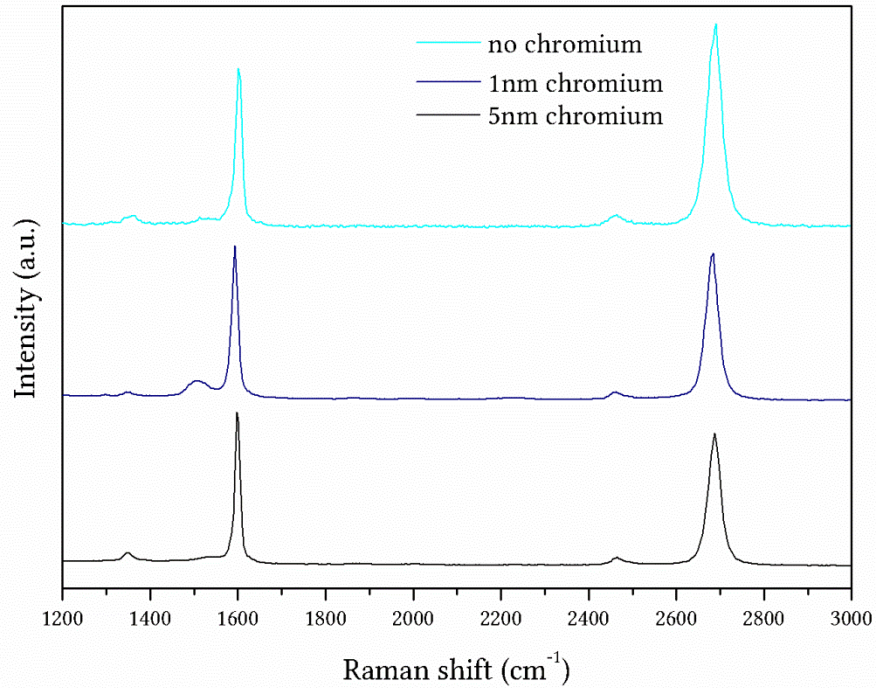


Figure 63: Raman spectra of graphene with no chromium [top], 1 nm sputtered chromium [middle] and 5 nm sputtered chromium [bottom]

5.4. Printing silver ink

It was reported elsewhere that the wettability of graphene lies somewhere between the wettability of graphite and the wettability of the substrate [53] [54]. This behaviour was also observed during the fabrication of silver contacts, leading to thicker ink lines on bare wafers than on graphene (see Figure 64).

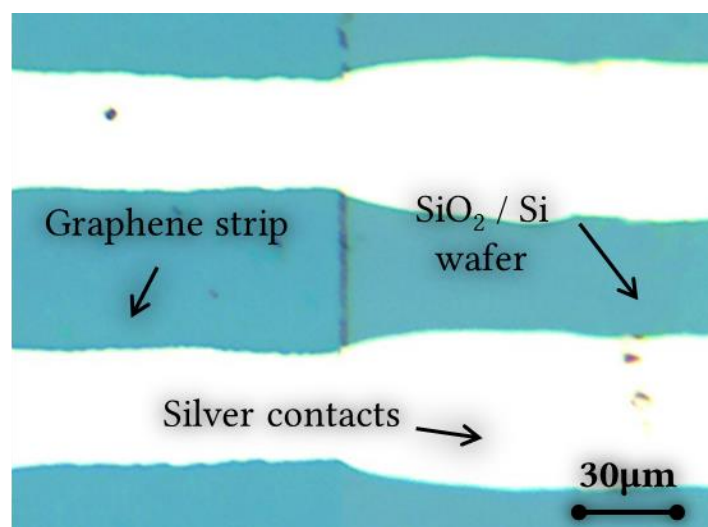


Figure 64: Optical microscopy image of the different width of sintered silver ink lines on graphene (left) and SiO₂/Si wafer (right)

Pure bulk silver has the lowest electrical resistivity of all metals, $1.587 \times 10^{-8} \Omega\text{m}$ [55]. However, this value cannot be expected in silver features as fabricated in this study. Impurities, pores and the like prevent it. The chosen sintering temperatures did raise the conductivity of the structures but was not high enough to cause extensive grain growth and thus eliminate pores. These sintering conditions were chosen in accordance with information obtained by experiments and provided by *Cabot* [56]. 10 min at 180 °C in air proved to be a quick and easy way of producing silver features that showed no obvious oxidation and high conductivity. The calculated bulk resistivity of $17.6 \mu\Omega\text{cm}$ is in agreement with the information published by the manufacturer [57].

Adding to the not ideal difference in work function between graphene and silver, a few reasons were found why silver ink cannot be considered to be the perfect electrode material in the production of graphene electronics. The graphene tended to rip during the sintering process due to the sudden vaporisation of solvents. Therefore in the production of graphene devices the ink was dried slowly and sintered afterwards. This procedure resulted in lower conductivities than the immediate sintering of wet ink. It may be that performing this step in an inert or slightly reducing atmosphere would minimise these losses in conductivity but investigations towards that end remain the subject of future studies. It was also noticed that the sintered silver lines started to oxidise in laboratory conditions and their resistivity increased by a factor of 1.5 in 56 days. Basically the described production route in this work could make flexible, transparent electronics possible, but silver electrodes are not transparent.

5.5. Electrical performance of the fabricated graphene devices

All GFETs produced on Si-Mat wafers performed as FETs and gave high charge carrier mobility values at room temperature. Electron mobilities of up to $2155 \text{ cm}^2\text{V}^{-1}\text{s}^{-1}$ and hole mobilities of up to $2078 \text{ cm}^2\text{V}^{-1}\text{s}^{-1}$ were calculated. Such high mobility values can only be obtained by graphene of good quality. These numbers are in the same order of magnitude as previously with other patterning methods produced graphene of this research group.

Residues that remain on the graphene surface after the transfer hugely impact its electrical properties [15]. It was shown elsewhere that the mobility of devices can be improved and the p-type doping counteracted by the removal of PMMA via vacuum annealing [45]. In this work vacuum annealing was applied to remedy this issue. Figure 65 follows one sample through two annealing steps. It can be observed that the charge

neutrality point shifts down towards zero making the determination of both electron and hole mobility possible.

It was observed that the performance of the devices deteriorated over time when stored at laboratory conditions. Figure 66 shows the sheet resistance curve of a device in ambient condition, after a 12 h vacuum anneal and the same sample 31 days after its production again in ambient conditions. The difference of the two curves that were measured in ambient conditions is clearly visible. The observed oxidation of the silver contacts could possibly be responsible for the decline in mobility as is the adsorption of contaminants (water ect.). Only the measurement carried out in vacuum shows the charge neutrality point.

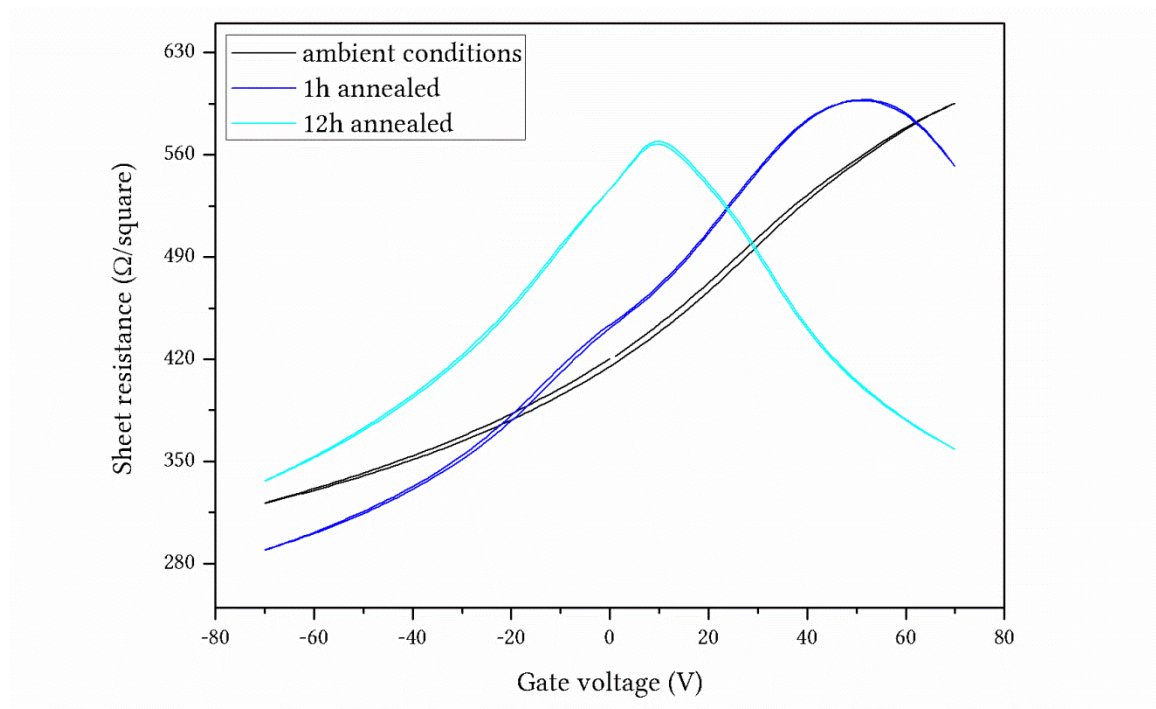


Figure 65: Comparison of sheet resistance vs. gate voltage, of sample D21.2. I U in ambient conditions [black], after a 1 h vacuum anneal [blue] and after a subsequent 12 h vacuum anneal [turquoise]

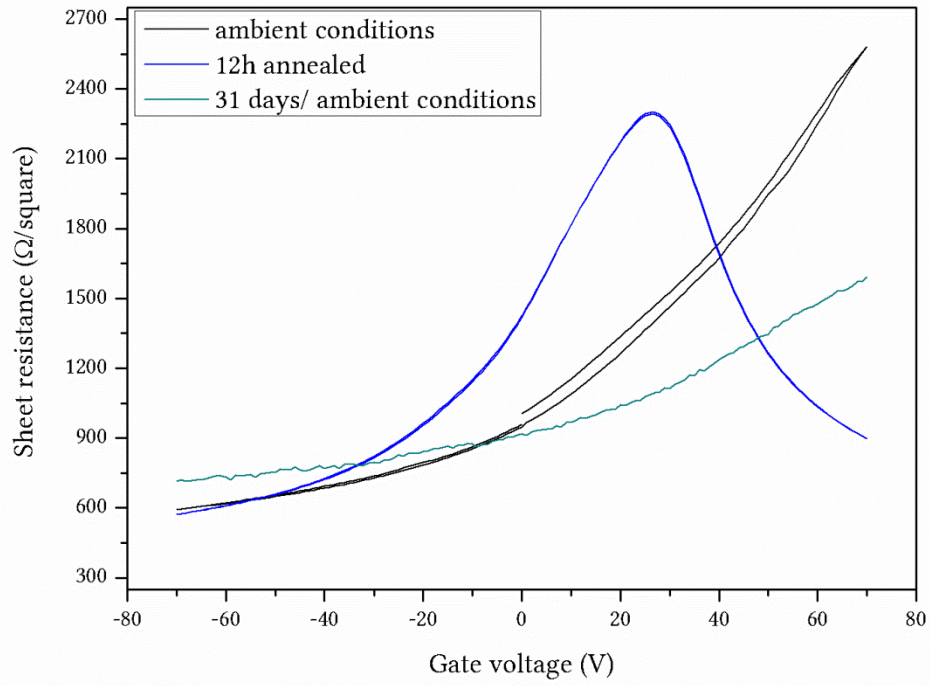


Figure 66: Comparison of sheet resistance vs. gate voltage, of sample D21.2. II L in ambient conditions [black], after an 12h vacuum anneal [blue] and 31 days after production in ambient conditions [turquoise]

6. Conclusion and future work

Graphene was grown on polished and unpolished copper foils. The growth on polished foils was found to exhibit decidedly less multilayer growth, an overall cleaner appearance and a Raman spectrum of superior quality.

The growth substrate, copper foils, were prepatterned with commercially available chromium containing marker ink (i.e. *Staedtler Lumocolor*[®] permanent marker) using inkjet printing to produce clearly defined graphene features. This prepatterned graphene growth had more precise edges on polished foils than on unpolished foils. Graphene strips arising from this method were contacted with silver electrodes by inkjet printing to form field effect transistors. Small amounts of silver ink solvent were able to migrate between graphene and the underlying substrate. These drops posed problems during sintering of the silver nanoparticles. The ink had to be dried slowly to prevent the solvent drops from bursting through and ripping the graphene upon evaporation. The produced GFETs showed p-doping and were vacuum annealed at 500 K to remove transfer residues. High charge carrier mobilities, of up to $2155 \text{ cm}^2\text{V}^{-1}\text{s}^{-1}$, were realised in these devices.

The obtained results show that it is possible to combine the high quality of CVD grown graphene with the flexibility afforded by inkjet printing.

Inkjet printing is limited in its lateral resolution and the presented process is not able to compete with conventional silicon micro-fabrication methods (e.g. lithography) in terms of feature size. It, however, is very well suited to the fabrication of bigger (tens of micron-scale) graphene structures as, for an example, needed in RFID antennas or similar devices. By eliminating the necessity of harsh post-growth patterning steps graphene structures on a wide variety of substrates could be realised with this process.

Like so many times in science, some questions have to stay unanswered and remain to be addressed in future work:

- Further investigations into the mechanism by which chromium influences the graphene growth and the possible use of chromium for the controlled suppression of multilayer growth should be carried out.
- The *Staedtler Lumocolor*[®] permanent marker ink used tended to clog the printer nozzles. An ink that is designed for inkjet printing and therefore does not block the

nozzles as easily should provide cleaner patterns. Different chromium containing inks should be tested or, alternatively, such an ink could be developed.

- Some ink residues remained on the samples during the cleaning steps and the graphene transfer. Either an improvement of the cleaning procedure or a different ink could solve this issue.
- Improvements of the sintering conditions of silver nanoparticle ink on graphene.
- Replacement of silver conductive ink with organic conductive ink as electrode material could be tested, e.g. PEDOT, or the sintering conditions of silver nanoparticle ink should be improved.
- The presented routine can be put into use to fabricate flexible, transparent devices on plastic foils, e.g. a RFID-antenna on PET.

Appendix

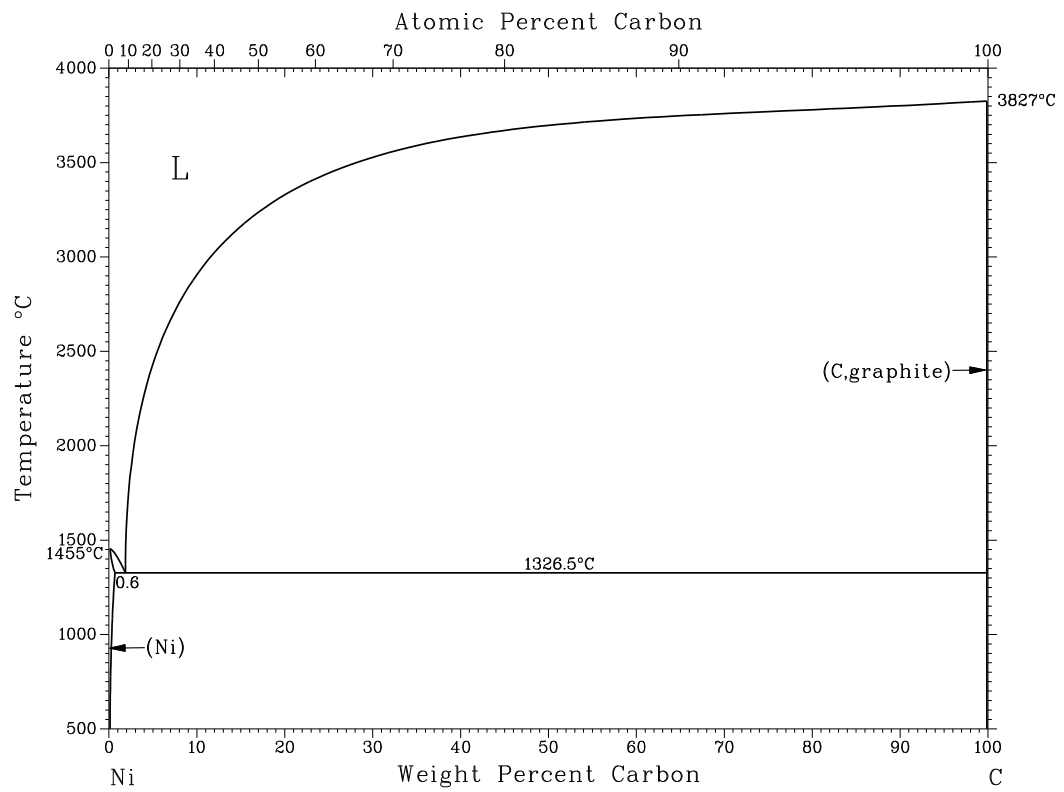


Figure 67: Phase diagram of carbon and nickel [reproduced from [34]]

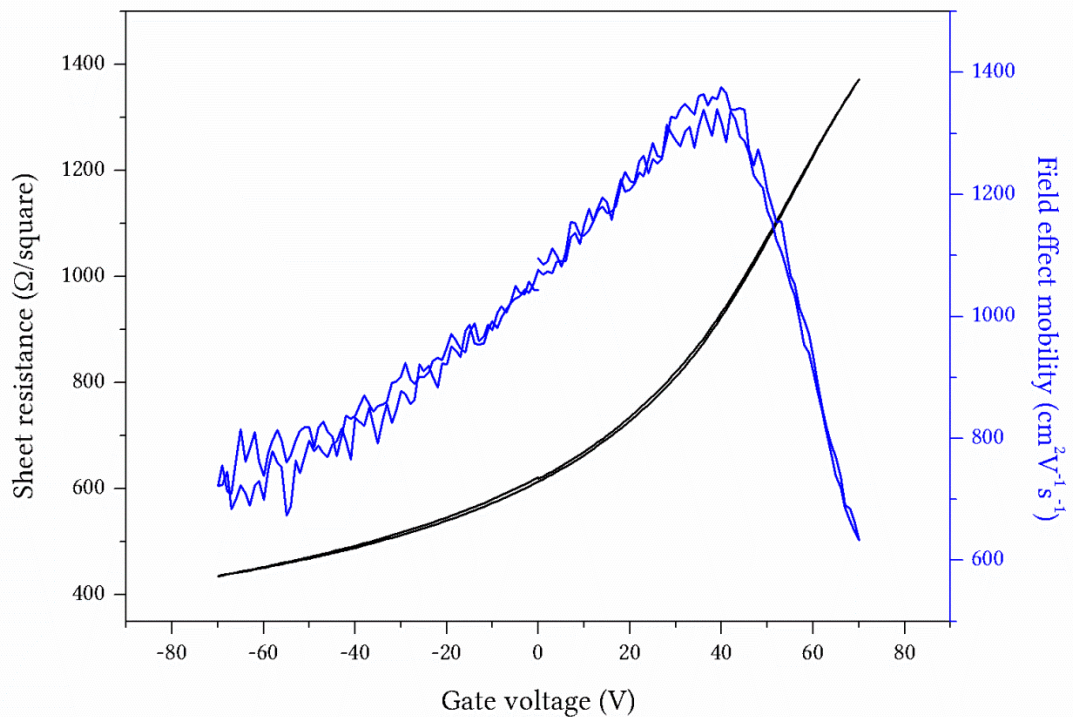


Figure 68:D21.2. 1 L ambient conditions

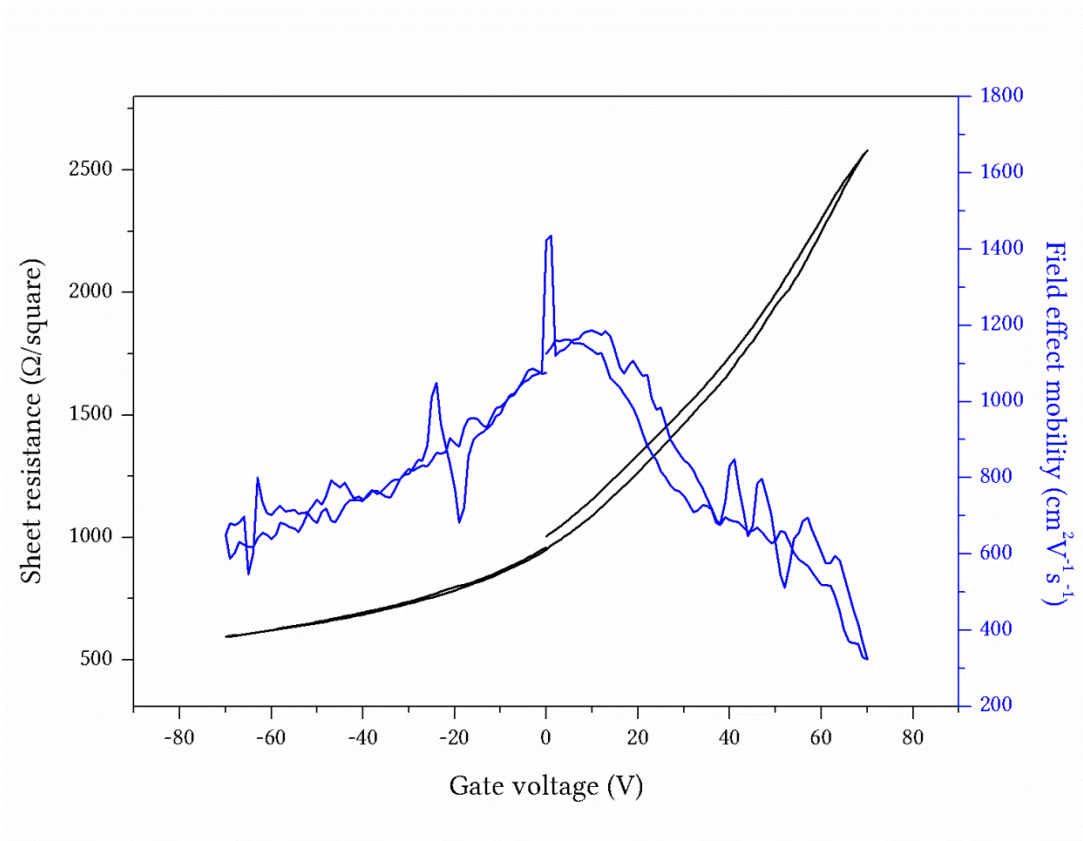


Figure 69:D21.2. II L ambient conditions

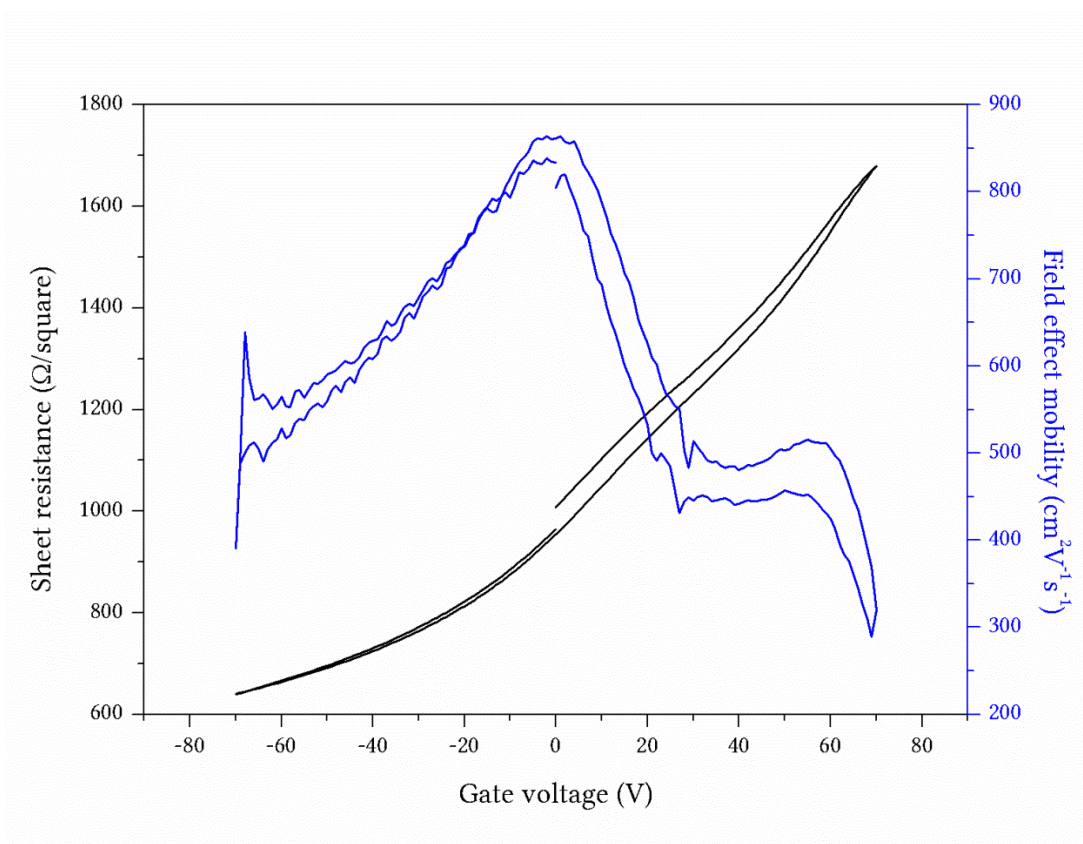


Figure 70: D21.2. II U ambient conditions

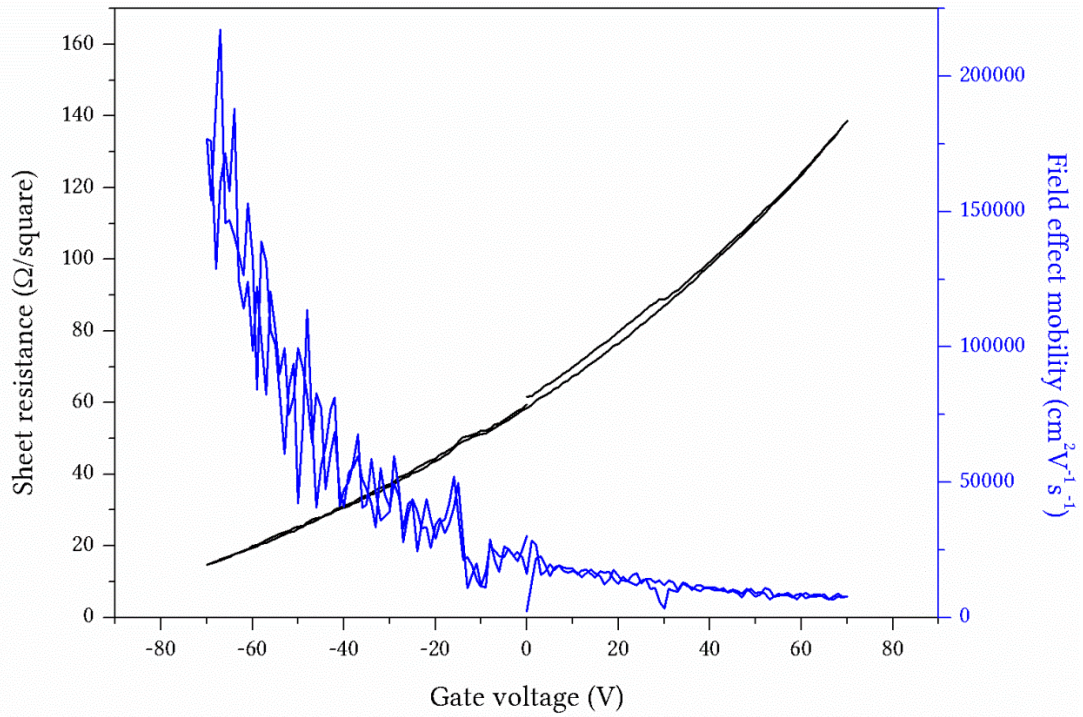


Figure 71: D21.2. III U ambient conditions

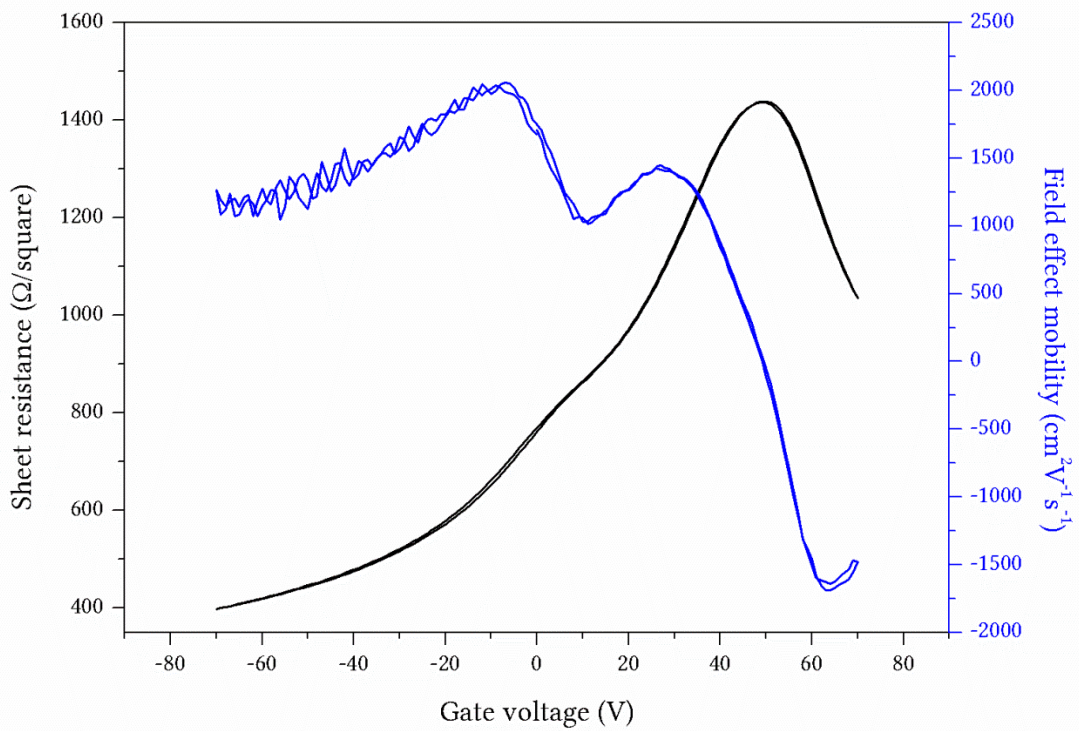


Figure 72:D21.2. I L 1h anneal

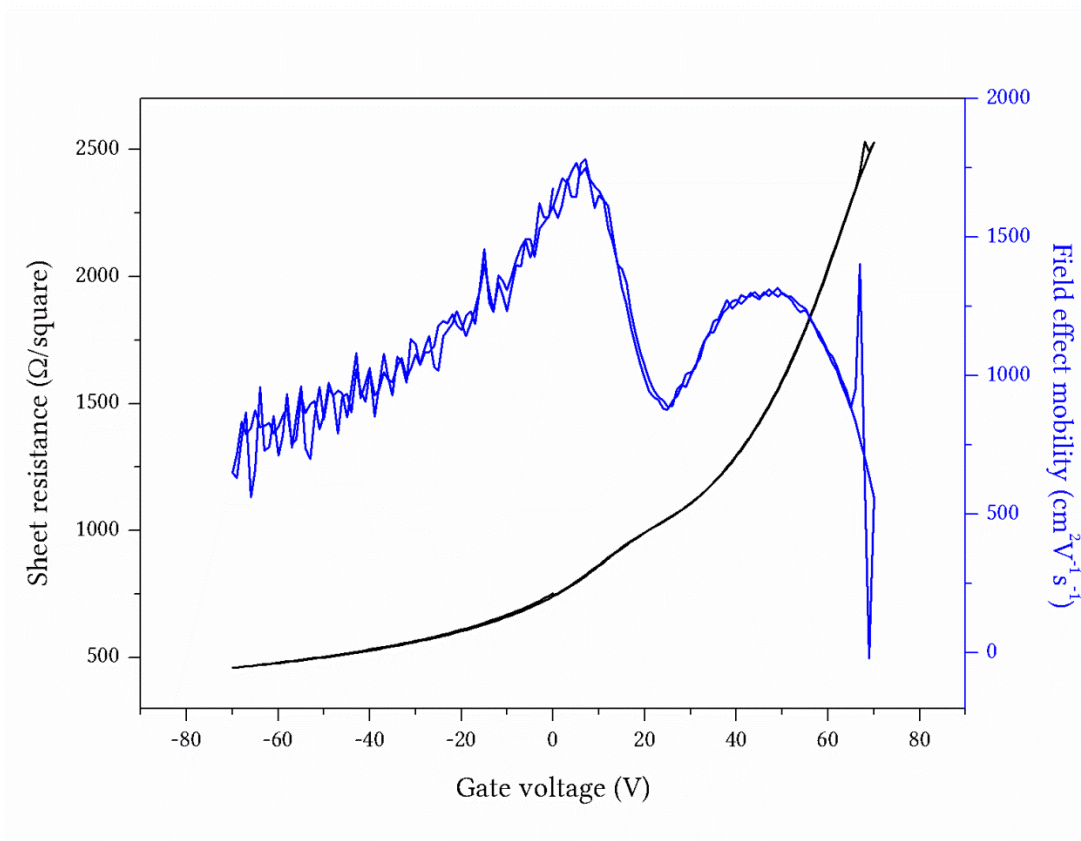


Figure 73: 21.2. II L 1h anneal

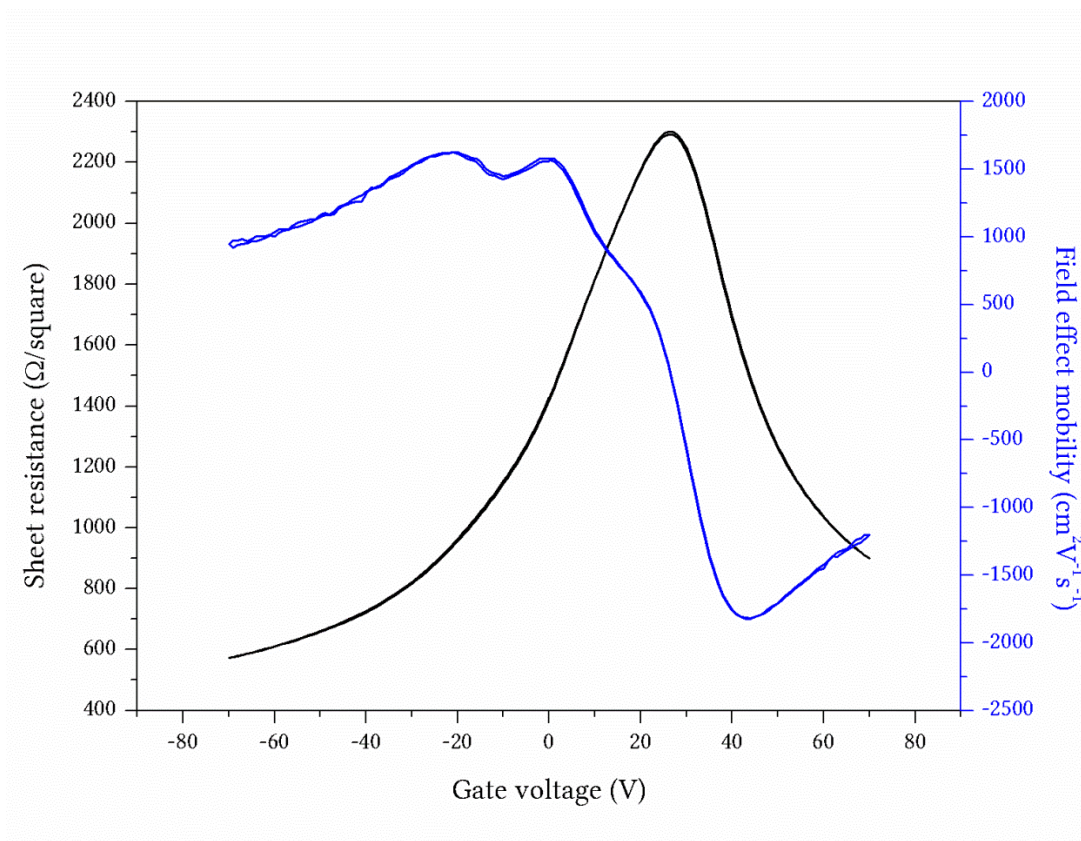


Figure 74: 21.2. II L 12h anneal

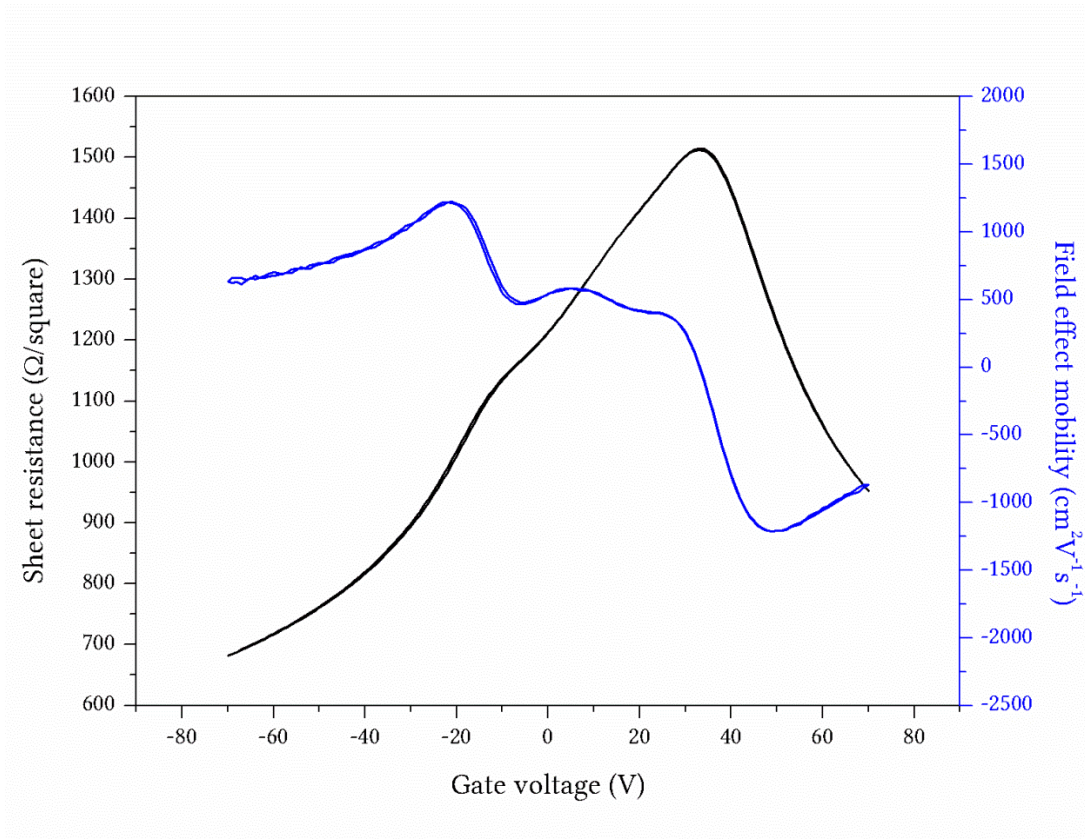


Figure 75: 21.2. II U 12h anneal

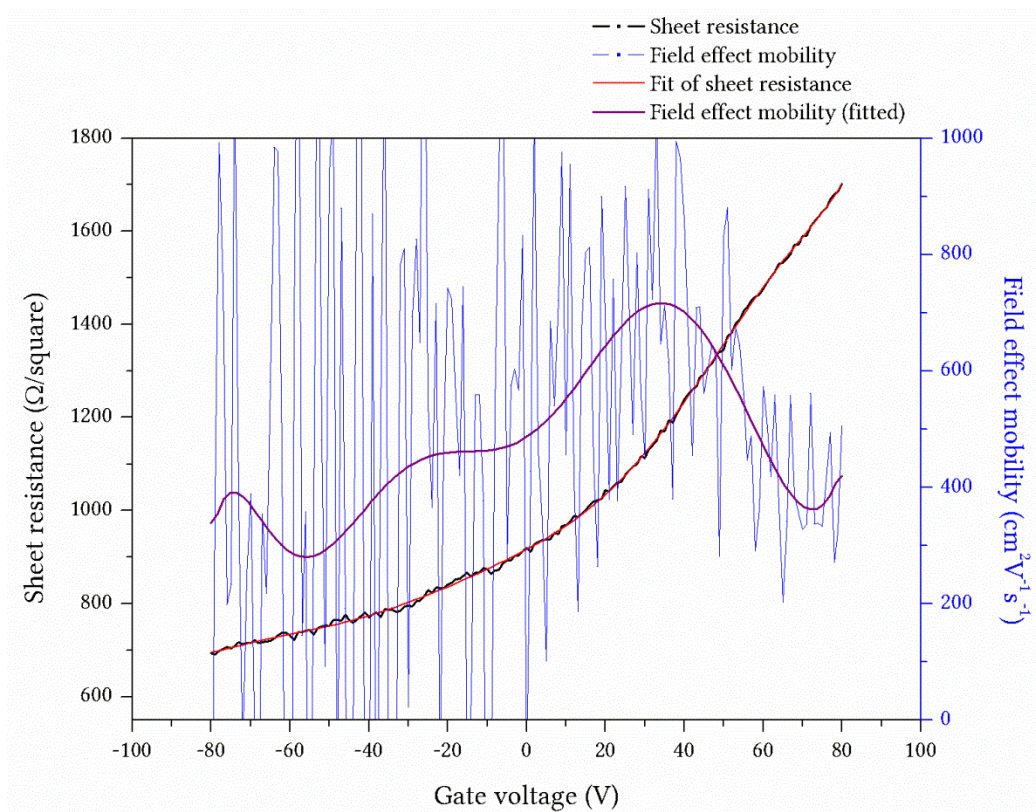


Figure 76: D21.2. II L measurement after 31 days in ambient conditions

List of Acronyms

2D	2-Dimensional
AFM	Atomic Force Microscopy
Ag	Silver
Al ₂ O ₃	Aluminium oxide
ALD	Atomic Layer Deposition
APS	Ammonium Persulfate
ARPES	Angle-Resolved Photoemission Spectroscopy
BSE	Back-scattered Electrons
CAD	Computer Aided Design
CH ₄	Methane
CNT	Carbon Nanotube
Cu	Copper
CVD	Chemical Vapour Deposition
DLS	Dynamic Light Scattering
DMF	Dimethylformamide
DOD	Drop on demand
EDX	Energy-dispersive X-ray spectroscopy
FE-SEM	Field Emission – Scanning Electron Microscopy
FET	Field Effect Transistor
FWHM	Full-Width at Half-Maximum
GFET	Graphene Field Effect Transistor
GO	Graphene Oxide
H ₂	Hydrogen
H ₃ PO ₄	Phosphoric acid
HCl	Hydrochloric acid
IPA	Isopropyl alcohol
IR	Infrared
ITO	Indium Tin Oxide
LP-CVD	Low Pressure – Chemical Vapour Deposition
n/a	not applicable
NMP	N-Methylpyrrolidone
PEDOT	Poly-3,4-ethylenedioxythiophene
PMMA	Poly(Methyl Methacrylate)
RF	Radio Frequency
RFID	Radio Frequency Identification
RGO	Reduced Graphene Oxide
RIE	Reactive Ion Etching
RMS	Root Mean Squared
SE	Secondary Electron
SEM	Scanning Electron Microscopy
Si	Silicon
SiC	Silicon Carbide
SiO ₂	Silicon Dioxide
TEM	Transmission Electron Microscopy
TFT	Thin Film Transistor
UV	Ultra Violet
XPS	X-ray Photoelectron Spectroscopy

List of References

- [1] R.S. Edwards et al., „Graphene synthesis: Relationship to applications,“ *Nanoscale*, 2013, 5, 1, pp. 38-51
- [2] E.Tekin et al., „Inkjet printing as a deposition and patterning tool for polymers and inorganic particles,“ *Soft Mater*, 2008, 4, pp. 703-713
- [3] J. Perelaer et al., „Printed electronics: the challenges involved in printing devices, interconnects and contacts based on inorganic materials,“ *Journal of Materials Chemistry*, 2010, 20, pp. 8446-8453
- [4] G. Cummis et al., „Inkjet printing of conductive materials: a review,“ *Circuit World*, 2012, 38, 4, pp. 193-213
- [5] F. Torrisi et al., „Inkjet-Printed Graphene Electronics,“ *ACS Nano*, 2012, 6, 4, pp. 2992-3006
- [6] M. Ha et al., „Printed, sub-3V digital circuits on plastic from aqueous carbon nanotube inks,“ *ACS Nano*, 2010, 4, 8, p. 4388-4395
- [7] K.I. Bolotin et al., „Ultrahigh electron mobility in suspended graphene,“ *Solid State Communications*, 2008, 146, p. 351-355
- [8] Y. Hernandez et al., „High-yield production of graphene by liquid-phase exfoliation of graphite,“ *Nature Nanotechnology*, 2008, 3, pp. 563-568
- [9] K. Shin et al., „Micropatterning of Graphene Sheets by Inkjet Printing and Its Wideband Dipole-Antenna Application,“ *Advanced Materials*, 2011, 23, p. 2113-2118
- [10] X. Li et al., „Large-Area Synthesis of High-Quality and Uniform Graphene Films on Copper Foils,“ *Science*, 2009, 324
- [11] N. Petrone et al., „Chemical Vapor Deposition-Derived Graphene with Electrical Performance of Exfoliated Graphene,“ *Nano Letters*, 2012, 12, pp. 2751-2756
- [12] F. Bonaccorso et al., „Production and processing of graphene and 2d crystals,“ *materialstoday*, 2012, 15, 12, pp. 564-589
- [13] P. Blake et al., „Graphene-Based Liquid Crystal Device,“ *Nano Letters*, 2008, 8, 6
- [14] S. Kumar et al., „Reliable processing of graphene using metal etchmasks,“ *Nanoscale Research Letters*, 2011, 6, 390
- [15] J.W. Suk et al., „Enhancement of the Electrical Properties of Graphene Growth by Chemical Vapor Deposition via Controlling the Effects of Polymer Residue,“ *Nano Letters*, 2013, 13, 4, p. 1462-1467
- [16] C. A. Howsare et al., „Substrate considerations for graphene synthesis on thin copper films,“ *Nanotechnology*, 2012, 23
- [17] N.S. Safron et al., „Barrier-Guided Growth of Micro- and Nano-Structured Graphene,“ *Advanced Materials*, 2012, 24, pp. 1041-1045
- [18] C. Soldano et al., „Production, properties and potential of graphene,“ *Carbon*, 2010, 48, 8, pp. 2127-2150
- [19] A. Geim et al., „The rise of graphene,“ *nature materials*, 2007, 6, 3, pp. 183-191
- [20] K.S. Novoselov et al., „Electric Field Effect in Atomically Thin Carbon Films,“ *Science*, 2004, 306, pp. 666-669
- [21] http://www.nobelprize.org/nobel_prizes/physics/laureates/2010/. [31 July 2013]

- [22] A.H. Castro Neto et al., „The electronic properties of graphene,“ *Reviews of Modern Physics*, 2009, 81, pp. 109-162
- [23] K.S. Novoselov et al., „Two-dimensional atomic crystals,“ *PNAS*, 2005, 102, 30
- [24] K.S. Novoselov et al., „A roadmap for graphene,“ *Nature*, 2012, 490, pp. 192-200
- [25] P. Blake et al., „Making graphene visible,“ *Applied Physics Letters*, 2007, 91
- [26] S.V. Morozov et al., „Giant Intrinsic Carrier Mobilities in Graphene and Its Bilayer,“ *Physical Review Letters*, 2008, 100, 1
- [27] A.A. Balandin, „Thermal properties of graphene and nanostructured carbon materials,“ *Nature Materials*, 2011, 10, pp. 569-581
- [28] C. Lee et al., „Measurement of the Elastic Properties and Intrinsic Strength of Monolayer Graphene,“ *Science*, 2008, 321, pp. 385-388
- [29] A.C. Ferrari et al., „Raman Spectrum of Graphene and Graphene Layers,“ *Physical Review Letters*, 2006.
- [30] http://www.sait.samsung.co.kr/saithome/Page.do?method=main&pagePath=02_research/&pageName=highperformance. [13 August 2013]
- [31] http://www.emsdiasum.com/microscopy/products/grids/graphene_tem.aspx. [12 August 2013]
- [32] H. Mehdipour et al., „Kinetics of Low-Pressure, Low-Temperature Graphene Growth: Toward Single-Layer, Single-Crystalline Structure,“ *ACS Nano*, 2012, 6, 11, pp. 10276-10286
- [33] Z. Sun et al., „Large-Area Bernal-Stacked Bi-, Tri-, and Tetralayer Graphene,“ *ACS Nano*, 2012, 6, 11, p. 9790–9796
- [34] T. B. Massalaski, *Binary Alloy Phase Diagrams*, Materials Park, Ohio: ASM International, 1990
- [35] Z. Yan et al., „Toward the Synthesis of Wafer-Scale Single-Crystal Graphene on Copper Foils,“ *ACS Nano*, 2012, 6, 10, pp. 9110-9117
- [36] S. Kumar et al., „CVD growth and processing of graphene for electronic applications,“ *Physica status solidi b*, 2011, 248, 11, pp. 2604-2608
- [37] A.C. Ferrari et al., „Raman spectroscopy as a versatile tool for studying the properties of graphene,“ *Nature nanotechnology*, 2013, 8, pp. 235-246
- [38] A.C. Ferrari, „Raman spectroscopy of graphene and graphite: Disorder, electron-phonon coupling, doping and nonadiabatic effects,“ *Solid State Communications*, 2007, 143, pp. 47-57
- [39] T.M.G. Mohiuddin et al., „Uniaxial strain in graphene by Raman spectroscopy: G peak splitting, Grüneisen parameters, and sample orientation,“ *Physical Review B*, 2009, 79
- [40] M. Kalbac et al., „The Influence of Strong Electron and Hole Doping on the Raman Intensity of Chemical Vapor-Deposition Graphene,“ *ACS Nano*, 2010, 4, 10, pp. 6055-6063
- [41] H. Hiura et al., „Determination of the Number of Graphene Layers: Discrete Distribution of the Secondary Electron Intensity Stemming from Individual Graphene Layers,“ *Applied Physics Express*, 2010, 3
- [42] A. Ismach et al., „Direct Chemical Vapor Deposition of Graphene on Dielectric Surfaces,“ *Nano Letters*, 2010, 10, pp. 1542-1548
- [43] V. Kochat et al., „High contrast imaging and thickness determination of graphene with in-column secondary electron microscopy,“ *Journal of Applied Physics*, 2011, 110, 1
- [44] S. Kumar et al., „Gas phase controlled deposition of high quality large-area graphene films,“ *Chemical Communications*, 2010, 46, pp. 1422-1424

- [45] A. Pirkle et al., „The effect of chemical residues on the physical and electrical properties of chemical vapor deposited graphene transferred to SiO₂,“ *Applied Physics Letters*, 2011, 99
- [46] E. Tekin et al., „Inkjet printing as a deposition and patterning tool for polymers and inorganic particles,“ *Soft Matter*, 2008, 4, pp. 703-713
- [47] D. Shin et al., „Impact of effective volume ratio of a dispersant to silver nano-particles on silicon solar cell efficiency in direct ink-jet metallization,“ *Journal of Micromechanics and Microengineering*, 2012, 22
- [48] S. Jeong et al., „Stable Aqueous Based Cu Nanoparticle Ink for Printing Well-Defined Highly Conductive Features on a Plastic Substrate,“ *Langmuir*, 2011, 27, pp. 3144-3149
- [49] D.A. Roberson et al., „Microstructural and Process Characterization of Conductive Traces Printed from Ag Particulate Inks,“ *materials*, 2011, 4, pp. 963-979
- [50] <http://www.sigmaaldrich.com/catalog/product/aldrich/719048?lang=en®ion=IE>. [30 January 2013]
- [51] K.X.Chen et al., „Rensselaer Polytechnic Institute,“ [Online] <http://www.ecse.rpi.edu/~schubert/Course-Teaching-modules/A037-Four-point-probe-measurement-of-semiconductor-sheet-resistance.pdf>. [17 January 2013]
- [52] M. Scheiber et al., „Transparent ultrathin conducting carbon films,“ *Applied Surface Science*, 2010, 265, 21, pp. 6186-6190
- [53] J. Rafiee et al., „Wetting transparency of graphene,“ *Nature Materials*, 2012, 11, pp. 217-222
- [54] C. Shih et al., „Breakdown in the Wetting Transparency of Graphene,“ *Physical Review Letters*, 2012, 109
- [55] David R. Lide, *CRC Handbook of Chemistry and Physics: A ready-reference book of chemical and physical data*. 90. Edition, CRC Taylor & Francis, Boca Raton Fla., 2009.
- [56] <http://www.cabot-corp.com/wcm/download/en-us/nb/ATTH4YZ5.doc>. [18 July 2013].
- [57] <http://www.sigmaaldrich.com/catalog/product/aldrich/719048?lang=en®ion=IE>. [30 January 2013].